UC Berkeley

UC Berkeley Electronic Theses and Dissertations

Title

Study of large electroweak logarithms at high energy in collider experiments

Permalink

https://escholarship.org/uc/item/1f44q239

Author

Ferland, Nicolas

Publication Date

2019

Peer reviewed|Thesis/dissertation

eScholarship.org Powered by the California Digital Library
University of California

Study of large electroweak logarithms at high energy in collider experiments

by

Nicolas Ferland

A dissertation submitted in partial satisfaction of the

requirements for the degree of

Doctor of Philosophy

in

Physics

in the

Graduate Division

of the

University of California, Berkeley

Committee in charge:

Doctor Christian Bauer, Co-chair
Professor Lawrence Hall, Co-chair
Professor Richard Borcherds
Professor Hitoshi Murayama

Spring 2019

Study of large electroweak logarithms at high energy in collider experiments

Copyright 2019
by
Nicolas Ferland

Abstract

Study of large electroweak logarithms at high energy in collider experiments

by

Nicolas Ferland

Doctor of Philosophy in Physics

University of California, Berkeley

Doctor Christian Bauer, Co-chair

Professor Lawrence Hall, Co-chair

Using the known resummation of virtual corrections together with knowledge of the leading-log structure of real radiation in a parton shower, we derive analytic expressions for the resummed real radiation after they have been integrated over all of phase space. Performing a numerical analysis for both the 13 TeV LHC and a 100 TeV pp collider, we show that resummation of the real corrections is at least as important as resummation of the virtual corrections, and that this resummation has a sizable effect for partonic center of mass energies exceeding $\sqrt{s} = \mathcal{O}(\text{few TeV})$. For partonic center of mass energies $\sqrt{s} \gtrsim 10$ TeV, which can be reached at a 100 TeV collider, resummation becomes an O(1) effect and needs to be included even for rough estimates of the cross-sections.

We compute the leading-order evolution of parton distribution functions for all Standard Model fermions and bosons up to energy scales far above the electroweak scale, where electroweak symmetry is restored. Our results include the 52 PDFs of the unpolarized proton, evolving according to the SU(3), SU(2), U(1), mixed SU(2)×U(1) and Yukawa interactions. We illustrate the numerical effects on parton distributions at large energies, and show that this can lead to important corrections to parton luminosities at a future 100 TeV collider.

We present a resummation of those double-logarithmically enhanced electroweak correction that arise in pp colliders because protons are not SU(2) singlets, by solving DGLAP equations in the full Standard Model. We then show how to match these results with those of fixed-order electroweak calculations. At a 100 TeV pp collider, contributions beyond order α are $\sim 10\%$ at partonic center-of-mass energies of a few TeV. These are mainly due to initial states with massive vector bosons.

Contents

Contents **i**

List of Figures **iii**

List of Tables **vi**

1 Introduction **1**
1.1 Running couplings 4

2 Resummation of electroweak Sudakov logarithms for real radiation **6**
2.1 The structure of logarithmic terms in the perturbative expansion 7
2.2 Fixed order calculations of the virtual and real contributions 8
2.3 LL resummation of the leading logarithms 11
2.4 Results 20

3 Standard Model Parton Distributions at Very High Energies **27**
3.1 The evolution of parton distributions in the full Standard Model 29
3.2 Implementation details 42
3.3 Results 45

4 Combining initial-state resummation with fixed-order calculations of electroweak corrections **54**
4.1 Standard Model parton luminosities and their expansion 57
4.2 Resummation of logarithms in inclusive di-lepton production 65

5 Conclusions **73**

Bibliography **76**

A Equations used in the forward evolution **82**
A.1 SU(3) interaction 82
A.2 U(1) interaction 83
A.3 SU(2) interaction 83

A.4 Yukawa interaction 84
A.5 Mixed interaction 85

B The partonic Born cross sections for di-lepton production 86

List of Figures

2.1 The cross-section summed over all lepton flavors for the 13 TeV LHC. On the top we show the individual corrections relative to the Born cross-section as defined in Eq. (2.66), in the middle the relative size of the resummation as defined in Eq. (2.67), while on the bottom we show the total perturbartive correction relative to the Born as defined in Eq. (2.68). Virtual corrections are shown in black, while real corrections with a Z, photon, W^+, W^- are shown in green, orange, red and blue. Resummed corrections are shown in solid lines, while fixed order results are dashed. The x-axis denotes the fraction of the partonic center of mass energy relative to the collider center of mass energy. 21
2.2 The cross-section summed over all lepton flavors for a 100 TeV pp collider on the right. All colors are the same as in Fig. 2.1. 22
2.3 The cross-section for e^+e^- for the 13 TeV LHC on the left, and 100 TeV pp collider on the right. All colors are the same as in Fig. 2.1. Note that the scaling of the y axis is different for the LHC and the 100 TeV collider. 23
2.4 The cross-section for $\bar{\nu}\nu$ for the 13 TeV LHC on the left, and 100 TeV pp collider on the right. All colors are the same as in Fig. 2.1. 24
2.5 The cross-section summed for $e^+\nu$ for the 13 TeV LHC on the left, and 100 TeV pp collider on the right. All colors are the same as in Fig. 2.1. 25
2.6 The cross-section for $\bar{\nu}e^-$ for the 13 TeV LHC on the left, and 100 TeV pp collider on the right. All colors are the same as in Fig. 2.1. 26

3.1 Quark and gluon PDFs in the full unbroken SM, divided by their values assuming pure QCD evolution only. Left- and right-handed quark chiralities are solid and dashed, respectively. The thin gray lines show where the scales on the x- and/or y-axes switch between linear and logarithmic. 49
3.2 Asymmetry between up-isospin and down-isospin left-handed quark PDFs, defined in Eq. (3.116), in the full unbroken SM, compared to the result when only QCD evolution is included. 50
3.3 Electroweak bosons PDF normalized by the gluon PDF. The thin gray lines show where the scales on the x- and/or y-axes switch between linear and logarithmic. 51

3.4 Longitudinal gauge and Higgs bosons PDFs normalized by the gluon PDF. The Z_L PDF is the same as the h PDF. The hZ_L PDF is purely imaginary and we show the result divided by i. The thin gray line shows where the scales on the x- and/or y-axes switch between linear and logarithmic. 52
3.5 First generation lepton PDFs normalized by the gluon PDF. Since we treat leptons as massless, and all leptons have the same initial condition, the results for the other 2 generations are identical. The thin gray line shows where the scales on the x- and/or y-axes switch between linear and logarithmic. 52
3.6 Quark anti-quark luminosity in the full unbroken SM, divided by their values assuming pure QCD evolution only. 53
3.7 Vq and Hq luminosity in the full unbroken SM, divided by the average of $u\bar{u}$ and $d\bar{d}$ luminosity assuming pure QCD evolution only. 53

4.1 Scaling of the expanded PDFs with the parameter r, which multiplies $\alpha_{I=1,2,M}$. On the left, we show the left-handed quarks of the first generation, in the middle the right-handed quarks of the first generation, and on the right the vector bosons. One can clearly see that the expanded PDFs are linear in α_I. 60
4.2 The ratio of the "noEW" and expanded SM PDFs relative to the PDF evaluated in the full SM for left-handed quarks. 61
4.3 The ratio of the "noEW" and expanded SM PDFs relative to the PDF evaluated in the full SM for the massless vector bosons. 61
4.4 The ratio of the "noEW" and expanded SM PDFs relative to the PDF evaluated in the full SM for the transversely-polarized massive vector bosons. 62
4.5 Plots showing luminosities for various choices of initial states. We show in black $\mathcal{L}^{\rm SM}$, in red $\mathcal{L}^{\rm noEW}$, in blue $\left[\mathcal{L}^{\rm SM}\right]_\alpha$ and for V_TV_T initial states in orange $\left[\mathcal{L}^{\rm SM}\right]_\alpha^{\rm mod}$. 64
4.6 The differential cross section $m_{\ell\ell}^4 {\rm d}\sigma/{\rm d}m_{\ell\ell}(p_{T\ell} > 100\text{ GeV})$ for a 100 TeV collider, showing the makeup of the total cross section in terms of the individual initial states. 66
4.7 The expansion of the various contributions to $m_{\ell\ell}^4 {\rm d}\sigma/{\rm d}m_{\ell\ell}(p_{T\ell} > 100\text{ GeV})$ for a 100 TeV collider. We show in black the result obtained using $\mathcal{L}^{\rm SM}$, in red that using $\mathcal{L}^{\rm noEW}$, in blue that using $\left[\mathcal{L}^{\rm SM}\right]_\alpha$ and for V_TV_T initial states in orange that using $\left[\mathcal{L}^{\rm SM}\right]_\alpha^{\rm mod}$. 67
4.8 The expansion of the complete result $m_{\ell\ell}^4 {\rm d}\sigma/{\rm d}m_{\ell\ell}(p_{T\ell} > 100\text{ GeV})$ for a 100 TeV collider. The colors are the same as in Fig. 4.7. 68
4.9 The differential cross section $m_{\ell\ell}^4 {\rm d}\sigma/{\rm d}m_{\ell\ell}(p_{T\ell} > 100\text{ GeV})$ for a 27 TeV and 1 PeV collider, showing the makeup of the total cross section in terms of the individual initial states. 69
4.10 The expansion of the various contributions to $m_{\ell\ell}^4 {\rm d}\sigma/{\rm d}m_{\ell\ell}(p_{T\ell} > 100\text{ GeV})$ for a 27 TeV collider. The colors are the same as in Fig. 4.7. 70
4.11 The expansion of the various contributions to $m_{\ell\ell}^4 {\rm d}\sigma/{\rm d}m_{\ell\ell}(p_{T\ell} > 100\text{ GeV})$ for a 1 PeV collider. The colors are the same as in Fig. 4.7. 71

4.12 The expansion of the complete result $m_{\ell\ell}^4 \mathrm{d}\sigma/\mathrm{d}m_{\ell\ell}(p_{T\ell} > 100 \text{ GeV})$ for a 27 TeV and 1 PeV collider. The colors are the same as in Fig. 4.7 72

List of Tables

3.1 The 52 PDFs required for the SM evolution can written in a basis with definite conserved quantum numbers. $(5n_g + 4)$ PDFs contribute to the $\{0, +\}$ state, $(5n_g + 1)$ to the $\{0, -\}$, $(2n_g + 2)$ to each to the $\{1, +\}$ and $\{1, -\}$ and 1 to the $\{2, +\}$, where $n_g = 3$ stands for number of generations. 32
3.2 Momentum fractions (%) carried by various parton species at scale $q = 10$ TeV. 47
3.3 Momentum fractions (%) carried by various parton species at scale $q = 100$ TeV. 48

4.1 The scaling of the PDFs with the EW coupling constant. 56

B.1 Born cross sections for $q\bar{q}$ and W^+W^- going to lepton pairs. Here e stands for the charged lepton. The cross sections for $BA \to \ell\bar{\ell}'$ are the same as $AB \to \ell\bar{\ell}'$ with $t \leftrightarrow u$. 86
B.2 Born cross sections for VV in the unbroken basis going to lepton pairs. Here M stands for the mixed B/W_3 PDF. The cross sections for $BA \to \ell\bar{\ell}'$ are the same as $AB \to \ell\bar{\ell}'$ with $t \leftrightarrow u$. 88
B.3 Born cross sections for VV in the broken basis going to lepton pairs. Here $\tilde{M}$ stands for the mixed γ/Z PDF. The cross sections for $BA \to \ell\bar{\ell}'$ are the same as $AB \to \ell\bar{\ell}'$ with $t \leftrightarrow u$. 88

Acknowledgments

I would like to thank my advisor, Christian Bauer, for mentoring me. You have been an excellent guide and support during my graduate school.

I would like to thank Bryan Webber for contributing to this research.

Chapter 1

Introduction

The Standard Model of particle physics describe all known non-gravitational interactions between particles. It includes 3 gauge groups U(1), SU(2) and SU(3). U(1) and SU(2) are spontaneously broken to $U(1)_{em}$, the electromagnetic symmetry, by the Higgs vacuum expectation value. Due to this symmetry, the electromagnetic interaction do not change the internal properties of a particle, while the weak interaction, the broken part of U(1) and SU(2), changes particles into other particles, such as charged leptons into neutrinos, up-type quarks into down-type quarks, and protons into neutrons and vice versa. Spontaneous symmetry breaking arises when the ground state of a theory is not invariant under a symmetry of its Lagrangian. In this case, low energy systems are not symmetric, but as the energy increases over the energy scale that breaks the symmetry the symmetry of the Lagragian appears since the system stops being dominated by its ground state. This energy scale is the electroweak boson mass because below this scale, the universe is free of real electroweak boson while above, electroweak bosons are radiated. This increase in symmetry happens only double logarithmically such that the energy must be many times larger than the electroweak scale for physical processes to have the electroweak symmetry. On the other hand, the Higgs vacuum expectation value create the parity symmetry by pairing left and right chiral fermions in massive fermions, and this symmetry is broken as the energy gets higher than the electroweak scale.

The electroweak, U(1) and SU(2), Lagrangian can be equivalently written with bosons (B, W^μ) respecting explicitly the symmetry but being unphysical, that is having a non-diagonal mass matrix caused by the Higgs vacuum expectation value, or with bosons being physical (A, $W^\pm$, Z) but not respecting explicitly the symmetry. The massive bosons ($W^\pm$, Z) have also longitudinal modes which comes from the complex Higgs field which is H^0, $H^\pm$ when the symmetry is explicit and $W_L^\pm$, Z_L and h when physical bosons are used, where h is the Higgs boson. Both sets of bosons are valid at all energies. The difference is that the physical bosons are mixed by the interaction and preserved by propagation, while the symmetric bosons are preserved by the interaction but mixed by propagation. The mixing due to propagation is due to the mass matrix, so when the electroweak bosons masses is negligible compare to the energy, the symmetric bosons are simpler to use. However, in any

experiment the initial and final states are observed at low energy and thus are expressed in the physical bosons.

There are many proposed future colliders including the Compact Linear Collider, the International Linear Collider and the Future Circular Collider. The Future Circular Collider would start as a electron-electron collider at the Higgs pole mass, but would then be upgraded to a 100 TeV proton-proton collider. If it is built, this collider will offer new prospects to study the Standard Model at high energy and potentially observe physics beyond the Standard Model. It will also be at an energy largely beyond the electroweak scale, and would thus show the effects of the electroweak symmetry. Those effects have been studied in [1].

Also, important measurements that are planned for the Future Circular Collider include the trilinear and quadrilinear Higgs self-interactions, which will be measured by the multiple Higgs production rates. Therefore, it is important to know how the electroweak interaction will modify the Higgs production and its background. In addition, electroweak bosons will be an important background to many Beyond the Standard Model signals. Also, in many Beyond the Standard Model models, there are new electroweakly charged particles which are more massive than the Standard Model particles. Those particles will likely be produced by Standard Model electroweak boson fusion and detected by decays into Standard Model electroweak bosons, so their rate of production and their mode of detection will be greatly affected by changes in the production and detection of the Standard Model electroweak bosons.

Experiments at the Large Hadron Collider are now probing the structure of matter at scales comparable with, and even beyond, the characteristic scale of electroweak symmetry breaking. So far, no evidence has been found for a breakdown of the Standard Model (SM) in particle collisions. Indeed, there is a logical possibility that the SM remains a good description of hard scattering processes up to scales far beyond those of any conceivable particle colliders. It is therefore of interest to examine the features predicted by the SM for collider events well above the electroweak scale. For this purpose, Monte Carlo event generators including all the SM interactions on an equal footing are necessary. Such generators would be useful for investigating the limits of LHC searches, the potential of possible future colliders and cosmic processes at ultrahigh energies.

It is well known that perturbative corrections in scattering processes have infrared (IR) sensitivity to soft and collinear emissions. For electroweak corrections involving massive Z and W bosons, the mass of the vector bosons regulates the IR divergences, such that the IR sensitivity yields logarithmic dependence on the ratio of the vector boson mass over the partonic center of mass energy

$$\mathrm{L}_s \equiv \ln \frac{s}{m_V^2}\,, \tag{1.1}$$

where s denotes the square of the partonic energy scale of the process, while m_V is a scale of order the masses of the Z and W bosons. Both virtual and real corrections give rise to such logarithmic corrections, and as usual, their effect cancels in fully inclusive observables.

This situation is very similar to the more common situation of gauge theories with massless gauge bosons, such as QCD, for which both virtual and real corrections are IR divergent, and the divergence cancels in the sum that enters in any physical observable. In exclusive processes, there are double logarithmic corrections that can be resummed to all orders, leading to Sudakov form factors. However, in electroweak processes, there are two main differences: First, for massive gauge bosons, both virtual and real contribution are separately finite (albeit with logarithmic dependence on the ratio of the mass of the vector boson to the center of mass energy), such that there is no need to combine them for physical observables. Second, even if the measurement is completely inclusive over the final state, the initial beams of colliders are typically not SU(2) singlets, such that there are additional double logarithms that appear even in observables and final states that are fully inclusive with respect to extra boson emission [3–18]. Thus, essentially any measurement has logarithmic sensitivity to the ratio m_V^2/s, such that for high enough center of mass energies electroweak corrections become very large. And since the beams of any current or proposed future collider are not SU(2) symmetric, no observable measured at such colliders can be symmetric, irrespective of how inclusively one defines the observable and the final state. For processes with non-symmetric final states, such as charged lepton pair production, even if fully inclusive with respect to electroweak boson emission, there will be additional double logarithms.[1]

Thus, in general every order of electroweak perturbation theory comes with two extra powers of logarithms of the form $\ln s/m_V^2$. This means that electroweak perturbation theory is an expansion of the form

$$\langle O\rangle = \langle O\rangle^{(0)} + \alpha_2 \mathrm{L}_s^2 \langle O\rangle^{(1)} + \left[\alpha_2 \mathrm{L}_s^2\right]^2 \langle O\rangle^{(2)} + \mathcal{O}(\alpha_2^n \mathrm{L}_s^{2n-m})\,, \tag{1.2}$$

where α_2 is the SU(2) coupling. Electroweak (EW) perturbation theory, therefore, becomes badly convergent at large partonic energies. However, the convergence can be improved by identifying the double-logarithmic terms and resumming them to all orders.

Much effort has been put into understanding the electroweak logarithms arising from virtual corrections [5, 6, 19–32, 34, 40, 41]. A general result for the logarithmic dependence at one-loop has been derived in [21, 22], and a general method for the resummation of these logarithms has been developed in [32, 34]. This method uses SCET which has been developed in [42–45]. While real radiation of electroweak gauge bosons typically leads to different experimental signatures, in many cases some amount of real radiation is included in the event samples. For example, in many analyses missing energy is not vetoed, such that radiation of Z bosons which decay to neutrinos is included, and any analysis that is inclusive over the number of jets includes real radiation of hadronically decaying vector bosons.

Logarithmic dependence from real emission, however, has, before we start working on it, been studied much less. The $\mathcal{O}(\alpha)$ correction from real emission can of course easily be included using phase space integrations over tree-level matrix elements, and a study of the effect of such real radiation on many experimental observables was performed in [46]. It was

[1] The other extreme case where the observable is completely exclusive over the extra electroweak radiation has been studied many times before [4, 5, 19–39].

found that the real corrections can have a sizable effect, albeit typically not quite as large as the virtual corrections. The effects of real radiation have recently been studied in [47,48].

In Chap. 2 [49], we present the impact of electroweak correction resummation on the Drell-Yan cross-section. This motivate the inclusion of the resummation in fully differentiable calculations for an arbitrary number of radiated electroweak bosons. In Chap. 3 [18], we implement the differentiable electroweak correction resummation of initial state by including the electroweak interaction in the parton distribution functions evolution. This procedure approximates the electroweak bosons mass to be zero which misses important terms included in fixed order electroweak corrections, this is why in Chap. 4 [50] we developped a procedure to combine those calculations.

1.1 Running couplings

The one-loop running of the gauge couplings α_I $(I = 1, 2, 3)$ is given by

$$\frac{2\pi}{\alpha_I(q_2)} = \frac{2\pi}{\alpha_I(q_1)} + \beta_I \ln \frac{q_2}{q_1}\,, \tag{1.3}$$

where, for n_g generations and n_H Higgs doublets,

$$\beta_1 = -\frac{1}{3}\rho_1 = -\frac{20}{9}n_g - \frac{1}{6}n_H = -\frac{41}{6}, \tag{1.4}$$

$$\beta_2 = \frac{2}{3}\left(11 - \rho_{V2}\right) = \frac{22}{3} - \frac{4}{3}n_g - \frac{1}{6}n_H = \frac{19}{6}, \tag{1.5}$$

$$\beta_3 = 11 - \rho_3 = 11 - \frac{4}{3}n_g = 7\,. \tag{1.6}$$

At scale $M_Z = 91.2$ GeV we take

$$\sin^2\theta_W = \frac{\alpha_1}{\alpha_1 + \alpha_2} = 0.23\,, \quad \alpha = \alpha_2 \sin^2\theta_W = \frac{1}{128}\,, \quad \alpha_3 = 0.118\,, \tag{1.7}$$

which gives

$$\alpha_1(M_Z) = 0.0101 \quad \alpha_2(M_Z) = 0.0340 \quad \alpha_3(M_Z) = 0.118\,. \tag{1.8}$$

We set all Yukawa couplings to zero, except for the top Yukawa coupling $\alpha_Y = y_t^2/4\pi$. Its running receives significant Yukawa and QCD contributions:

$$q\frac{\partial \alpha_Y}{\partial q} = \frac{\alpha_Y}{2\pi}\left(\beta_Y \alpha_Y - \beta_S \alpha_3\right)\,, \tag{1.9}$$

where $\beta_Y = 9/2$ and $\beta_S = 8$. The solution is

$$\frac{1}{\alpha_Y(q_2)} = \frac{\delta}{\alpha_3(q_2)} - \left[\frac{\delta}{\alpha_3(q_1)} - \frac{1}{\alpha_Y(q_1)}\right]\left[\frac{\alpha_3(q_1)}{\alpha_3(q_2)}\right]^{\gamma}\,, \tag{1.10}$$

where

$$\gamma = \frac{\beta_S}{\beta_3} = \frac{24}{33 - 4n_g} = \frac{8}{7}\,, \tag{1.11}$$

$$\delta = \frac{\beta_Y}{\beta_S - \beta_3} = \frac{27}{8n_g - 18} = \frac{9}{2}\,. \tag{1.12}$$

We take $m_t(m_t) = 163$ GeV, which implies $\alpha_Y(m_t) = 0.0349$, and $\alpha_3(m_t) = 0.109$.

We also define

$$s_W(q) = \sqrt{\frac{\alpha_1(q)}{\alpha_1(q) + \alpha_2(q)}}$$

$$c_W(q) = \sqrt{\frac{\alpha_2(q)}{\alpha_1(q) + \alpha_2(q)}}\,, \tag{1.13}$$

and

$$\alpha_W(q) = \alpha_2(q)\,, \qquad \alpha_Z(q) = \frac{\alpha_2(q)}{c_W(q)}\,, \qquad \alpha_{em} = \frac{\alpha_2(q)}{s_W(q)}\,. \tag{1.14}$$

Chapter 2

Resummation of electroweak Sudakov logarithms for real radiation

We consider the Drell-Yan cross sections $\sigma_{pp\to\ell_1\ell_2}$ and $\sigma_{pp\to\ell_1\ell_2 V}$. Here ℓ denotes either an electron, positron or a neutrino, and V denotes either a Z, a photon or a W boson. For Drell-Yan production at NLO accuracy, the first cross section includes the tree-level and the one-loop virtual correction, while the second cross section denotes the real radiation of a gauge boson. Collectively, we will represent these two cross sections as $\sigma_{pp\to\ell_1\ell_2 X}$.

To calculate this hadronic scattering cross-sections one starts as always by factorizing the short distance partonic scattering from the non-perturbative physics describing the binding of partons into hadrons

$$\sigma_{pp\to\text{final}} = \sum_{ab} \int \mathrm{d}x_a \mathrm{d}x_b \, f_a(x_a, \sqrt{s}) f_b(x_b, \sqrt{s}) \, \hat{\sigma}_{ab\to\text{final}}(x_a, x_b, s) \,, \tag{2.1}$$

where $f_i(x_i)$ are the parton distribution functions to find parton i in the proton p with momentum fraction x_i, and $\hat{\sigma}_{ab\to\text{final}}(x_a, x_b)$ denotes the partonic scattering cross-section. By Lorentz invariance, the dependence of the partonic cross-sections on the momentum fractions x_i is only through the product $s = x_a x_b S$, where S is the square of the hadronic energy scale, and not through the rapidity $Y = \ln(x_a/x_b)/2$. Thus, one can write

$$\frac{\mathrm{d}\sigma_{pp\to\text{final}}}{\mathrm{d}s} = \sum_{ab} \mathcal{L}_{ab}(s) \, \hat{\sigma}_{ab\to\text{final}}(s) \,, \tag{2.2}$$

where the parton luminosity is defined as

$$\mathcal{L}_{ab}(s) = \int \mathrm{d}x_a \mathrm{d}x_b \, f_a(x_a, \sqrt{s}) f_b(x_b, \sqrt{s}) \, \delta(s - x_a x_b S) \,. \tag{2.3}$$

It is the purpose of this chapter to derive simple analytical expressions for the resummation of electroweak Sudakov logaritms at leading logarithmic (LL) accuracy. To achieve this, we combine knowledge of the resummation of the virtual corrections, together with the

known IR structure of real radiation from parton showers. This allows us to obtain simple analytical results which we present here. This approach is similar to the one used in [19], where these effects were discussed focussing on e^+e^- collider. We then use these results to give expressions for the individual contributions to the hadronic cross-sections $\sigma_{pp\to\ell_1\ell_2X}$ as a function of the center of mass energy $\sqrt{s}$. We reproduce the well known fact that resummation has a large effect on the virtual contribution for $\sqrt{s} \gtrsim 2$ TeV. The resummation of the real corrections changes the fixed order results by more than 40% for $\sqrt{s} \gtrsim 2$ TeV, and this effect grows to about 200% for $\sqrt{s} \sim 25$ TeV.

2.1 The structure of logarithmic terms in the perturbative expansion

To first order in electroweak perturbation theory the partonic scattering cross-section can be written as

$$\hat{\sigma}_{ij\to\ell_1\ell_2X} = \hat{\sigma}^{(0)}_{ij\to\ell_1\ell_2} + \hat{\sigma}^{(1)}_{ij\to\ell_1\ell_2X}\,, \tag{2.4}$$

where $\hat{\sigma}^{(0)}_{ij\to\ell_1\ell_2}$ denotes the Born cross-section, and $\hat{\sigma}^{(1)}_{ij\to\ell_1\ell_2X}$ the $\mathcal{O}(\alpha)$ correction. This first order perturbative correction can be decomposed into a virtual and real contribution, and each of these two terms can be further separated by the flavor of the vector boson in the loop or real final state. This gives

$$\hat{\sigma}^{(1)}_{ij\to\ell_1\ell_2X} = \sum_V \left[\hat{\sigma}^V_{ij\to\ell_1\ell_2} + \hat{\sigma}_{ij\to\ell_1\ell_2V}\right]\,. \tag{2.5}$$

Here the first term describes the contribution from one-loop diagrams with $V = \{Z, W^\pm, \gamma\}$ in the loop, while the second term is given by the real radiation of an electroweak gauge boson V.

Each of the terms on the right hand side of Eq. (2.5), contains double and single logarithmic terms of the form $\alpha\, L_V$ and $\alpha\, L_V^2$. By the KLN theorem [51], these logarithmically enhanced terms cancel when we sum over complete gauge multiplets. Thus, the completely inclusive cross-section has no logarithmically enhanced terms (called "finite" below)

$$\sum_{a,b,\ell_1,\ell_2} \hat{\sigma}^{(1)}_{ab\to\ell_1\ell_2X} = \text{finite}\,. \tag{2.6}$$

The sum of the initial state is over $a, b \in \{u, d\}$, that of the final state is over $\ell_1, \ell_2 \in \{e^+, e^-, \nu\}$, and we sum over the virtual contributions, and well as the real contributions with either a Z, a photon or W in the final state. Since the logarithmic enhancement depends on the mass of the vector boson, the logarithmic corrections from Z bosons, photons, and W bosons cancel separately between real and virtual corrections. Furthermore, since the

emission of a Z boson or a photon does not change the flavor of a fermion, the cancellation of the terms enhanced by L_Z happens for each flavor assignment separately. This gives

$$\hat{\sigma}^{Z}_{ab\to\ell_1\ell_2} + \hat{\sigma}_{ab\to\ell_1\ell_2 Z} = \text{finite}\,, \qquad \hat{\sigma}^{\gamma}_{ab\to\ell_1\ell_2} + \hat{\sigma}_{ab\to\ell_1\ell_2\gamma} = \text{finite}\,. \tag{2.7}$$

The emission of W bosons, on the other hand, changes the flavor of the fermion. This implies that the cancellation of the terms enhance by L_W only happens after summing over all flavors

$$\sum_{a,b,\ell_1,\ell_2} \left[\hat{\sigma}^{W}_{ab\to\ell_1\ell_2} + \hat{\sigma}_{ab\to\ell_1\ell_2 W}\right] = \text{finite}\,. \tag{2.8}$$

An important consequence of Eq. (2.8) is that a finite answer is only obtained if one sums over all initial state flavors. Thus, the hadronic cross-section given in Eq. (2.2) still contains contributions enhanced logarithmically by factors of L_W. This is because each initial state flavor is multiplied by a different parton luminosity, such that the sum over initial state flavors cannot be observed.

2.2 Fixed order calculations of the virtual and real contributions

In this section we consider the fixed order expansion of the virtual corrections $\hat{\sigma}^{V}_{ab\to\ell_1\ell_2}$ and the real contributions $\hat{\sigma}_{ab\to\ell_1\ell_2 V}$. For both terms, we quote here only the dominant contributions that are enhanced by two powers of L_V.

For completeness, we start with the Born cross-sections, including the contributions from both photon and Z exchange for the neutral initial and final states, and from W exchange in the charged cases. They are given by

$$\begin{aligned}
\hat{\sigma}^{B}_{u\bar{u}\to e^-e^+} &= N\,\frac{85\alpha_1^2 + 6\alpha_1\alpha_2 + 9\alpha_2^2}{54} \\
\hat{\sigma}^{B}_{u\bar{u}\to \nu\bar{\nu}} &= N\,\frac{17\alpha_1^2 - 6\alpha_1\alpha_2 + 9\alpha_2^2}{54} \\
\hat{\sigma}^{B}_{d\bar{d}\to e^-e^+} &= N\,\frac{25\alpha_1^2 - 6\alpha_1\alpha_2 + 9\alpha_2^2}{54} \\
\hat{\sigma}^{B}_{d\bar{d}\to \nu\bar{\nu}} &= N\,\frac{5\alpha_1^2 + 6\alpha_1\alpha_2 + 9\alpha_2^2}{54} \\
\hat{\sigma}^{B}_{u\bar{d}\to \nu e^+} &= N\,\frac{2\alpha_2^2}{3} \\
\hat{\sigma}^{B}_{d\bar{u}\to e^-\nu} &= N\,\frac{2\alpha_2^2}{3}\,,
\end{aligned} \tag{2.9}$$

where we have defined the constant

$$N = \frac{\pi}{8N_C s}\,, \tag{2.10}$$

with $N_C = 3$ denoting the number of colors. All coupling constant are evaluated at the scale $\sqrt{s}$, the center of mass energy, $\alpha_i = \alpha_i(\sqrt{s})$.

The virtual corrections from W exchange that are enhanced by two powers of the logarithm are easily obtained for example using [21] and are given by

$$\begin{aligned}
\hat{\sigma}^{W^\pm}_{u\bar{u}\to e^-e^+} &= -N\,\frac{\alpha_W\,L_W^2}{4\pi}\,\frac{11\alpha_1^2+6\alpha_1\alpha_2+9\alpha_2^2}{27}\\
\hat{\sigma}^{W^\pm}_{u\bar{u}\to \nu\bar{\nu}} &= -N\,\frac{\alpha_W\,L_W^2}{4\pi}\,\frac{3\alpha_1^2-2\alpha_1\alpha_2+3\alpha_2^2}{9}\\
\hat{\sigma}^{W^\pm}_{d\bar{d}\to e^-e^+} &= -N\,\frac{\alpha_W\,L_W^2}{4\pi}\,\frac{5\alpha_1^2-6\alpha_1\alpha_2+9\alpha_2^2}{27}\\
\hat{\sigma}^{W^\pm}_{d\bar{d}\to \nu\bar{\nu}} &= -N\,\frac{\alpha_W\,L_W^2}{4\pi}\,\frac{\alpha_1^2+2\alpha_1\alpha_2+3\alpha_2^2}{9}\\
\hat{\sigma}^{W^\pm}_{u\bar{d}\to \nu e^+} &= -N\,\frac{\alpha_W\,L_W^2}{4\pi}\,\frac{4\alpha_2^2}{3}\\
\hat{\sigma}^{W^\pm}_{d\bar{u}\to e^-\nu} &= -N\,\frac{\alpha_W\,L_W^2}{4\pi}\,\frac{4\alpha_2^2}{3}\,.
\end{aligned} \tag{2.11}$$

Those from Z exchange are given by

$$\begin{aligned}
\hat{\sigma}^{Z}_{u\bar{u}\to e^-e^+} &= -N\,\frac{\alpha_Z\,L_Z^2}{4\pi}\,\frac{(99-366s_W^2+2210s_W^4)\alpha_1^2+(9-30s_W^2+26s_W^4)\,(6\alpha_1\alpha_2+9\alpha_2^2)}{486}\\
\hat{\sigma}^{Z}_{u\bar{u}\to \nu\bar{\nu}} &= -N\,\frac{\alpha_Z\,L_Z^2}{4\pi}\,\frac{(81-12s_W^2+136s_W^4)\alpha_1^2+(9-12s_W^2+8s_W^4)\,(-6\alpha_1\alpha_2+9\alpha_2^2)}{486}\\
\hat{\sigma}^{Z}_{d\bar{d}\to e^-e^+} &= -N\,\frac{\alpha_Z\,L_Z^2}{4\pi}\,\frac{5(9-24s_W^2+100s_W^4)\alpha_1^2+(9-24s_W^2+20s_W^4)\,(-6\alpha_1\alpha_2+9\alpha_2^2)}{486}\\
\hat{\sigma}^{Z}_{d\bar{d}\to \nu\bar{\nu}} &= -N\,\frac{\alpha_Z\,L_Z^2}{4\pi}\,\frac{(27-6s_W^2+10s_W^4)\alpha_1^2+(9-6s_W^2+2s_W^4)\,(6\alpha_1\alpha_2+9\alpha_2^2)}{486}\\
\hat{\sigma}^{Z}_{u\bar{d}\to \nu e^+} &= -N\,\frac{\alpha_Z\,L_Z^2}{4\pi}\,\frac{2(9-18s_W^2+14s_W^4)\alpha_2^2}{27}\\
\hat{\sigma}^{Z}_{d\bar{u}\to e^-\nu} &= -N\,\frac{\alpha_Z\,L_Z^2}{4\pi}\,\frac{2(9-18s_W^2+14s_W^4)\alpha_2^2}{27}\,.
\end{aligned} \tag{2.12}$$

The virtual corrections from photon exchange that are enhanced by two powers of the loga-

rithm are easily obtained and are given by

$$\begin{aligned}
\hat{\sigma}^{\gamma}_{u\bar{u}\to e^-e^+} &= -N\,\frac{\alpha_{em}\,L_\gamma^2}{4\pi}\,\frac{85\alpha_1^2+6\alpha_1\alpha_2+9\alpha_2^2}{54}\,\frac{26}{9}\\
\hat{\sigma}^{\gamma}_{u\bar{u}\to \nu\bar{\nu}} &= -N\,\frac{\alpha_{em}\,L_\gamma^2}{4\pi}\,\frac{17\alpha_1^2-6\alpha_1\alpha_2+9\alpha_2^2}{54}\,\frac{8}{9}\\
\hat{\sigma}^{\gamma}_{d\bar{d}\to e^-e^+} &= -N\,\frac{\alpha_{em}\,L_\gamma^2}{4\pi}\,\frac{25\alpha_1^2-6\alpha_1\alpha_2+9\alpha_2^2}{54}\,\frac{20}{9}\\
\hat{\sigma}^{\gamma}_{d\bar{d}\to \nu\bar{\nu}} &= -N\,\frac{\alpha_{em}\,L_\gamma^2}{4\pi}\,\frac{5\alpha_1^2-6\alpha_1\alpha_2+9\alpha_2^2}{54}\,\frac{2}{9}\\
\hat{\sigma}^{\gamma}_{u\bar{d}\to \nu e^+} &= -N\,\frac{\alpha_{em}\,L_\gamma^2}{4\pi}\,\frac{2\alpha_2^2}{3}\,\frac{14}{9}\\
\hat{\sigma}^{\gamma}_{d\bar{u}\to e^-\nu} &= -N\,\frac{\alpha_{em}\,L_\gamma^2}{4\pi}\,\frac{2\alpha_2^2}{3}\,\frac{14}{9}\,,
\end{aligned} \tag{2.13}$$

where the logarithms depend on a scale Λ, below which a photon is no longer resolved,

$$L_\gamma \equiv \ln\left(\frac{\Lambda^2}{s}\right)\,. \tag{2.14}$$

The double-logarithmically enhanced real corrections with a Z boson or a photon in the final state are related to the corresponding virtual corrections via

$$\hat{\sigma}_{q_1\bar{q}_2\to\ell_1\ell_2 Z} = -\hat{\sigma}^{Z}_{q_1\bar{q}_2\to\ell_1\ell_2}\,, \tag{2.15}$$

$$\hat{\sigma}_{q_1\bar{q}_2\to\ell_1\ell_2\gamma} = -\hat{\sigma}^{\gamma}_{q_1\bar{q}_2\to\ell_1\ell_2}\,, \tag{2.16}$$

which directly follow from Eq. (2.7), for those with a W^+ boson in the final state we find

$$\begin{aligned}
\hat{\sigma}_{u\bar{d}\to e^-e^+W^+} &= N\,\frac{\alpha_W\,L_W^2}{4\pi}\,\frac{5\alpha_1^2+27\alpha_2^2}{54}\\
\hat{\sigma}_{u\bar{d}\to \nu\bar{\nu}W^+} &= N\,\frac{\alpha_W\,L_W^2}{4\pi}\,\frac{\alpha_1^2+27\alpha_2^2}{54}\\
\hat{\sigma}_{u\bar{u}\to e^-\bar{\nu}W^+} &= N\,\frac{\alpha_W\,L_W^2}{4\pi}\,\frac{17\alpha_1^2+27\alpha_2^2}{54}\\
\hat{\sigma}_{d\bar{d}\to e^-\bar{\nu}W^+} &= N\,\frac{\alpha_W\,L_W^2}{4\pi}\,\frac{5\alpha_1^2+27\alpha_2^2}{54}\,,
\end{aligned} \tag{2.17}$$

while those with a W^- are given by

$$\begin{aligned}
\hat{\sigma}_{d\bar{u}\to e^- e^+ W^-} &= N\,\frac{\alpha_W\,L_W^2}{4\pi}\,\frac{5\alpha_1^2+27\alpha_2^2}{54}\\
\hat{\sigma}_{d\bar{u}\to \nu\bar{\nu} W^-} &= N\,\frac{\alpha_W\,L_W^2}{4\pi}\,\frac{\alpha_1^2+27\alpha_2^2}{54}\\
\hat{\sigma}_{u\bar{u}\to \nu e^+ W^-} &= N\,\frac{\alpha_W\,L_W^2}{4\pi}\,\frac{17\alpha_1^2+27\alpha_2^2}{54}\\
\hat{\sigma}_{d\bar{d}\to \nu e^+ W^-} &= N\,\frac{\alpha_W\,L_W^2}{4\pi}\,\frac{5\alpha_1^2+27\alpha_2^2}{54}\,.
\end{aligned} \tag{2.18}$$

From these results one can obtain the inclusive cross-sections, which have been summed over all final state flavors

$$\begin{aligned}
\hat{\sigma}_{u\bar{u}} &= -N\,\frac{\alpha_W\,L_W^2}{4\pi}\,\frac{\alpha_1^2-3\alpha_2^2}{9}\\
\hat{\sigma}_{d\bar{d}} &= -N\,\frac{\alpha_W\,L_W^2}{4\pi}\,\frac{\alpha_1^2-3\alpha_2^2}{9}\\
\hat{\sigma}_{u\bar{d}} &= N\,\frac{\alpha_W\,L_W^2}{4\pi}\,\frac{\alpha_1^2-3\alpha_2^2}{9}\\
\hat{\sigma}_{d\bar{u}} &= N\,\frac{\alpha_W\,L_W^2}{4\pi}\,\frac{\alpha_1^2-3\alpha_2^2}{9}\,.
\end{aligned} \tag{2.19}$$

From these expressions one can very easily validate that in $\sum_{ab}\hat{\sigma}_{ab}$ all double logarithms cancel.

2.3 LL resummation of the leading logarithms

Virtual corrections

To resum the electroweak Sudakov logarithms for for the virtual contributions we follow the work of [34, 37], which uses renormalization group equations in SCET. The calculation proceeds in three steps. At the scale $\mu_Q^2 \sim s$, one matches the full theory onto 4-fermion operators in SCET, where each of the fermion is represented by a different collinear sector in SCET. One then runs the theory from the scale μ_Q to the scale $\mu_V \sim m_V$, at which point the massive gauge bosons are integrated out of the theory and electroweak symmetry is broken. As long as $s \gg m_V^2$, the mass of the vector boson can be set to zero in the matching onto SCET at the scale μ_Q, and in the calculation of the anomalous dimension which governs the running from μ_Q to μ_V. This implies that one can use an unbroken SU(2), simplifying these calculations substantially.

In [34, 37], this resummation was carried out in full generality to NLL′ accuracy. For the purposes of this work, we only work to LL accuracy, which simplifies the structure significantly. The first simplification is that only tree level matching is required both at the

high and low scale. Furthermore, no operator mixing arises in the running from the high to the low scale. This will allow us to write relatively simple analytical formulae.

As already mentioned, in the effective theory between μ_Q and μ_V one can use unbroken electroweak symmetry, such that there are a total of 7 operator that contribute

$$\begin{aligned}\mathcal{L} =& C_{QLT}\, Q^T L^T + C_{QLS}\, Q^S L^S + C_{ULS}\, U^S L^S + C_{DLS}\, D^S L^S \\ &+ C_{QES} Q^S E^S + C_{UES}\, U^S E^S + C_{DES}\, D^S E^S\,,\end{aligned} \tag{2.20}$$

where we have defined the fermion bilinears in either triplet or singlet representation

$$F^S = \bar{F}\gamma^\mu F\,, \qquad F^T = \bar{F}\tau^a\gamma^\mu F\,. \tag{2.21}$$

Here Q and L denote left-handed quark and lepton fields, respectively, while U, D and E denote the right handed up-type quarks, down-type quarks and electron fields. The tree level matching is given by

$$\begin{aligned} s\, C^{(0)}_{QLT} &= 4\pi\alpha_2 \\ s\, C^{(0)}_{IFS} &= 4\pi\alpha_1\, Y_I Y_F\,, \end{aligned} \tag{2.22}$$

where I and F denote the initial and final fermions of each singlet operator, and Y_i is the hypercharge of particle i. The hypercharge normalization used is

$$Y_i = Q_i - T^3_i\,, \tag{2.23}$$

where Q_i is the electromagnetic charge of the fermion $f = q/\ell$ and T^3_i is the weak isospin.

In general, the renormalization group can mix these operators, however this mixing only arises starting at NLL. Since we are only interested in LL accuracy we can write

$$\mu\frac{\mathrm{d}}{\mathrm{d}\mu}O_i(\mu) = \Gamma_i(\mu)\ln\frac{\mu^2}{s}O_i(\mu)\,, \tag{2.24}$$

where the cusp anomalous dimension is

$$\Gamma_i(\mu) = \sum_j \left[\frac{\alpha_1(\mu)}{2\pi}Y_j^2 + \frac{\alpha_2(\mu)}{2\pi}T_j^2\right]_i\,. \tag{2.25}$$

Here $[T_j]^2_i$ is the SU(2) Casimir of the j'th fermion (3/4 for left-handed fermions and 0 for right-handed fermions) in O_i.

The solution to this RGE can easily be written down analytically, and one finds for the Wilson coefficients at the low scale

$$C_i(\mu_V) = U_i^{LL}(\mu_V, \mu_Q)C_i(\mu_Q)\,. \tag{2.26}$$

Working in the limit $\alpha_i \ln m_V^2/s \sim 1$, one obtains the simple result

$$U_i^{LL}(\mu_V, \mu_Q; s) = \frac{\exp\left[-\Gamma_i(\sqrt{s}) \ln^2 \frac{\mu_V}{\sqrt{s}}\right]}{\exp\left[-\Gamma_i(\sqrt{s}) \ln^2 \frac{\mu_Q}{\sqrt{s}}\right]} . \tag{2.27}$$

For $\mu_Q = \sqrt{s}$ and $\mu_V = m_V$ this result simplifies to

$$U_i \equiv U_i^{LL}(m_V, \sqrt{s}; s) = \exp\left[-\Gamma_i(\sqrt{s}) \ln^2 \frac{m_V}{\sqrt{s}}\right] . \tag{2.28}$$

Note that the anomalous dimension and therefore the evolution Kernel only depends on the type of initial and final state particles. Thus, we have

$$U_{IFS} = U_{IFT} \equiv U_{IF} . \tag{2.29}$$

The SU(2) $\otimes$ U(1) gauge structure is broken at $\mu_V = m_V$ to the $\mathrm{U(1)_{em}}$, and below that scale only the photon remains as gauge degree of freedom. Thus, below the scale m_V one continues to run to a scale μ_Λ, at which point the photon becomes unresolved. This running is determined by the cusp anomalous dimension

$$\Gamma^{\mathrm{em}}(\mu) = \frac{\alpha_{\mathrm{em}}(\mu)}{2\pi} Q_{\mathrm{tot}}^2 , \tag{2.30}$$

where

$$Q_{\mathrm{tot}}^2 \equiv \sum_i Q_i^2 \tag{2.31}$$

is the sum of the square of the electromagnetic charges of all particles in the operator. The evolution Kernel between μ_V and μ_Λ is

$$U_{Q_{\mathrm{tot}}^2}^{\mathrm{em}}(\mu_\Lambda, \mu_V; s) = \frac{\exp\left[-\frac{\alpha_{\mathrm{em}}}{2\pi} Q_{\mathrm{tot}}^2 \ln^2 \frac{\mu_\Lambda}{\sqrt{s}}\right]}{\exp\left[-\frac{\alpha_{\mathrm{em}}}{2\pi} Q_{\mathrm{tot}}^2 \ln^2 \frac{\mu_V}{\sqrt{s}}\right]} . \tag{2.32}$$

We obtain the simple results for the resummed virtual corrections,

$$\begin{aligned}
\hat{\sigma}^{\rm LL}_{u\bar{u}\to e^-e^+} &= N\,\frac{4\left(4\,U_{UL}^2+U_{QE}^2+16\,U_{UE}^2\right)\alpha_1^2+U_{QL}^2\left(\alpha_1+3\alpha_2\right)^2}{54}\,\left[U^{\rm em}_{26/9}\left(\Lambda,m_V;s\right)\right]^2\\
\hat{\sigma}^{\rm LL}_{u\bar{u}\to \nu\bar{\nu}} &= N\,\frac{16\,U_{UL}^2\alpha_1^2+U_{QL}^2\left(\alpha_1-3\alpha_2\right)^2}{54}\,\left[U^{\rm em}_{8/9}\left(\Lambda,m_V;s\right)\right]^2\\
\hat{\sigma}^{\rm LL}_{d\bar{d}\to e^-e^+} &= N\,\frac{4\left(U_{DL}^2+U_{QE}^2+4\,U_{DE}^2\right)\alpha_1^2+U_{QL}^2\left(\alpha_1-3\alpha_2\right)^2}{54}\,\left[U^{\rm em}_{20/9}\left(\Lambda,m_V;s\right)\right]^2\\
\hat{\sigma}^{\rm LL}_{d\bar{d}\to \nu\bar{\nu}} &= N\,\frac{4\,U_{DL}^2\alpha_1^2+U_{QL}^2\left(\alpha_1+3\alpha_2\right)^2}{54}\,\left[U^{\rm em}_{2/9}\left(\Lambda,m_V;s\right)\right]^2\\
\hat{\sigma}^{\rm LL}_{u\bar{d}\to \nu e^+} &= N\,\frac{2\,U_{QL}^2\alpha_2^2}{3}\,\left[U^{\rm em}_{14/9}\left(\Lambda,m_V;s\right)\right]^2\\
\hat{\sigma}^{\rm LL}_{d\bar{u}\to e^-\nu} &= N\,\frac{2\,U_{QL}^2\alpha_2^2}{3}\,\left[U^{\rm em}_{14/9}\left(\Lambda,m_V;s\right)\right]^2\,.
\end{aligned}\tag{2.33}$$

Note that since $\alpha_1/\alpha_2=\tan^2(\theta_W)\sim 0.32$, the term proportional to α_1^2 (which depends on various different evolution Kernels) is numerically suppressed compared to the term proportional to $(\alpha_1\pm 3\alpha_2)^2$. Thus, to a good approximation, each leptonic final state gets the same suppression factor U_{QL} from the resummation.

A simple check of our results is that they reproduce the Born results given in Eq. (2.9) if we set all resummation Kernels to unity, and that they reproduce the fixed order results in Eqs.(2.11), (2.12), and (2.13) if we use the expansion $U_i^2=1-2\Gamma_i\ln^2\frac{m_V}{\sqrt{s}}+\ldots$ and $\left[U^{\rm em}_{Q^2_{\rm tot}}\left(\Lambda,m_V;s\right)\right]^2=1+\frac{\alpha_{\rm em}(\mu)}{\pi}Q^2_{tot}\left(\ln^2\frac{m_V}{\sqrt{s}}-\ln^2\frac{\Lambda}{\sqrt{s}}\right)+\ldots$.

Real corrections

In this section we will calculate the resummation of the real emissions. We first give the results for the case of a single SU(2) gauge symmetry, and then extend the results to the case of the broken SU(2) $\otimes$ U(1) of the standard model.

Simple SU(2)

For a single SU(2) symmetry, the virtual results can be obtained from Eq. (2.33) by setting $\alpha_1=\alpha_{\rm em}=0$. It will be useful to rewrite them in a slightly different form, separating the contributions from the different helicities

$$\hat{\sigma}^{\rm LL}_{q_1^Hq_2^H\to\ell_1^H\ell_2^H}=\hat{\sigma}^{B}_{q_1^Hq_2^H\to\ell_1^H\ell_2^H}\Delta^{\rm SU(2)}_{q_1^Hq_2^H\ell_1^H\ell_2^H}(m_V^2,s;s)\,.\tag{2.34}$$

The resummed logarithms are now contained in the factor $\Delta^{\rm SU(2)}_{q_1^Hq_2^H\ell_1^H\ell_2^H}(m_V^2,s;s)$. The superscript H denotes that each fermion has a fixed helicity. The Born cross-sections are given

by

$$\hat{\sigma}^{B}_{q^H q^H \to \ell^H \ell^H} = N \frac{8\,\alpha_2^2 \left(T^3_{q^H} T^3_{\ell^H} \right)^2}{3}$$
$$\hat{\sigma}^{B}_{q_1^L q_2^L \to \ell_1^L \ell_2^L} = N \frac{2\alpha_2^2}{3}\,, \tag{2.35}$$

where $T^3_{q^H}$ denotes the weak isospin of the fermion q/ℓ with helicity H. The factor $\Delta^{\mathrm{SU}(2)}$resums the leading logarithms and is given by

$$\Delta^{\mathrm{SU}(2)}_{q_1^H q_2^H \ell_1^H \ell_2^H}(m_V^2, s; s) = \exp\left[-\frac{A^{\mathrm{SU}(2)}_{q_1^H q_1^H \ell_1^H \ell_2^H}}{2} \ln^2 \frac{m_V^2}{s} \right]\,, \tag{2.36}$$

where

$$A^{\mathrm{SU}(2)}_{q_1^H q_1^H \ell_1^H \ell_2^H} = \frac{\alpha_2}{2\pi} \sum_i T_i^2\,, \tag{2.37}$$

and the sum over i runs over all particles $i \in \{q_1^H, q_1^H, \ell_1^H, \ell_2^H\}$. Summing Eq. (2.34) over all possible helicity structures, we reproduce Eq. (2.33) in the limit $\alpha_1 = \alpha_{\mathrm{em}} = 0$.

By rewriting our result as in Eq. (2.34), one notices that it can be interpreted as the exclusive cross-section for the scattering process $q_1^H q_2^H \to \ell_1^H \ell_2^H$, where $\Delta^{\mathrm{SU}(2)}_{q_1^H q_2^H \ell_1^H \ell_2^H}(m^2, s; s)$ is a Sudakov factor describing the probability of not having an emission of electroweak gauge bosons between the scales s and m_V^2 for a process with center of mass energy s. Since of course the emission of a massive gauge boson always gives rise to a scale above m_V^2, this exclusive cross-section is by definition equal to the virtual result.

Eq. (2.34) is precisely the result that a parton shower would predict for the exclusive cross-section[1], and one can use insight from parton shower evolution to derive the expressions for real gauge boson radiation. The real emission of a gauge boson is given in a parton shower by the product of Altarelli-Parisi splitting functions, which describe the emission with a given transverse momentum k_T^2, multiplied by a Sudakov factor, which gives the no-branching probability above the value of k_T^2 as explained in [52]. Thus, the total inclusive real radiation cross-section (the cross section with one or more extra gauge bosons in the final state) is given by

$$\begin{aligned}\hat{\sigma}^{\mathrm{LL}}_{q_1^H q_2^H \to \ell_1^H \ell_2^H + nV} &= \hat{\sigma}^{B}_{q_1^H q_2^H \to \ell_1^H \ell_2^H} \int_{m_V^2}^{s} \mathrm{d}k_T^2 \, \frac{\mathrm{d}}{\mathrm{d}k_T^2} \Delta^{\mathrm{SU}(2)}_{q_1^H q_2^H \ell_1^H \ell_2^H}(k_T^2, s; s) \\ &= \hat{\sigma}^{B}_{q_1^H q_2^H \to \ell_1^H \ell_2^H} \left[1 - \Delta^{\mathrm{SU}(2)}_{q_1^H q_2^H \ell_1^H \ell_2^H}(m_V^2, s; s) \right]\,. \end{aligned} \tag{2.38}$$

[1]Note that our Sudakov factor for the initial state particles does not include the ratios of PDFs that usually arise in backward evolution. This ratio of PDFs only contributes to NLL.

Such an inclusive cross-section makes sense only if the measurement is not breaking the SU(2) symmetry. This is because the inclusive cross section is defined at a scale $\mu \sim k_T$, while the SU(2) symmetry is only broken at the scale $\mu \sim m_V$. This implies that the flavor structure one would obtain at the scale k_T can be changed by the further emissions of extra gauge bosons, making an inclusive measurement with definite flavor structure (which is what breaks the symmetry) ill defined.

Continuing to work in an unbroken SU(2) theory, one can also define the exclusive real radiation cross section (the cross section with exactly one extra gauge boson in the final state). This requires adding an extra no-branching probability from the scale k_T^2 to the scale m_V^2, which accounts for the fact that no extra gauge bosons are emitted from the fermions and the extra gauge boson with lower k_T^2. This extra factor is given by

$$\Delta^{\mathrm{SU}(2)}_{q_1^H q_2^H \ell_1^H \ell_2^H V}(m_V^2, k_T^2; s) \equiv \Delta_V(m_V^2, k_T^2; \hat{k}_T^2) \Delta^{\mathrm{SU}(2)}_{q_1^H q_2^H \ell_1^H \ell_2^H}(m_V^2, k_T^2; s)\,, \tag{2.39}$$

where the term Δ_V gives the probability of not emitting extra gauge bosons off the emitted vector boson

$$\Delta_V(m_V^2, k_T^2; k_T^2) = \exp\left[-\frac{\alpha_2\, C_A}{4\pi} \ln^2 \frac{m_V^2}{k_T^2}\right]\,, \tag{2.40}$$

while the second term describes the no-emissions probability below k_T off the fermions

$$\Delta^{\mathrm{SU}(2)}_{q_1^H q_2^H \ell_1^H \ell_2^H}(m_V^2, k_T^2; s) \equiv \frac{\Delta^{\mathrm{SU}(2)}_{q_1^H q_2^H \ell_1^H \ell_2^H}(m_V^2, s; s)}{\Delta^{\mathrm{SU}(2)}_{q_1^H q_2^H \ell_1^H \ell_2^H}(k_T^2, s; s)}\,. \tag{2.41}$$

Combining everything together, one therefore finds

$$\begin{aligned}
&\hat{\sigma}^{\mathrm{LL}}_{q_1^H q_2^H \to \ell_1^H \ell_2^H + V} \\
&\quad = \hat{\sigma}^B_{q_1^H q_2^H \to \ell_1^H \ell_2^H} \int_{m_V^2}^s \mathrm{d}k_T^2\, \frac{\mathrm{d}}{\mathrm{d}k_T^2} \left[\Delta^{\mathrm{SU}(2)}_{q_1^H q_2^H \ell_1^H \ell_2^H}(k_T^2, s; s)\right] \Delta^{\mathrm{SU}(2)}_{q_1^H q_2^H \ell_1^H \ell_2^H V}(m_V^2, k_T^2; s) \\
&\quad = \hat{\sigma}^B_{q_1^H q_2^H \to \ell_1^H \ell_2^H}\, A^{\mathrm{SU}(2)}_{q_1^H q_1^H \ell_1^H \ell_2^H}\, \Delta^{\mathrm{SU}(2)}_{q_1^H q_2^H \ell_1^H \ell_2^H}(m_V^2, s; s) \int_{m_V^2}^s \frac{\mathrm{d}k_T^2}{k_T^2} \ln \frac{s}{k_T^2} \Delta_V(m_V^2, k_T^2; k_T^2)\,.
\end{aligned} \tag{2.42}$$

The integral can be performed easily, and we write a general result

$$\begin{aligned}
I_\beta(m_V^2, s) &\equiv \int_{m_V^2}^s \frac{\mathrm{d}k_T^2}{k_T^2} \ln \frac{s}{k_T^2} \left[\Delta_V(m_V^2, k_T^2; k_T^2)\right]^\beta \\
&= \frac{2\pi}{\alpha_2\, \beta\, C_A} \left[\frac{\sqrt{\alpha_2\, \beta\, C_A}}{2} \ln \frac{m_V^2}{s}\, \mathrm{Erf}\left(\sqrt{\frac{\alpha_2\, \beta\, C_A}{4\pi}}\, \ln \frac{m_V^2}{s}\right) + \left[\Delta_V(m_V^2, s; s)\right]^\beta - 1\right]\,.
\end{aligned} \tag{2.43}$$

With this result, the exclusive cross section for a single emission is given by

$$\hat{\sigma}^{\mathrm{LL}}_{q_1^H q_2^H \to \ell_1^H \ell_2^H + V} = \hat{\sigma}^B_{q_1^H q_2^H \to \ell_1^H \ell_2^H}\, A^{\mathrm{SU}(2)}_{q_1^H q_1^H \ell_1^H \ell_2^H}\, \Delta^{\mathrm{SU}(2)}_{q_1^H q_2^H \ell_1^H \ell_2^H}(m_V^2, s; s)\, I_1(m_V^2, s)\,. \tag{2.44}$$

Full SU(2) $\otimes$ U(1)

We now extend the results obtained with a single SU(2) gauge symmetry to include the full SU(2) $\otimes$ U(1) gauge structure. The Born cross-section is now given by

$$\begin{aligned}\hat{\sigma}^B_{q^H q^H \to \ell^H \ell^H} &= N \, \frac{8 \left(\alpha_2 T^3_{q^H} T^3_{\ell^H} + \alpha_1 Y_{q^H} Y_{\ell^H} \right)^2}{3} \\ \hat{\sigma}^B_{q_1^L q_2^L \to \ell_1^L \ell_2^L} &= N \, \frac{2\alpha_2^2}{3} \,, \end{aligned} \tag{2.45}$$

where as before $T^3_{f^H}$ denotes the weak isospin of the fermion $f = q/\ell$ with helicity H and Y_{f^H} denotes the hypercharge of the fermion $f = q/\ell$ with helicity H. The hypercharge normalization used is given by Eq. (2.23).

We can write the LL cross section as the Born cross section times a Sudakov factor. However, contrary to the case of a single SU(2) symmetry, in the broken SU(2)$\otimes$U(1) symmetry of the standard model, below the scale $\mu = m_V$ one needs to continue to evolve the operators with the electromagnetic running. This gives

$$\hat{\sigma}^{\rm LL}_{q_1^H q_2^H \to \ell_1^H \ell_2^H} = \hat{\sigma}^B_{q_1^H q_2^H \to \ell_1^H \ell_2^H} \Delta_{q_1^H q_2^H \ell_1^H \ell_2^H}(m_V^2, s; s) \, \Delta^{\rm em}_{q_1^H q_2^H \ell_1^H \ell_2^H}(\Lambda^2, m_V^2; s) \,. \tag{2.46}$$

The Sudakov factor from s to m_V^2 factors into two pieces, one for the SU(2) symmetry and one for the U(1)

$$\Delta_{q_1^H q_2^H \ell_1^H \ell_2^H}(m_V^2, s; s) = \Delta^{\rm SU(2)}_{q_1^H q_2^H \ell_1^H \ell_2^H}(m_V^2, s; s) \, \Delta^{\rm U(1)}_{q_1^H q_2^H \ell_1^H \ell_2^H}(m_V^2, s; s) \,. \tag{2.47}$$

The SU(2) contribution was given in Eq. (2.36), while the term coming from the U(1) symmetry is given by

$$\Delta^{\rm U(1)}_{q_1^H q_2^H \ell_1^H \ell_2^H}(m_V^2, s; s)) = \exp \left[- \frac{A^{U(1)}_{q_1^H q_2^H \ell_1^H \ell_2^H}}{2} \ln^2 \frac{m_V^2}{s} \right] \,, \tag{2.48}$$

with

$$A^{\rm U(1)}_{q_1^H q_1^H \ell_1^H \ell_2^H} = \frac{\alpha_1}{2\pi} \sum_i Y_i^2 \,. \tag{2.49}$$

The running below m_V is determined only by the total charge of the operator, and one finds

$$\Delta^{\rm em}_{q_1^H q_2^H \ell_1^H \ell_2^H}(\Lambda^2, m_V^2; s) = \exp \left[- \frac{\alpha_{\rm em} Q^2_{\rm tot}}{4\pi} \left(\ln^2 \frac{\Lambda^2}{s} - \ln^2 \frac{m_V^2}{s} \right) \right] \,. \tag{2.50}$$

Summing over all possible helicity structures, we reproduce the resummed results of Sec. 2.3.

To obtain the resummation of the real radiation, we follow the steps of Sec. 2.3, taking into account the full SU(2)$\otimes$U(1) structure above m_V^2 and the running due to the photon

below m_V^2. For the $W^\pm$ bosons, the U(1) symmetry does not contribute, but one needs to be careful about the flavor structure when breaking the electroweak symmetry. One finds

$$\begin{aligned}
&\hat{\sigma}^{\mathrm{LL}}_{q_1^H q_2^H \to \ell_1^H \ell_2^H + W^\pm} \\
&\quad = \left[\Delta_{q_1^H q_2^H \ell_1^H \ell_2^H}(m_V^2, s; s)\, \Delta^{\mathrm{em}}_{q_1^H q_2^H \ell_1^H \ell_2^H W^\pm}(\Lambda^2, m_V^2; s) \int_{m_V^2}^{s} \frac{\mathrm{d}k_T^2}{k_T^2} \ln \frac{s}{k_T^2} \Delta_V(m_V^2, k_T^2; k_T^2) \right] \\
&\qquad \times \left(\hat{\sigma}^B_{q'^H_1 q_2^H \to \ell_1^H \ell_2^H} A^{W^\pm}_{q_1^H} + \hat{\sigma}^B_{q_1^H q'^H_2 \to \ell_1^H \ell_2^H} A^{W^\pm}_{q_2^H} + \hat{\sigma}^B_{q_1^H q_2^H \to \ell'^H_1 \ell_2^H} A^{W^\pm}_{\ell_1^H} + \hat{\sigma}^B_{q_1^H q_2^H \to \ell_1^H \ell'^H_2} A^{W^\pm}_{\ell_2^H} \right) \\
&\quad = \left[\Delta_{q_1^H q_2^H \ell_1^H \ell_2^H}(m_V^2, s; s)\, \Delta^{\mathrm{em}}_{q_1^H q_2^H \ell_1^H \ell_2^H W^\pm}(\Lambda^2, m_V^2; s)\, I_1(m_V^2, s) \right] \\
&\qquad \times \left(\hat{\sigma}^B_{q'^H_1 q_2^H \to \ell_1^H \ell_2^H} A^{W^\pm}_{q_1^H} + \hat{\sigma}^B_{q_1^H q'^H_2 \to \ell_1^H \ell_2^H} A^{W^\pm}_{q_2^H} + \hat{\sigma}^B_{q_1^H q_2^H \to \ell'^H_1 \ell_2^H} A^{W^\pm}_{\ell_1^H} + \hat{\sigma}^B_{q_1^H q_2^H \to \ell_1^H \ell'^H_2} A^{W^\pm}_{\ell_2^H} \right) ,
\end{aligned} \tag{2.51}$$

where f' is the fermion f becomes after having radiated a $W^\pm$ that is $u' = d$, $d' = u$, $l' = \nu$ and $\nu' = l$ and for any flavor set which allows a $W^\pm$ emission there is one of the Born cross section which is zero because its electromagnetic charge is not conserved. Also, we broke $A^{\mathrm{SU(2)}}_{q_1^H q_1^H \ell_1^H \ell_2^H}$ in its component related to the emission of a $W^\pm$, that is

$$A^{\mathrm{SU(2)}}_{q_1^H q_1^H \ell_1^H \ell_2^H} = A^{W^3}_{q_1^H q_1^H \ell_1^H \ell_2^H} + \sum_i A_i^{W^\pm} , \tag{2.52}$$

with

$$A^{W^\pm}_{f^L} = \frac{\alpha_2}{4\pi} , \qquad A^{W^\pm}_{f^R} = 0 , \qquad A^{W^3}_{q_1^H q_1^H \ell_1^H \ell_2^H} = \frac{\alpha_2}{2\pi} \sum_i (T_i^3)^2 . \tag{2.53}$$

For the emissions of Z bosons and photons, one needs to take into account the mixing between the third component of the SU(2) gauge symmetry and the U(1) gauge symmetry. The emission of a W^3 boson is given by

$$\begin{aligned}
\hat{\sigma}^{\mathrm{LL}}_{q_1^H q_2^H \to \ell_1^H \ell_2^H + W^3} = \hat{\sigma}^B_{q_1^H q_2^H \to \ell_1^H \ell_2^H} A^{\mathrm{W^3}}_{q_1^H q_1^H \ell_1^H \ell_2^H}\, \Delta_{q_1^H q_2^H \ell_1^H \ell_2^H}(m_V^2, s; s) \\
\times \Delta^{\mathrm{em}}_{q_1^H q_2^H \ell_1^H \ell_2^H}(\Lambda^2, m_V^2; s) \int \frac{\mathrm{d}k_T^2}{k_T^2} \ln \frac{s}{k_T^2} \Delta_V(m_V^2, k_T^2; k_T^2) ,
\end{aligned} \tag{2.54}$$

while for the emission of a U(1) boson B

$$\begin{aligned}
\hat{\sigma}^{\mathrm{LL}}_{q_1^H q_2^H \to \ell_1^H \ell_2^H + B} = \hat{\sigma}^B_{q_1^H q_2^H \to \ell_1^H \ell_2^H} A^{\mathrm{U(1)}}_{q_1^H q_1^H \ell_1^H \ell_2^H}\, \Delta_{q_1^H q_2^H \ell_1^H \ell_2^H}(m_V^2, s; s) \\
\times \Delta^{\mathrm{em}}_{q_1^H q_2^H \ell_1^H \ell_2^H}(\Lambda^2, m_V^2; s) \int \frac{\mathrm{d}k_T^2}{k_T^2} \ln \frac{s}{k_T^2} .
\end{aligned} \tag{2.55}$$

To combine these two expressions into the emission of a Z boson, we have to mix the amplitude of the emission of a W^3 with the amplitude of the emission of a B. Each individual

emission is given by breaking the coefficient $A^{W^3}_{q_1^H q_1^H \ell_1^H \ell_2^H}$ and $A^{\mathrm{U}(1)}_{q_1^H q_1^H \ell_1^H \ell_2^H}$ in their components for an emission from one fermion, and the amplitude is given by the square root of this emission. We mix the amplitudes using that

$$Z = s_W B - c_W W^3 \,, \tag{2.56}$$

where $c_W = \cos(\theta_W)$ and $s_W = \sin(\theta_W)$. This gives

$$\begin{aligned}\hat{\sigma}^{\mathrm{LL}}_{q_1^H q_2^H \to \ell_1^H \ell_2^H + Z} = \hat{\sigma}^{B}_{q_1^H q_2^H \to \ell_1^H \ell_2^H}\, \Delta_{q_1^H q_2^H \ell_1^H \ell_2^H}(m_V^2, s; s)\, \Delta^{\mathrm{em}}_{q_1^H q_2^H \ell_1^H \ell_2^H}(\Lambda^2, m_V^2; s) \\ \times \int_{m_V^2}^{s} \frac{\mathrm{d}k_T^2}{k_T^2} \ln \frac{s}{k_T^2} R_{q_1^H q_2^H \ell_1^H \ell_2^H}(m_V^2, k_T^2) \,,\end{aligned} \tag{2.57}$$

where we have defined

$$R_{q_1^H q_2^H \ell_1^H \ell_2^H}(m_V^2, k_T^2) = \alpha_W \sum_i \left(s_W \sqrt{\frac{A_i^{U(1)}}{\alpha_W}} - c_W \sqrt{\frac{A_i^{W^3}}{\alpha_W} \Delta_V(m_V^2, k_T^2; k_T^2)} \right)^2 \,, \tag{2.58}$$

with

$$A^{\mathrm{U}(1)}_{f^H} = \frac{\alpha_1}{2\pi} Y^2_{f^H} \,, \qquad A^{W^3}_{f^H} = \frac{\alpha_1}{2\pi} (T^3_{f^H})^2 \,. \tag{2.59}$$

By using the simple relations

$$\sqrt{\frac{A^{\mathrm{U}(1)}_{f^H}}{\alpha_W}} = \sqrt{\frac{1}{2\pi}} \frac{s_W}{c_W} Y_{f^H} \,, \qquad \sqrt{\frac{A^{W^3}_{f^H}}{\alpha_W}} = \sqrt{\frac{1}{2\pi}} T^3_{f^H} \,, \tag{2.60}$$

we obtain the final result for the Z boson emission cross section

$$\hat{\sigma}^{\mathrm{LL}}_{q_1^H q_2^H \to \ell_1^H \ell_2^H + Z} = \hat{\sigma}^{B}_{q_1^H q_2^H \to \ell_1^H \ell_2^H}\, \Delta_{q_1^H q_2^H \ell_1^H \ell_2^H}(m_V^2, s; s)\, \Delta^{\mathrm{em}}_{q_1^H q_2^H \ell_1^H \ell_2^H}(\Lambda^2, m_V^2; s) \tag{2.61}$$

$$\begin{aligned}&\times \int_{m_V^2}^{s} \frac{\mathrm{d}k_T^2}{k_T^2} \ln \frac{s}{k_T^2} \Bigg(s_W^2 A^{\mathrm{U}(1)}_{q_1^H q_2^H \ell_1^H \ell_2^H} - A^{\mathrm{mixing}}_{q_1^H q_2^H \ell_1^H \ell_2^H} \sqrt{\Delta_V(m_V^2, k_T^2; k_T^2)} \\ &\qquad + c_W^2 A^{W^3}_{q_1^H q_2^H \ell_1^H \ell_2^H} \Delta_V(m_V^2, k_T^2; k_T^2) \Bigg) \\ &= \hat{\sigma}^{B}_{q_1^H q_2^H \to \ell_1^H \ell_2^H}\, \Delta_{q_1^H q_2^H \ell_1^H \ell_2^H}(m_V^2, s; s)\, \Delta^{\mathrm{em}}_{q_1^H q_2^H \ell_1^H \ell_2^H}(\Lambda^2, m_V^2; s) \\ &\qquad \Bigg(s_W^2 A^{\mathrm{U}(1)}_{q_1^H q_2^H \ell_1^H \ell_2^H} \frac{1}{2} \ln^2 \frac{m_V^2}{s} \\ &\qquad - A^{\mathrm{mixing}}_{q_1^H q_2^H \ell_1^H \ell_2^H} I_{\frac{1}{2}}(m_V^2, s) + c_W^2 A^{W^3}_{q_1^H q_2^H \ell_1^H \ell_2^H} I_1(m_V^2, s) \Bigg) \,,\end{aligned} \tag{2.62}$$

where

$$A^{\text{mixing}}_{q_1^H q_2^H \ell_1^H \ell_2^H} = \frac{\alpha_{\text{em}}}{\pi} \sum_i T_i^3 Y_i \,. \tag{2.63}$$

For the emission of a photon, we use that, for a scale higher than the electroweak bosons masses, the photon is a mixing of the B and W^3 bosons.

$$\gamma = c_W B + s_W W^3 \,, \tag{2.64}$$

while, for a scale lower than the electroweak bosons masses, the photon can still be produced proportionally to the derivative of its no-branching probability $\Delta^{\text{em}}_{q_1^H q_2^H \ell_1^H \ell_2^H}(k_T^2, m_V^2; s)$.

$$\begin{aligned}
\hat{\sigma}^{\text{LL}}_{q_1^H q_2^H \to \ell_1^H \ell_2^H + \gamma} &= \hat{\sigma}^{B}_{q_1^H q_2^H \to \ell_1^H \ell_2^H}\, \Delta_{q_1^H q_2^H \ell_1^H \ell_2^H}(m_V^2, s; s) \\
&\quad \times \Bigg[\Delta^{\text{em}}_{q_1^H q_2^H \ell_1^H \ell_2^H}(\Lambda^2, m_V^2; s) \Bigg(c_W^2 A^{\text{U(1)}}_{q_1^H q_2^H \ell_1^H \ell_2^H} \frac{1}{2} \log^2(\frac{m_V^2}{s}) \\
&\qquad + A^{\text{mixing}}_{q_1^H q_2^H \ell_1^H \ell_2^H} I_{\frac{1}{2}}(m_V^2, s) + s_W^2 A^{W^3}_{q_1^H q_2^H \ell_1^H \ell_2^H} I_1(m_V^2, s) \Bigg) + \\
&\qquad \int_{\Lambda^2}^{m_V^2} \mathrm{d}k_T^2 \frac{\mathrm{d}}{\mathrm{d}k_T^2} \left[\Delta^{\text{em}}_{q_1^H q_2^H \ell_1^H \ell_2^H}(k_T^2, m_V^2; s) \right] \Delta^{\text{em}}_{q_1^H q_2^H \ell_1^H \ell_2^H}(\Lambda^2, k_T^2; s) \Bigg] \\
&= \hat{\sigma}^{B}_{q_1^H q_2^H \to \ell_1^H \ell_2^H}\, \Delta_{q_1^H q_2^H \ell_1^H \ell_2^H}(m_V^2, s; s) \Delta^{\text{em}}_{q_1^H q_2^H \ell_1^H \ell_2^H}(\Lambda^2, m_V^2; s) \\
&\quad \times \Bigg[c_W^2 A^{\text{U(1)}}_{q_1^H q_2^H \ell_1^H \ell_2^H} \frac{1}{2} \log^2(\frac{m_V^2}{s}) + A^{\text{mixing}}_{q_1^H q_2^H \ell_1^H \ell_2^H} I_{\frac{1}{2}}(m_V^2, s) + \\
&\qquad s_W^2 A^{W^3}_{q_1^H q_2^H \ell_1^H \ell_2^H} I_1(m_V^2, s) + \frac{\alpha Q_{\text{tot}}^2}{4\pi} \left(\ln^2 \frac{\Lambda^2}{s} - \ln^2 \frac{m_V^2}{s} \right) \Bigg] \,.
\end{aligned} \tag{2.65}$$

2.4 Results

In this section we analyze both the cross section with virtual corrections and those with real corrections for both the the 13 TeV LHC and a 100 TeV proton-proton collider. The main reason to present the results for a 100 TeV collider is that it is the main candidate to succeed to the LHC and the importance of our results increase with the energy. Our results show that resumming both the real and virtual logarithms is essential for a 100 TeV collider.

We begin by explaining the format used in all of our plots: solid lines represent the resummed LL corrections, while dashed lines are the fixed order double logarithmic correction. Black lines correspond to the virtual corrections while the real corrections with Z, photon, W^+ and W^- are shown in red, orange, blue and green, respectively. For each plot, we show on the top the perturbative corrections relative to the Born, in the middle the relative size of

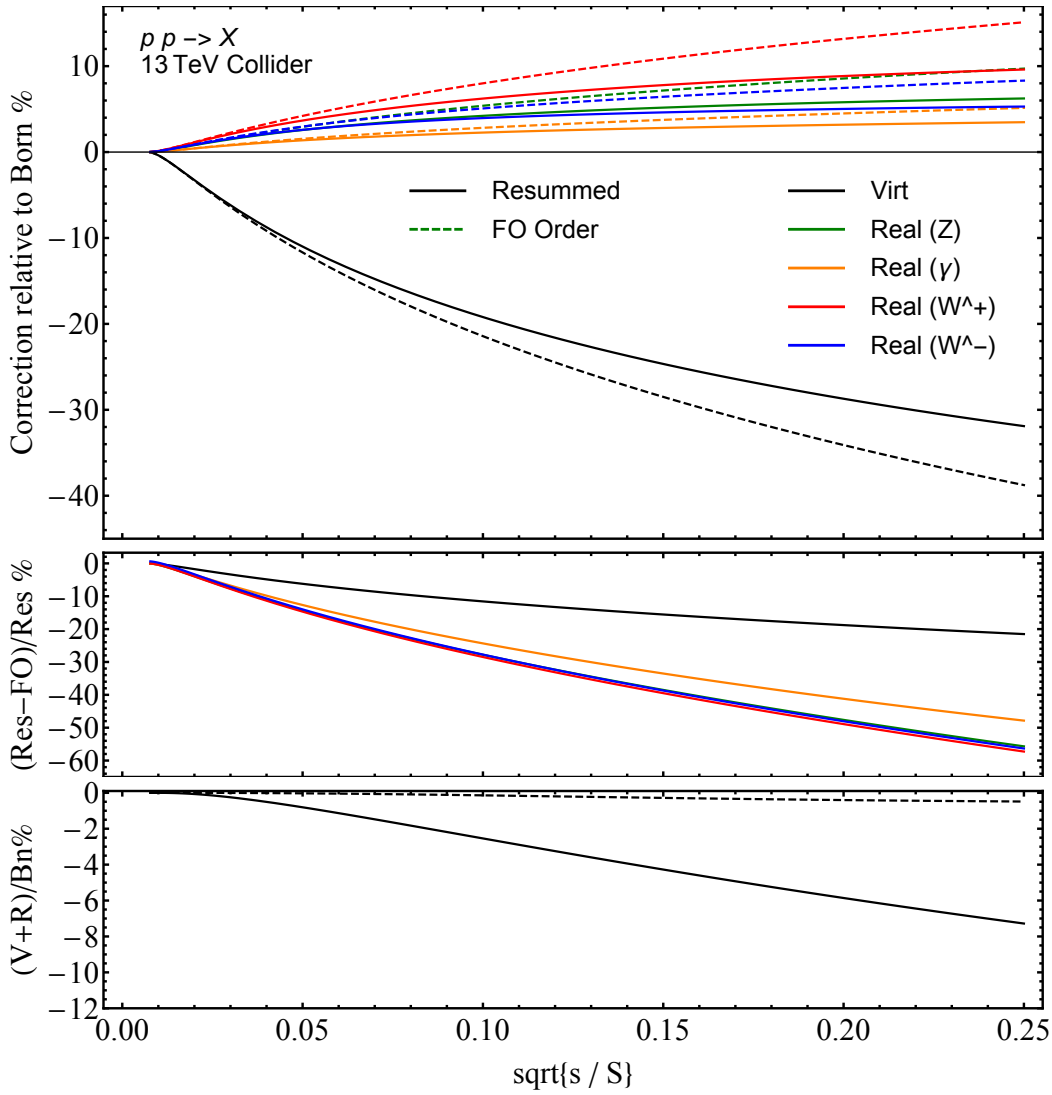

Figure 2.1: The cross-section summed over all lepton flavors for the 13 TeV LHC. On the top we show the individual corrections relative to the Born cross-section as defined in Eq. (2.66), in the middle the relative size of the resummation as defined in Eq. (2.67), while on the bottom we show the total perturbartive correction relative to the Born as defined in Eq. (2.68). Virtual corrections are shown in black, while real corrections with a Z, photon, W^+, W^- are shown in green, orange, red and blue. Resummed corrections are shown in solid lines, while fixed order results are dashed. The x-axis denotes the fraction of the partonic center of mass energy relative to the collider center of mass energy.

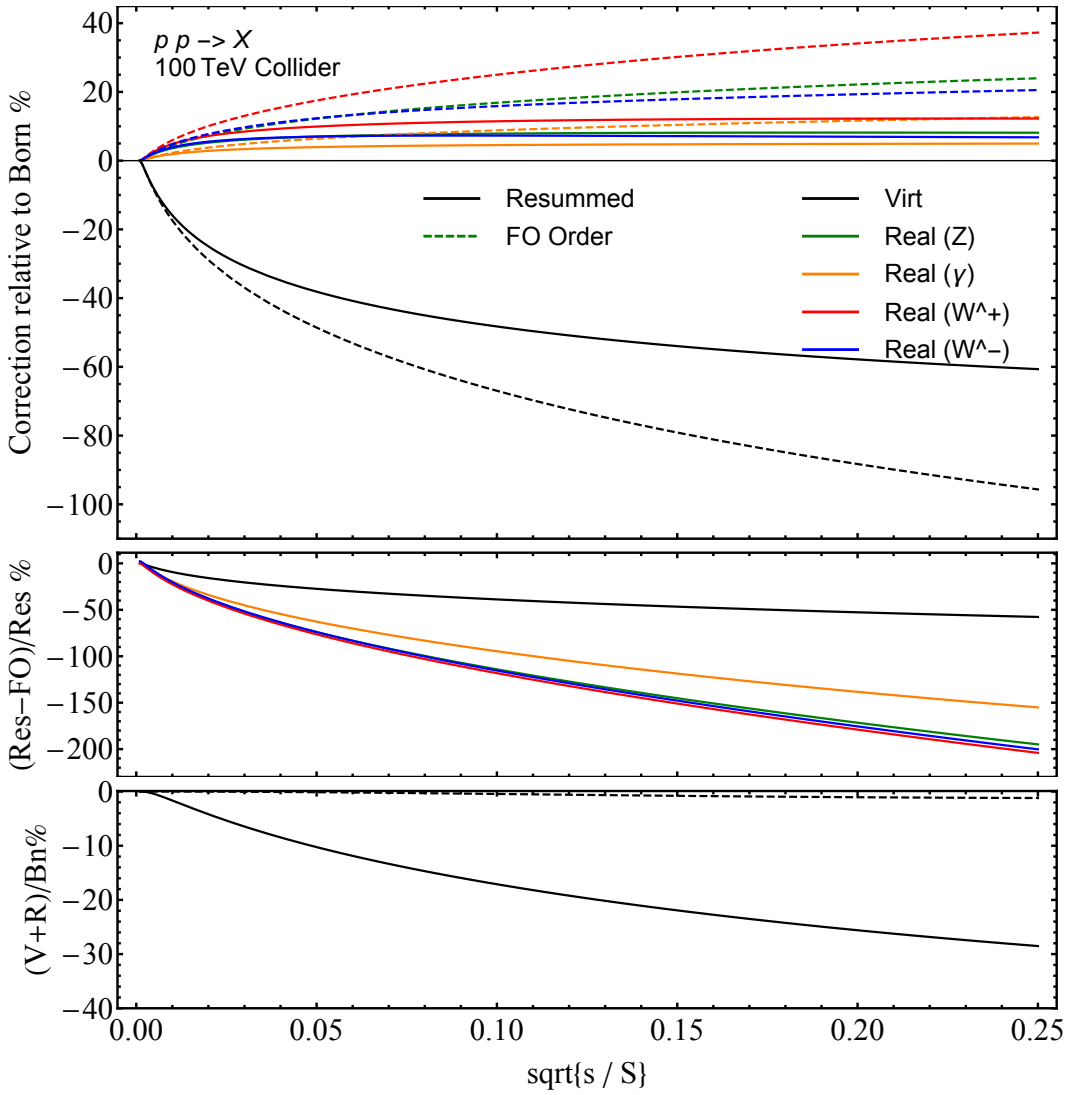

Figure 2.2: The cross-section summed over all lepton flavors for a 100 TeV pp collider on the right. All colors are the same as in Fig. 2.1.

the resummation and on the bottom the total perturbative correction after summing virtual and real relative to the Born. To be more precise, on the top we plot for virtual and real

$$\text{Virt}: \quad \frac{\sigma_{pp\to\ell_1\ell_2} - \sigma^{\text{B}}_{pp\to\ell_1\ell_2}}{\sigma^{\text{B}}_{pp\to\ell_1\ell_2}}, \qquad \text{Real (V)}: \quad \frac{\sigma_{pp\to\ell_1\ell_2 V}}{\sigma^{\text{B}}_{pp\to\ell_1\ell_2}}, \tag{2.66}$$

using either the resummed or fixed order expression. In the middle we show for the virtual

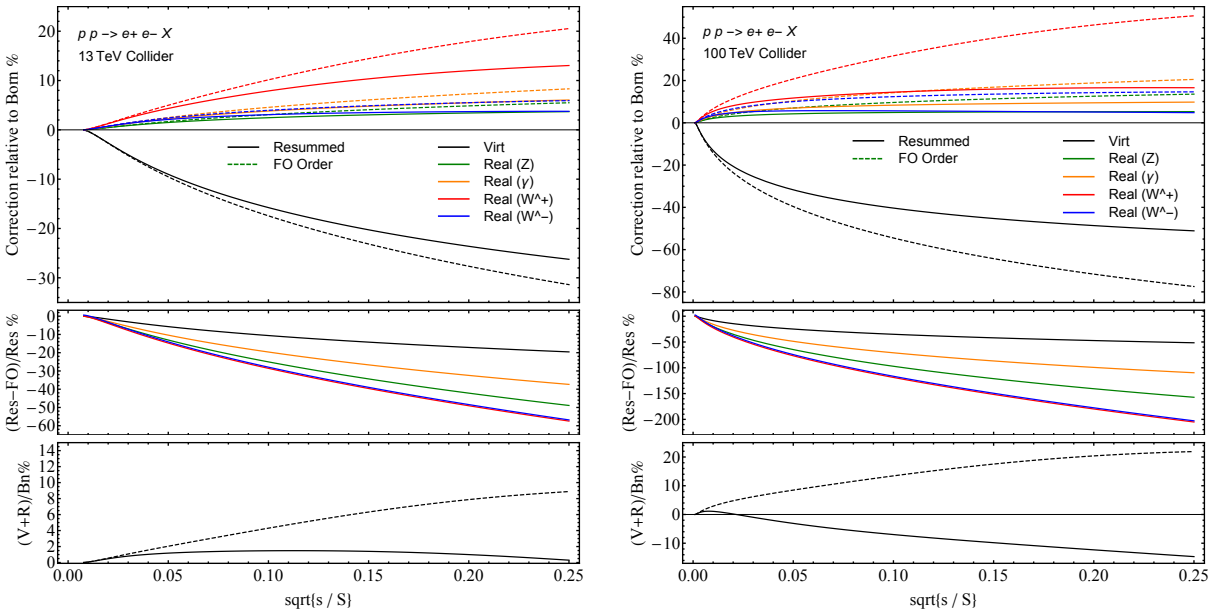

(a) 13 TeV LHC

(b) 100 TeV collider

Figure 2.3: The cross-section for e^+e^- for the 13 TeV LHC on the left, and 100 TeV pp collider on the right. All colors are the same as in Fig. 2.1. Note that the scaling of the y axis is different for the LHC and the 100 TeV collider.

contribution

$$\text{Virt}: \quad \frac{\sigma^{\text{FO}}_{pp\to\ell_1\ell_2} - \sigma^{\text{Res}}_{pp\to\ell_1\ell_2}}{\sigma^{\text{Res}}_{pp\to\ell_1\ell_2}}\,, \qquad \text{Real (V)}: \quad \frac{\sigma^{\text{FO}}_{pp\to\ell_1\ell_2 V} - \sigma^{\text{Res}}_{pp\to\ell_1\ell_2 V}}{\sigma^{\text{Res}}_{pp\to\ell_1\ell_2 V}}\,, \tag{2.67}$$

while for the lower plot we show

$$\frac{\sigma_{pp\to\ell_1\ell_2} + \sigma_{pp\to\ell_1\ell_2 V} - \sigma^{\text{B}}_{pp\to\ell_1\ell_2}}{\sigma^{\text{B}}_{pp\to\ell_1\ell_2}}\,, \tag{2.68}$$

for both fixed order and resummed. All effects are shown as a percentage.

We start with the result for the fully inclusive cross-section, where we sum over the flavors of all final state particles. In other words, we are summing over the virtual corrections for any lepton flavor, and the real corrections for any lepton flavor and gauge boson type. In terms of equations, for the fixed order result, the virtual are obtained by summing over all terms in Eqs. (2.11), (2.12), and (2.13); while the real are given by Eqs. (2.15), (2.17), (2.18), and (2.16). The resummed result are given by Eqs. (2.33), (2.62), (2.51), and (2.65). All those results are for $\Lambda = m_Z$, that is we are resolving the photon only down to the mass of the Z. A lower Λ would reduce all the exclusive cross section but the real cross

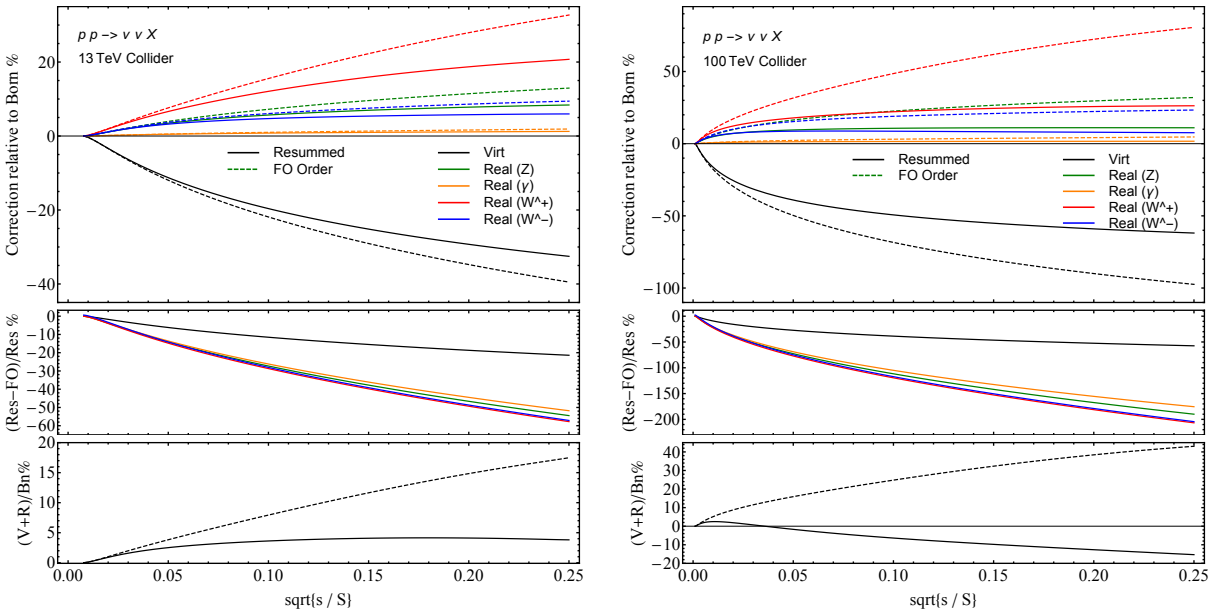

(a) 13 TeV LHC

(b) 100 TeV collider

Figure 2.4: The cross-section for $\bar{\nu}\nu$ for the 13 TeV LHC on the left, and 100 TeV pp collider on the right. All colors are the same as in Fig. 2.1.

section for photon as calculated in eq. (2.65) which will increase up to a value of Λ low enough than $\frac{\alpha Q_{\rm tot}^2}{4\pi}\left(\ln^2\frac{\Lambda^2}{s}-\ln^2\frac{m_V^2}{s}\right)=1-c_W^2 A^{\rm U(1)}_{q_1^H q_2^H \ell_1^H \ell_2^H}\frac{1}{2}\log^2(\frac{m_V^2}{s})-A^{\rm mixing}_{q_1^H q_2^H \ell_1^H \ell_2^H} I_{\frac{1}{2}}(m_V^2,s)-s_W^2 A^{W^3}_{q_1^H q_2^H \ell_1^H \ell_2^H} I_1(m_V^2,s)$, and then decrease if Λ continues to be lowered.

The results for the virtual and real contributions both at fixed and resummed order are shown in Fig. 2.1 for the LHC and in Fig. 2.2 for the 100 TeV collider. For the LHC, the corrections from virtual contributions range from $\mathcal{O}(15\%)$ at $\sqrt{s}\sim 1$ TeV to $\mathcal{O}(30\%)$ at $\sqrt{s}\sim 3$ TeV, while the real corrections for a given gauge boson are about a factor of 3 smaller individually. However, as can be seen from the ratio plot in the middle, the relative effect of the resummation is more than twice bigger for the real correction compared to the virtual correction. This clearly shows that the size of the resummation effect cannot be inferred from the size of the fixed order correction alone. The relative effect of the resummation for the virtual reaches from $\mathcal{O}(10\%)$ at $\sqrt{s}\sim 1$ TeV to $\mathcal{O}(20\%)$ at $\sqrt{s}\sim 3$ TeV while the relative effect of the resummation for the real reaches from $\mathcal{O}(20\%)$ at $\sqrt{s}\sim 1$ TeV to $\mathcal{O}(50\%)$ at $\sqrt{s}\sim 3$ TeV.

In the lower part of the plot for the fixed order, one can see that after summing the virtual and real, the perturbative corrections largely cancel, but a small effect at the $\mathcal{O}(1\%)$ level persists. For a fully inclusive cross section the logarithmically enhanced virtual and

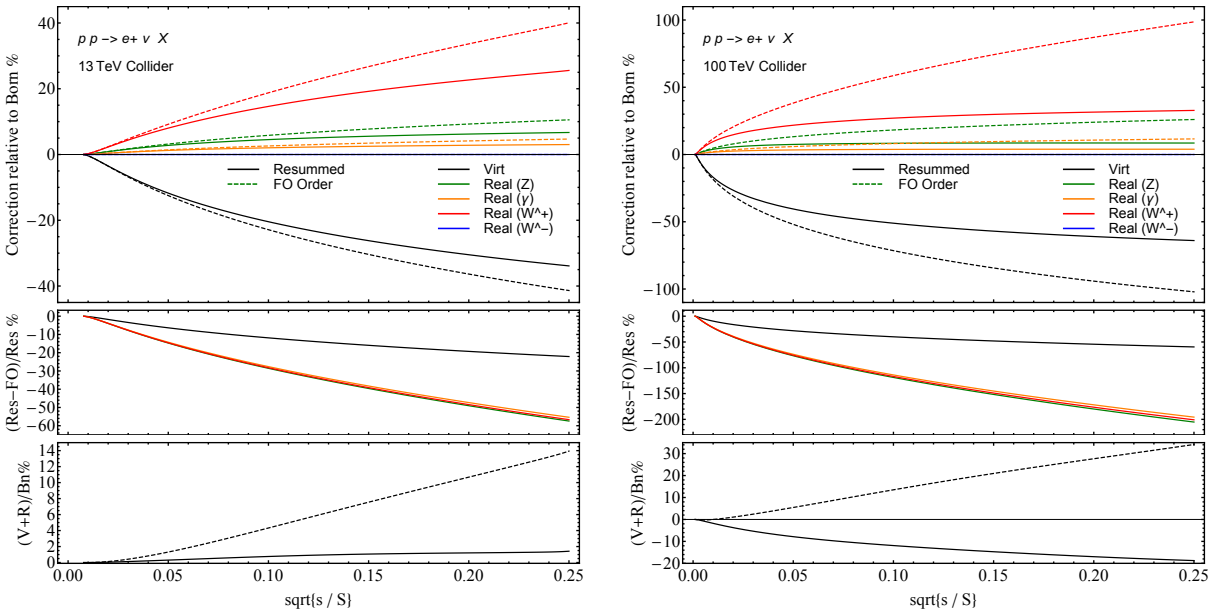

(a) 13 TeV LHC

(b) 100 TeV collider

Figure 2.5: The cross-section summed for $e^+\nu$ for the 13 TeV LHC on the left, and 100 TeV pp collider on the right. All colors are the same as in Fig. 2.1.

real corrections cancel against each other, up to the fact that the pp initial state is not an iso-singlet. The large cancellation can be understood from Eq. (2.19), which shows that switching the flavor of initial state anti-quark changes the sign of the partonic cross-section. Since pdf's for sea quarks are similar in magnitude, one expects $f_{\bar{u}/p} \sim f_{\bar{d}/p}$, explaining the cancellation. For the resummed result on the other hand, there is no cancellation. That is because even if the initial state is an SU(2) singlet, the cancellation would occur only for an inclusive result, that is summing the virtual to the real for any number of gauge boson. The remaining correction for the resummed result is thus mostly due to the production of more than one gauge boson with also an order 1% correction due to the initial state not being an SU(2) singlet. This remaining correction ranges from 2% at $\sqrt{s} \sim 5$ TeV to 7% at $\sqrt{s} \sim 25$ TeV.

For the 100 TeV collider, the results are qualitatively the same, but given the much larger reach in energy, the overall size of the effects are much larger. The virtual contributions range from $\mathcal{O}(30\%)$ at $\sqrt{s} \sim 5$ TeV to $\mathcal{O}(60\%)$ at $\sqrt{s} \sim 25$ TeV, with the real corrections again roughly a factor of 3 smaller. The relative size of the resummation, is also much larger, and at $\sqrt{s} \sim 25$ TeV changes the result by $\mathcal{O}(50\%)$ for the virtual and by $\mathcal{O}(200\%)$ for the real corrections. Thus, at such large energies, resummation has to be included to get a reliable estimate of the effects, not only for virtual corrections but also for the real emissions. Once

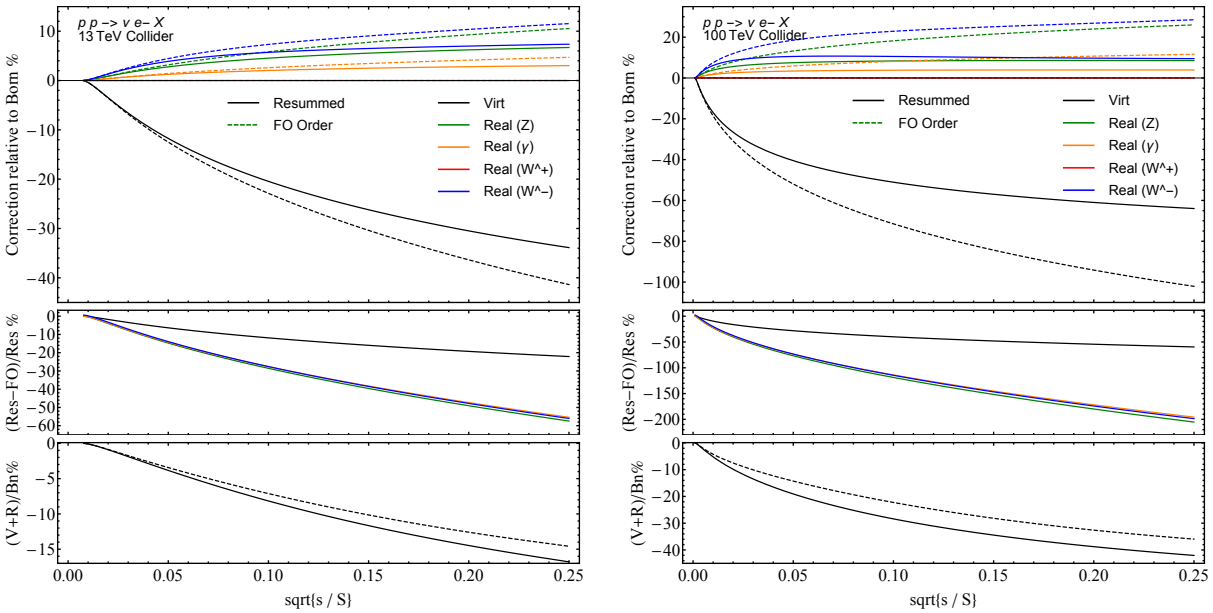

(a) 13 TeV LHC

(b) 100 TeV collider

Figure 2.6: The cross-section for $\bar{\nu}e^-$ for the 13 TeV LHC on the left, and 100 TeV pp collider on the right. All colors are the same as in Fig. 2.1.

the virtual and real corrections are added at fixed order, the total corrections again are very small, at the percent level; while for the resummed result, the total correction ranges from $\mathcal{O}(10\%)$ at $\sqrt{s} \sim 5$ TeV to $\mathcal{O}(30\%)$ at $\sqrt{s} \sim 25$ TeV.

Next, we consider the results for final states with specific leptons flavors. From the Figures 2.3 to 2.6, one can see that at the LHC, the virtual corrections range from $\mathcal{O}(15\%)$ at $\sqrt{s} \sim 1$ TeV to $\mathcal{O}(30\%)$ at $\sqrt{s} \sim 3$ TeV, with the exact numbers depending on the leptonic final state chosen, while at a 100 TeV collider they can exceed 50% at $\sqrt{s} \sim 25$ TeV. Resummation at the LHC changes the virtual corrections by $\mathcal{O}(10\%)$ at $\sqrt{s} \sim 1$ TeV to $\mathcal{O}(20\%)$ at $\sqrt{s} \sim 3$ TeV, while at a 100 TeV collider the effect can become as large as 50%. Resummation at the LHC changes the real corrections by $\mathcal{O}(20\%)$ at $\sqrt{s} \sim 1$ TeV to $\mathcal{O}(60\%)$ at $\sqrt{s} \sim 3$ TeV, while at a 100 TeV collider the effect can become as large as 200%. After summing over virtual and real corrections, the remaining perturbative corrections grow with energy are much larger than in the fully inclusive case. This is of course expected, since by specifying the leptonic final state, we are not considering an inclusive final state any longer.

Chapter 3

Standard Model Parton Distributions at Very High Energies

To construct a general-purpose SM event generator,[1] the three phases of a hard collision, namely initial-state parton showering, parton-parton collision and final-state showering, need to be simulated including all SM particles and interactions. For the initial-state showering, parton distribution functions (PDFs) for all the SM fermions and bosons need to be computed and tabulated beforehand, so that showering can be generated backwards from the hard process, guided by the scale dependence of the PDFs [54, 55].

Recently, a final-state parton shower including emissions from all interactions in the Standard Model was developed [56], which illustrated the importance of electroweak splittings at high energies. For initial-state radiation the generalization of the DGLAP [57–59] evolution equations using all the Standard Model interactions has been worked out in [12], but so far no numerical implementation of these results has been published.

As already mentioned, understanding the DGLAP evolution of PDFs using all interactions of the SM is a required first step in developing a complete initial state parton shower. Moreover, it already allows us to study many new qualitative features of very high-energy processes, such as lepton-initiated processes in hadron collisions and the polarization induced by electroweak PDF evolution.

The inclusion of QED corrections into parton distributions is a well established procedure [60–67]. However, above the electroweak scale around 100 GeV, the contributions of other electroweak bosons become non-negligible and new effects appear [3–17]. PDFs of leptons, vector and scalar bosons are generated dynamically, and left- and right-handed fermions evolve differently. There are also comparable effects in the third generation of quarks due to their Yukawa interactions. Some effects of the SU(2) interaction are double-logarithmically enhanced, due to the non-singlet nature of the incoming states.

The PDF evolution equations for the full Standard Model have been presented in Ref. [12]. In the present chapter we recast those equations in a form suitable for event generation and

[1] For a review of existing generators, see ref. [53].

solve them numerically for a given set of input distributions at the electroweak scale. The resulting PDF set extends through the region of interest for future colliders and well beyond, so that we can study the onset of the regime where all the SM interactions start to become comparable.

Our solutions to the SM evolution equations are obtained in the approximation of exact SU(3)×SU(2)×U(1) symmetry. That is, we neglect fermion and Higgs masses and the Higgs vacuum expectation value, the effects of these being power-suppressed at high scales. We impose an infra-red cutoff m_V on interactions that involve the emission of an electroweak vector boson, $V = W^i$ for SU(2) or B for U(1). Leading-order evolution kernels and one-loop running couplings are used. All the electroweak PDFs are generated dynamically from the QCD plus photon PDFs, starting from a matching scale $q_V \sim m_V$. In practice we take $q_V = m_V = 100$ GeV. In Sec. 3.3 we show some effects of varying these parameters, to provide an indication of uncertainties due to subleading logarithms and power-suppressed terms.

For the evolution of the photon, we decompose its PDF into W^3, B and mixed B/W^3 components at the input scale, evolve these components, and reconstruct the photon PDF from them at higher scales using the running SU(2) and U(1) couplings. For the top quark, we set the PDF to zero below the top mass scale and then use the leading-order massless evolution kernels, as for other fermions. This treatment of the transition region around the electroweak scale is clearly over-simplified but it should give a reliable indication of the magnitude of electroweak effects at higher energies.

The accuracy of our resulting PDFs is leading logarithmic, with subleading logarithmic effects included where possible, but not in a complete way. Contributions to the evolution from the U(1), SU(3) and Yukawa interactions are therefore correct at the single logarithmic level. However, as mentioned above, the SU(2) interactions give rise to double logarithmic effects in the PDF evolution, such that single logarithmic effects in SU(2) non-singlet quantities are not fully under control.

The organization of the chapter is as follows. In Sec. 3.1 we define the relevant parton distribution functions for unpolarized proton beams and the general form of their evolution equations, paying particular attention to the conservation of momentum in the presence of the cutoff m_V for vector boson emission. After specifying all the necessary splitting functions and running couplings, we write the explicit evolution equations associated with the five interactions: SU(3), U(1), SU(2), Yukawa and mixed U(1)×SU(2), for all the SM partons in a flavor basis. As usual for DGLAP evolution, we do not include 4 point interactions which are suppressed at high energies.

For a numerical implementation, as described in Sec. 3.2, the flavor basis is not convenient, as too many coupled equations are involved. Instead we use the basis of conserved quantum numbers introduced in Ref. [12]. As shown there, the double-logarithmic evolution of SU(2) non-singlet PDFs can then be factored out, which stabilizes and accelerates the solution of the equations. In this way we are able to evolve all the SM PDFs to arbitrarily high scales with satisfactory speed and precision. In practice we evolve up to 10^8 GeV, where the approach to asymptotic behavior is well established.

3.1 The evolution of parton distributions in the full Standard Model

Definition of the parton distribution functions

The standard definition of an x-weighted parton distribution is given by the matrix element of a bi-local operator, separated along the lightcone. For fermions, one finds the standard definition, but without spin averaging as we are separating the fermions into left- and right-handed. Thus, each fermion has only one possible spin determined by its helicity and the sign of its momentum

$$f_i(x,\mu) = x\int\frac{dy}{2\pi}\,e^{-i\,2x\bar{n}\cdot p\,y}\langle p|\,\bar{\psi}^{(i)}(y)\,\bar{\not{n}}\,\psi^{(i)}(-y)|p\rangle\,, \tag{3.1}$$

$$f_{\bar{i}}(x,\mu) = x\int\frac{dy}{2\pi}\,e^{-i\,2x\bar{n}\cdot p\,y}\langle p|\,\psi^{(i)}(y)\,\bar{\not{n}}\,\bar{\psi}^{(i)}(-y)|p\rangle\,, \tag{3.2}$$

where μ is the renormalization scale. Since we have separate left- and right-handed PDFs, for each generation there are a total of 8 quark PDFs and 6 lepton PDFs to consider, giving a total of 42 fermion PDFs.

Parton distributions functions of the vector bosons are given by

$$f_V(x,\mu) = \frac{2}{\bar{n}\cdot p}\int\frac{dy}{2\pi}\,e^{-i\,2x\bar{n}\cdot p\,y}\,\bar{n}_\mu\bar{n}^\nu\langle p|\,V^{\mu\lambda}(y)V_{\lambda\nu}(-y)|p\rangle\Big|_{\text{spin avg.}}\,. \tag{3.3}$$

Since SU(3) is unbroken, we consider a single PDF to describe the gluon field. For the SU(2) $\otimes$ U(1) symmetry, on the other hand, one needs to take the symmetry breaking into account. For the W^+ and W^- boson we simply include separate PDFs for each of the two gauge bosons. For the B and W_3, however, one needs to be more careful to take the mixed contributions of these two bosons into account. Such contributions arise from the fact that the left-handed fermions and Higgs carry both isospin and hypercharge. This implies that besides B and W_3 PDFs one needs to include a mixed PDF, which is given by[2]

$$f_{BW}(x) = \frac{2}{\bar{n}\cdot p}\int\frac{dy}{2\pi}\,e^{-i\,2x\bar{n}\cdot p\,y}\,\bar{n}^\mu\bar{n}_\nu\langle p|\,B_{\mu\lambda}(y)W_3^{\lambda\nu}(-y)|p\rangle\Big|_{\text{spin avg.}} + \text{h.c.}\,. \tag{3.4}$$

From these PDFs one can then construct the PDF for the photon, the transversely-polarized Z^0 and their mixed state as a transformation of the PDF for the B, the W_3 and their mixed state. Using $A = c_W B + s_W W_3$ and $Z^0 = -s_W B + c_W W_3$ one finds

$$\begin{pmatrix} f_\gamma \\ f_Z \\ f_{\gamma Z} \end{pmatrix} = \begin{pmatrix} c_W^2 & s_W^2 & c_W s_W \\ s_W^2 & c_W^2 & -c_W s_W \\ -2c_W s_W & 2c_W s_W & c_W^2 - s_W^2 \end{pmatrix} \begin{pmatrix} f_B \\ f_{W_3} \\ f_{BW} \end{pmatrix}\,, \tag{3.5}$$

[2]Note that our definition of the mixed PDF f_{BW} is the sum of BW_3 and W_3B contributions, and similarly for the mixed PDF $f_{\gamma Z}$.

and thus

$$\begin{pmatrix} f_B \\ f_{W_3} \\ f_{BW} \end{pmatrix} = \begin{pmatrix} c_W^2 & s_W^2 & -c_W s_W \\ s_W^2 & c_W^2 & c_W s_W \\ 2c_W s_W & -2c_W s_W & c_W^2 - s_W^2 \end{pmatrix} \begin{pmatrix} f_\gamma \\ f_Z \\ f_{\gamma Z} \end{pmatrix} . \tag{3.6}$$

For the electroweak input at scale $\mu = q_V$ we have $f_\gamma(x, q_V) \neq 0$ and $f_Z(x, q_V) = f_{\gamma Z}(x, q_V) = 0$, so the input conditions at that scale are

$$f_B = c_W^2 \, f_\gamma \,, \quad f_{W_3} = s_W^2 \, f_\gamma \,, \quad f_{BW} = 2 c_W s_W \, f_\gamma \,. \tag{3.7}$$

Thus, when relating the PDFs at the input scale $\mu = q_V$ in Eq. (3.7), one chooses $s_W \equiv s_W(q_V)$ and $c_W \equiv c_W(q_V)$. After evolving these three unbroken PDFs to a higher scale q, the physical photon and Z^0 PDFs are reconstructed using the corresponding running values of $c_W(q)$ and $s_W(q)$.

Finally, one needs to include PDFs for the scalar bosons. One writes

$$f_H(x) \;=\; x \int \frac{dy}{2\pi} \, e^{-i\, 2x\bar{n}\cdot p\, y} \left\langle p \right| \Phi(y) \Phi(-y) \left| p \right\rangle , \tag{3.8}$$

and PDFs for each of the 4 Higgs fields H^0, $\bar{H}^0$, H^+ and H^- are included. The relationship to the 4 Higgs fields in the unbroken basis to the physical Higgs and the longitudinal gauge bosons is as follows: The $H^\pm$ PDFs correspond to those of the longitudinally polarized $W^\pm$. In the notation of Ref. [12], the neutral Higgs fields are

$$H^0 = \frac{(h - i Z_L)}{\sqrt{2}} \,, \qquad \bar{H}^0 = \frac{(h + i Z_L)}{\sqrt{2}} \,, \tag{3.9}$$

where h and Z_L represent the Higgs and the longitudinal Z^0 fields, respectively. The corresponding PDFs are

$$f_{H^0} \;=\; \frac{1}{2} \left[f_h + f_{Z_L} + i \left(f_{h Z_L} - f_{Z_L h} \right) \right] , \tag{3.10}$$

$$f_{\bar{H}^0} \;=\; \frac{1}{2} \left[f_h + f_{Z_L} - i \left(f_{h Z_L} - f_{Z_L h} \right) \right] , \tag{3.11}$$

and one can also define the mixed PDFs

$$f_{H^0 \bar{H}^0} \;=\; \frac{1}{2} \left[f_h - f_{Z_L} - i \left(f_{h Z_L} + f_{Z_L h} \right) \right] , \tag{3.12}$$

$$f_{\bar{H}^0 H^0} \;=\; \frac{1}{2} \left[f_h - f_{Z_L} + i \left(f_{h Z_L} + f_{Z_L h} \right) \right] . \tag{3.13}$$

Both of these mixed PDF carry non-zero hypercharge, such that they are not produced by the DGLAP evolution in the unbroken gauge theory as considered in this chapter[3]. Thus, one immediately finds

$$f_h - f_{Z_L} = f_{h Z_L} + f_{Z_L h} = 0 \,, \tag{3.14}$$

[3]They are only produced through insertions of the Higgs vacuum.

and

$$f_h = f_{Z_L} = \frac{1}{2}(f_{H^0} + f_{\bar{H}^0})\,, \qquad f_{hZ_L} = -f_{Z_L h} = -\frac{i}{2}(f_{H^0} - f_{\bar{H}^0})\,. \tag{3.15}$$

In summary, there are a total of 52 parton distribution functions that need to be considered. Apart from the QCD quark and gluon distributions, the charged leptons, and the neutral electroweak boson PDFs (3.7), all the other SM PDFs are set to zero at scale q_V and evolve according to the generalized DGLAP equations presented below.

For the input used here, and because fermion masses and Yukawa couplings are neglected except for the top quark, several fermion PDFs are identical. The lepton PDFs are independent of generation. Also the right-handed fermion and antifermion PFDs are identical, apart from the top quark, unless they are different at the matching scale q_V. This is the case only for the up and down quarks. The right-handed top and anti-top are slightly different, since they interact through the Yukawa coupling with H^+ H^-, respectively. Thus the number of distinct right-handed quark PDFs is reduced from 12 to 9, the left-handed leptons from 12 to 4, and the right-handed leptons from 6 to 1, making a total of 36 non-identical PDFs.

General evolution equations

We consider the x-weighted PDFs of parton species i at momentum fraction x and scale q, $f_i(x,q)$. In general they satisfy evolution equations of the following forms:

$$\begin{aligned} q\frac{\partial}{\partial q} f_i(x,q) &= \sum_I \frac{\alpha_I(q)}{\pi}\left[P^V_{i,I}(q)\, f_i(x,q) + \sum_j C_{ij,I}\int_x^{z^{ij,I}_{\max}(q)} \mathrm{d}z\, P^R_{ij,I}(z) f_j(x/z,q)\right] \\ &\equiv \sum_I \left[q\frac{\partial}{\partial q} f_i(x,q)\right]_I . \end{aligned} \tag{3.16}$$

Here, the sum over I goes over the different interactions in the Standard Model and the notation $[q\,\partial/\partial q f_i(x,q)]_I$ implies that we only keep the terms proportional to the coupling α_I when taking the derivative[4]. For the rest of the section, we will show the evolution of each $f_i(x,q)$. We choose $I = 1,2,3$ for the pure U(1), SU(2) and SU(3) gauge interactions, $I = Y$ for Yukawa interactions, and $I = M$ for the mixed interaction proportional to

$$\alpha_M(q) = \sqrt{\alpha_1(q)\,\alpha_2(q)}\,. \tag{3.17}$$

The first contribution, proportional to $P^V_{i,I}$, denotes the virtual contribution to the PDF evolution (the disappearance of a flavor i), while the second contribution is the real contribution (the appearance of flavor i due to the splitting of a flavor j). The maximum value of z in

[4]Note that $[\ldots]_I$ is only introduced for notational convenience and should not be interpreted as setting all other couplings to zero. In particular, the PDFs appearing on the right-hand side of Eq. (3.16) still depend on the value of all coupling constants.

the integration of the real contribution depends on the type of splitting and interaction, and we choose

$$z_{\max}^{ij,I}(q) = \begin{cases} 1 - \frac{m_V}{q} & \text{for } I = 1, 2, \text{ and } i, j \notin V \text{ or } i, j \in V \\ 1 & \text{otherwise} \end{cases} , \tag{3.18}$$

that is, we apply an infrared cutoff m_V, of the order of the electroweak scale, when a B or W boson is emitted. This regulates the divergence of the splitting function for those emissions as $z \to 1$. Such a cutoff is mandatory for $I = 2$ because there are PDF contributions that are SU(2) non-singlets. The evolution equations for SU(3) are regular in the absence of a cutoff, as hadron PDFs are color singlets. Similarly for U(1), the unpolarized PDFs have zero hypercharge,[5] but we include the same cutoff for $I = 1$, since the B and W_3 are mixed in the physical Z and γ states.

Note that the precise choice of the cutoff is somewhat arbitrary, and as already mentioned, we choose $m_V = 100$ GeV in this chapter. Changing this value changes our results by subleading logarithmic effect, at the same level as other effects not included. However, given that the SU(2) evolution is double logarithmic, this implies that the ambiguity is single logarithmic for the SU(2) coupling. By matching our results to fixed order, one would account for these term at first order in α_2. This is beyond the scope of this chapter.

While the flavor basis chosen above is the most intuitive basis, the fact that all 52 PDFs are coupled to one another makes it quite difficult to solve the evolution equations. To decouple some of the equations, it helps to change the basis such that the ingredients have quantum numbers that are conserved in the Standard Model. Choosing the total isospin $\mathbf{T}$ and CP as the quantum numbers, the PDFs for each set of quantum numbers required are shown in Table 3.1.

$\{\mathbf{T}, \text{CP}\}$	fields
$\{0, +\}$	$2n_g \times q_R\,, n_g \times \ell_R\,, n_g \times q_L\,, n_g \times \ell_L\,, g\,, W\,, B\,, H$
$\{0, -\}$	$2n_g \times q_R\,, n_g \times \ell_R\,, n_g \times q_L\,, n_g \times \ell_L\,, H$
$\{1, +\}$	$n_g \times q_L\,, n_g \times \ell_L\,, BW, H$
$\{1, -\}$	$n_g \times q_L\,, n_g \times \ell_L\,, W, H$
$\{2, +\}$	W

Table 3.1: The 52 PDFs required for the SM evolution can written in a basis with definite conserved quantum numbers. $(5n_g + 4)$ PDFs contribute to the $\{0, +\}$ state, $(5n_g + 1)$ to the $\{0, -\}$, $(2n_g + 2)$ to each to the $\{1, +\}$ and $\{1, -\}$ and 1 to the $\{2, +\}$, where $n_g = 3$ stands for number of generations.

Note that in general there can be additional mixed PDFs, which however are zero in our initial conditions and which are not generated in the evolution. In particular, there can be states mixing left-and right-handed fermions, but they are not present in the initial condition

[5] Although there can be contributions with non-zero hypercharge for transversely polarized beams [12].

when only considering unpolarized beams because those states are not Lorentz scalar. Thus, we can drop these states from our evolution.

The sum of momenta of all non-mixed PDFs in the particle basis is conserved, since it is the momentum of the proton. Momentum conservation applies independently for each interaction since physics would still be coherent if we removed one interaction from the Standard Model.

$$\sum_{i\neq \mathrm{BW}} \int_0^1 dx \left[q\frac{\partial}{\partial q} f_i(x,q)\right]_I = 0 \,\text{for}\, I = 1,2,3,Y,M\,. \tag{3.19}$$

This is equivalent to the sum over all $\mathbf{T} = 0$, CP $= +$ PDFs in the isospin and CP basis because only these states contribute to a sum over the PDFs in the particle basis. For the other values of $\mathbf{T}$ and CP, the PDFs correspond to differences of PDFs in the particle basis. For example an isospin 1 PDF is added in PDF of an up-type fermion, but subtracted in the down-type PDF, thus it has no effect on the sum.

Combining Eqs. (3.16) and (3.19) gives

$$\begin{aligned} 0 &= \sum_{i\neq \mathrm{BW}} P^V_{i,I} \int_0^1 dx\, f_i(x,q) + \sum_{i,j} C_{ij,I} \int_0^1 \mathrm{d}x \int_x^{z^{ij,I}_{\max}(q)} \mathrm{d}z\, P^R_{ij,I}(z)\, f_j(x/z,q) \\ &= \sum_{i\neq \mathrm{BW}} P^V_{i,I} \int_0^1 dx\, f_i(x,q) + \sum_{i,j} C_{ij,I} \int_0^{z^{ij,I}_{\max}(q)} \mathrm{d}z\, P^R_{ij,I}(z) \int_0^z dx f_j(x/z,q) \\ &= \sum_{i\neq \mathrm{BW}} P^V_{i,I} \langle f_i(q)\rangle + \sum_{i,j} C_{ij,I} \int_0^{z^{ij,I}_{\max}(q)} z\,\mathrm{d}z\, P^R_{ij,I}(z) \langle f_j(q)\rangle\,, \end{aligned} \tag{3.20}$$

where we have defined the momentum averaged PDF

$$\langle f_i(q)\rangle \equiv \int_0^1 dx\, f_i(x,q)\,. \tag{3.21}$$

Solving the equation for each of the $\langle f_i(q)\rangle$, since all the input particle PDFs can be set independently, we get

$$P^V_{i,I}(q) = -\sum_j C_{ji,I} \int_0^{z^{ji,I}_{\max}(q)} z\,\mathrm{d}z\, P^R_{ji,I}(z) \,\text{for}\, i \neq \mathrm{BW}\,. \tag{3.22}$$

Thus, momentum conservation determines the factor $P^V_{i,I}$ for all non-mixed fields in the particle basis.

Note that the result from momentum conservation agrees up to power corrections with the more traditional definition of the virtual corrections as loop insertions on the fields of

the PDF, which we denote by $\tilde{P}^V_{i,I}$. Summing over possible loops, one has

$$\begin{aligned}
\tilde{P}^V_{f_i,I}(q) &= -C_{ff,i,I}\int_0^{z^{ff,I}_{\max}(q)} \mathrm{d}z\, P^R_{ff,I}(z) \\
\tilde{P}^V_{V_i,I}(q) &= -\frac{C_{VV,i,I}}{2}\int_0^{z^{VV,I}_{\max}(q)} \mathrm{d}z\, P^R_{VV,I}(z) - \sum_{j\in f,h} C_{jV_i,I}\int_0^1 \mathrm{d}z\, P^R_{jV,I}(z) \\
\tilde{P}^V_{H_i,I}(q) &= -C_{HH,i,I}\int_0^{z^{HH,I}_{\max}(q)} \mathrm{d}z\, P^R_{HH,I}(z) - \sum_{j\in f} C_{jH_i,I}\int_0^1 \mathrm{d}z\, P^R_{fH,I}(z)\,,
\end{aligned} \tag{3.23}$$

where $\sum_{j\in f,h}$ is a sum over all fermions and Higgs bosons which are not antiparticles, and

$$C_{ff,i,I} = \sum_j C_{f_j f_i,I} \tag{3.24}$$

and similarly for $C_{VV,i,I}$ and $C_{HH,i,I}$. To see that Eqs. (3.22) and (3.23) agree with each other, we will work it out explicitly for the virtual contribution to a fermion. One uses for the fermions that $P^R_{Vf,I}(z) = P^R_{ff,I}(1-z)$ and $C_{ff,I} = C_{Vf,I}$ to obtain the correct relation:

$$\begin{aligned}
P^V_{f,I}(q) &= -C_{ff,I}\left[\int_0^{z_{\max}} z\,\mathrm{d}z\, P^R_{ff,I}(z) + \int_0^1 z\,\mathrm{d}z\, P^R_{Vf,I}(z)\right] \\
&= -C_{ff,I}\left[\int_0^{z_{\max}} z\,\mathrm{d}z\, P^R_{ff,I}(z) + \int_0^1 (1-z)\,\mathrm{d}z\, P^R_{ff,I}(z)\right] \\
&= \tilde{P}^V_{f,I}(q) + \ldots\,,
\end{aligned} \tag{3.25}$$

where $\ldots$ denotes power corrections in $1-z_{\max}$. The argument is exactly the same for $P^V_{H,I}(q)$, while for $P^V_{V,I}(q)$ one simply uses that $P^R_{VV,I}(z)$ and $P^R_{fV,I}(z)$, and $P^R_{hV,I}(z)$ and $P^R_{fH,I}(z)$, are symmetric in $z \leftrightarrow 1-z$ to write $\int z\,\mathrm{d}z = \int \mathrm{d}z/2$. In our implementation of the evolution equations, we use Eq. (3.22), to ensure exact momentum conservation without explicit power corrections.

Since the mixed PDF f_{BW} is a pure $\mathbf{T} = 1$ state, it does not contribute to the momentum sum. This implies that one cannot derive its associated virtual contribution from momentum conservation. However, using the traditional definition in terms of loops, one sees that in this case the U(1) and SU(2) virtual corrections each apply to only one of the two fields involved, and therefore

$$\tilde{P}^V_{BW,1}(q) = \frac{1}{2}P^V_{B,1}(q)\,, \qquad \tilde{P}^V_{BW,2}(q) = \frac{1}{2}P^V_{W,2}(q)\,, \tag{3.26}$$

while the virtual contribution is zero for the other interactions.

One can simplify the general evolution equations in Eq. (3.16) by defining a full Sudakov factor

$$\Delta_i(q) = \exp\left[\sum_I \int_{q_V}^q \frac{\mathrm{d}q'}{q'}\frac{\alpha_I(q')}{\pi} P^V_{i,I}(q')\right]\,, \tag{3.27}$$

as well as a partial Sudakov factor for each interaction

$$\Delta_{i,I}(q) = \exp\left[\int_{q_V}^{q} \frac{\mathrm{d}q'}{q'} \frac{\alpha_I(q')}{\pi} P^V_{i,I}(q')\right], \tag{3.28}$$

where q_V is an arbitrary cutoff, which for convenience we set equal to m_V. This allows us to write

$$\left[\Delta_{i,I}(q)\, q\frac{\partial}{\partial q}\frac{f_i(x,q)}{\Delta_{i,I}(q)}\right]_I = \frac{\alpha_I(q)}{\pi}\sum_j C_{ij,I} P^R_{ij,I} \otimes f_j\,, \tag{3.29}$$

where again the notation $[\ldots]_I$ implies that only terms from the interaction I are kept. This gives

$$\begin{aligned}\Delta_i(q)\, q\frac{\partial}{\partial q}\left[\frac{f_i(x,q)}{\Delta_i(q)}\right] &= \sum_I \left[\Delta_{i,I}(q)\, q\frac{\partial}{\partial q}\frac{f_i(x,q)}{\Delta_{i,I}(q)}\right]_I \\ &= \sum_I \frac{\alpha_I(q)}{\pi}\sum_j C_{ij,I} P^R_{ij,I} \otimes f_j\,, \end{aligned} \tag{3.30}$$

where

$$P^R_{ij,I} \otimes f_j \equiv \int_x^{z^{ij,I}_{\max}(q)} \mathrm{d}z\, P^R_{ij,I}(z) f_j(x/z,q)\,. \tag{3.31}$$

Splitting functions

The splitting functions depend only on the type of particles, which for the Standard Model are the spin 1/2 fermions, denoted by f, spin 1 gauge bosons, denoted by V, as well as spin 0 Higgs bosons, denoted by H.

Denoting the three gauge interactions of the Standard Model collectively by $I = G$, the splitting functions involving gauge bosons are given by

$$P^R_{ff,G}(z) = \frac{1+z^2}{1-z}\,, \tag{3.32}$$

$$P^R_{Vf,G}(z) = P_{ff,G}(1-z)\,, \tag{3.33}$$

$$P^R_{fV,G}(z) = \frac{1}{2}\left[z^2 + (1-z)^2\right], \tag{3.34}$$

$$P^R_{VV,G}(z) = 2\left[\frac{z}{1-z} + \frac{1-z}{z} + z(1-z)\right] \tag{3.35}$$

$$P^R_{HH,G}(z) = \frac{2z}{1-z}\,, \tag{3.36}$$

$$P^R_{VH,G}(z) = P^R_{HH,G}(1-z)\,, \tag{3.37}$$

$$P^R_{HV,G}(z) = z(1-z)\,. \tag{3.38}$$

The factor of 1/2 in P_{fV} has to be included since we are considering fermions with definite chirality. For the Yukawa interaction (Y), one obtains

$$P^R_{ff,Y}(z) = \frac{1-z}{2}\,, \tag{3.39}$$

$$P^R_{Hf,Y}(z) = P^R_{ff,Y}(1-z)\,, \tag{3.40}$$

$$P^R_{fH,Y}(z) = \frac{1}{2}\,. \tag{3.41}$$

$I = 3$: SU(3) interactions

We start by considering the well known case of SU(3) interactions. The relevant degrees of freedom are the gluon, as well as left and right-handed quarks. The coupling constants are (with $C_F = 4/3$, $C_A = 3$, $T_R = 1/2$)

$$C_{qq,3} = C_{gq,3} = C_F\,, \qquad C_{qg,3} = T_R\,, \qquad C_{gg,3} = C_A\,. \tag{3.42}$$

This gives for the evolution of a quark or gluon[6]

$$\left[\Delta_{q,3}\, q\frac{\partial}{\partial q}\frac{f_q}{\Delta_{q,3}}\right]_3 = \frac{\alpha_3}{\pi}\left[C_F P^R_{ff,G}\otimes f_q + T_R P^R_{fV,G}\otimes f_g\right], \tag{3.43}$$

$$\left[\Delta_{g,3}\, q\frac{\partial}{\partial q}\frac{f_g}{\Delta_{g,3}}\right]_3 = \frac{\alpha_3}{\pi}\left[C_A P^R_{VV,G}\otimes f_g + \sum_f C_F P^R_{Vf,G}\otimes f_q\right]. \tag{3.44}$$

The Sudakov factor can be obtained from Eq. (3.22) using the coupling constants in Eq. (3.42). This gives

$$P^V_{q,3}(q) = -C_F\int_0^1 z\,\mathrm{d}z\,\left[P^R_{ff,G}(z) + P^R_{Vf,G}(z)\right], \tag{3.45}$$

$$P^V_{g,3}(q) = -\int_0^1 z\,\mathrm{d}z\,\left[C_A\,P^R_{VV,G}(z) + 8\,n_g\,T_R\,P^R_{fV,G}(z)\right], \tag{3.46}$$

where we have used in the last line that there are 8 chiral quarks plus antiquarks per generation.

Since the gluon is massless, the upper limit in all the z integrations is equal to 1 [see Eq. (3.18)]. This implies that the convolutions $P^R_{ff,G}\otimes f_q$ and $P^R_{VV,G}\otimes f_g$ in Eqs. (3.43) and (3.44) are both divergent. However, at the same time the virtual splitting functions that enter the Sudakov factors $\Delta_{q,3}(q)$ and $\Delta_{g,3}(q)$ defined in Eq. (3.28) are also divergent, such that the divergences cancel in the evolution of the actual PDFs. Using +-distributions, as explained in Sec. 3.2, one obtains evolution equations that are free of any divergences, and which can be implemented numerically. Alternatively, for parton shower implementation, one can impose a cutoff of the form Eq. (3.18) with m_V replaced by a small parameter $m_g > \Lambda_{\rm QCD}$.

[6]From now on we omit the arguments of functions for brevity.

$I = 1$: U(1) interactions

For U(1) the relevant degrees of freedom are left- and right-handed fermions (denoted by the subscript f), as well as the U(1) gauge boson B. The couplings involving fermions and gauge bosons are

$$C_{ff,1} = C_{Bf,1} = Y_f^2\,, \qquad C_{fB,1} = N_f\,Y_f^2\,, \qquad C_{BB,1} = 0 \tag{3.47}$$

where the hypercharges of the different fermions are given by

$$Y_{q_L} = \frac{1}{6}\,, \qquad Y_{u_R} = \frac{2}{3}\,, \qquad Y_{d_R} = -\frac{1}{3}\,, \qquad Y_{\ell_L} = -\frac{1}{2}\,, \qquad Y_{e_R} = -1\,, \tag{3.48}$$

and the color factor N_f is equal to 3 for quarks and 1 for leptons. The couplings involving the Higgs bosons are

$$C_{hh,1} = C_{Bh,1} = C_{hB,1} = \frac{1}{4}\,, \tag{3.49}$$

where h here stands for any of the four Higgs boson PDFs.

Plugging this into the general evolution equation gives

$$\left[\Delta_{f,1}\,q\frac{\partial}{\partial q}\frac{f_f}{\Delta_{f,1}}\right]_1 = \frac{\alpha_1}{\pi}Y_i^2\left[P^R_{ff,G}\otimes f_f + N_f P^R_{fV,G}\otimes f_B\right], \tag{3.50}$$

$$\left[\Delta_{B,1}\,q\frac{\partial}{\partial q}\frac{f_B}{\Delta_{B,1}}\right]_1 = \frac{\alpha_1}{\pi}\left[\sum_f Y_f^2 P^R_{Vf,G}\otimes f_f + \frac{1}{4}\sum_h P^R_{VH,G}\otimes f_h\right], \tag{3.51}$$

$$\left[\Delta_{H,1}\,q\frac{\partial}{\partial q}\frac{f_h}{\Delta_{H,1}}\right]_1 = \frac{\alpha_1}{\pi}\frac{1}{4}\left[P^R_{HH,G}\otimes f_h + P^R_{HV,G}\otimes f_B\right]. \tag{3.52}$$

The virtual splitting functions, required for the Sudakov factor are given by

$$P^V_{f,1}(q) = -Y_f^2\left[\int_0^{1-\frac{m_V}{q}} z\,\mathrm{d}z\,P^R_{ff,G}(z) + \int_0^1 z\,\mathrm{d}z\,P^R_{Vf,G}(z)\right], \tag{3.53}$$

$$P^V_{B,1}(q) = -n_g\left(\frac{11}{9}N_C + 3\right)\int_0^1 z\,\mathrm{d}z\,P^R_{fV,G}(z) - \int_0^1 z\,\mathrm{d}z\,P^R_{HV,G}(z)\,, \tag{3.54}$$

$$P^V_{H,1}(q) = -\frac{1}{4}\left[\int_0^{1-\frac{m_V}{q}} z\,\mathrm{d}z\,P^R_{HH,G}(z) + \int_0^1 z\,\mathrm{d}z\,P^R_{VH,G}(z)\right], \tag{3.55}$$

where we have used in the second line that for each generation there are 4 left-handed quarks (one needs to count particles and antiparticles separately), 2 right-handed up-type quarks, 2 right-handed down-type quarks, 4 left-handed leptons and 2 right-handed electrons, and that there are a total of 4 Higgs bosons.

$I = 2$: SU(2) interactions

The SU(2) interactions are more complicated, since the emission of $W^{\pm}$ bosons changes the flavor of the emitting particle. This, combined with the SU(2) breaking in the input hadron PDFs, leads to double-logarithmic scale dependence in the DGLAP evolution, rather than only single-logarithmic dependence as in the evolution based on U(1) and SU(3).

The relevant coupling constants are (where u_L and d_L denote any up- and down-type left-handed fermion)

$$C_{u_L d_L,2} = C_{d_L u_L,2} = C_{W^+ u_L,2} = C_{W^- d_L,2} = \frac{1}{2}, \tag{3.56}$$

$$C_{u_L u_L,2} = C_{W_3 u_L,2} = C_{d_L d_L,2} = C_{W_3 d_L,2} = \frac{1}{4}, \tag{3.57}$$

$$C_{u_L W^+,2} = C_{d_L W^-,2} = N_f \frac{1}{2}, \tag{3.58}$$

$$C_{u_L W_3,2} = C_{d_L W_3,2} = N_f \frac{1}{4}, \tag{3.59}$$

$$C_{W^{\pm} W^{\pm},2} = C_{W^{\pm} W_3,2} = C_{W_3 W^{\pm},2} = 1, \tag{3.60}$$

where as before the color factor $N_f = 3$ for quarks, 1 for leptons. The couplings of the W_3 state to the Higgs are given by

$$C_{hh,2} = C_{W_3 h,2} = C_{h W_3,2} = \frac{1}{4}, \tag{3.61}$$

where again h stands for any of the 4 Higgs bosons, while those of the charged W states are given by

$$\begin{aligned} C_{H^+ H^0,2} &= C_{H^0 H^+,2} = C_{H^+ W^+,2} = C_{W^+ H^+,2} \\ &= C_{H^0 W^-,2} = C_{W^- H^0,2} = \frac{1}{2}. \end{aligned} \tag{3.62}$$

The couplings for the charge-conjugate states are the same.

This gives for the evolution of the fermions

$$\begin{aligned} \left[\Delta_{f_L,2}\, q \frac{\partial}{\partial q} \frac{f_{u_L}}{\Delta_{f_L,2}}\right]_2 &= \frac{\alpha_2}{\pi}\left\{P^R_{ff,G} \otimes \left[\frac{f_{d_L}}{2} + \frac{f_{u_L}}{4}\right]\right. \\ &\quad \left. + N_f P_{fV,G} \otimes \left[\frac{f_{W^+}}{2} + \frac{f_{W_3}}{4}\right]\right\}, \end{aligned} \tag{3.63}$$

$$\begin{aligned} \left[\Delta_{f_L,2}\, q \frac{\partial}{\partial q} \frac{f_{d_L}}{\Delta_{f_L,2}}\right]_2 &= \frac{\alpha_2}{\pi}\left\{P^R_{ff,G} \otimes \left[\frac{f_{u_L}}{2} + \frac{f_{d_L}}{4}\right]\right. \\ &\quad \left. + N_f P_{fV,G} \otimes \left[\frac{f_{W^-}}{2} + \frac{f_{W_3}}{4}\right]\right\}. \end{aligned} \tag{3.64}$$

For the W^+ and W_3 bosons we have

$$\left[\Delta_{W,2}\, q\frac{\partial}{\partial q}\frac{f_{W^+}}{\Delta_{W,2}}\right]_2 = \frac{\alpha_2}{\pi}\Bigg\{P^R_{VV,G}\otimes[f_{W^+}+f_{W_3}]+\frac{1}{2}P^R_{VH,G}\otimes[f_{H^+}+f_{\bar{H}^0}] + \sum_{\text{gen}}\frac{1}{2}P_{Vf,G}\otimes\left[f_{u_L}+f_{\bar{d}_L}+f_{\nu_L}+f_{\bar{\ell}_L}\right]\Bigg\}, \tag{3.65}$$

$$\left[\Delta_{W,2}\, q\frac{\partial}{\partial q}\frac{f_{W_3}}{\Delta_{W,2}}\right]_2 = \frac{\alpha_2}{\pi}\Bigg\{P^R_{VV,G}\otimes[f_{W^+}+f_{W^-}]+\frac{1}{4}P^R_{VH,G}\otimes\sum_h f_h + \frac{1}{4}\sum_{f_L}P^R_{Vf,G}\otimes f_{f_L}\Bigg\}, \tag{3.66}$$

where the sum in the last line is over all left-handed fermions and anti-fermions. The equation for the W^- can be obtained from that of the W^+ by charge conjugation.

Finally, for the Higgs bosons we have

$$\left[\Delta_{H,2}\, q\frac{\partial}{\partial q}\frac{f_{H^+}}{\Delta_{H,2}}\right]_2 = \frac{\alpha_2}{\pi}\Bigg\{P^R_{HH,G}\otimes\left[\frac{f_{H^0}}{2}+\frac{f_{H^+}}{4}\right] + P_{HV,G}\otimes\left[\frac{f_{W^+}}{2}+\frac{f_{W_3}}{4}\right]\Bigg\}, \tag{3.67}$$

$$\left[\Delta_{H,2}\, q\frac{\partial}{\partial q}\frac{f_{H^0}}{\Delta_{H,2}}\right]_2 = \frac{\alpha_2}{\pi}\Bigg\{P^R_{HH,G}\otimes\left[\frac{f_{H^+}}{2}+\frac{f_{H^0}}{4}\right] + P_{HV,G}\otimes\left[\frac{f_{W^-}}{2}+\frac{f_{W_3}}{4}\right]\Bigg\}. \tag{3.68}$$

The virtual splitting functions are

$$P^V_{f,2}(q) = -\frac{3}{4}\left[\int_0^{1-\frac{m_V}{q}} z\,\mathrm{d}z\, P^R_{ff,G}(z)+\int_0^1 z\,\mathrm{d}z\, P^R_{Vf,G}(z)\right], \tag{3.69}$$

$$P^V_{W,2}(q) = -2\int_0^{1-\frac{m_V}{q}} z\,\mathrm{d}z\, P^R_{VV,G}(z) - n_g(N_C+1)\int_0^1 z\,\mathrm{d}z\, P^R_{fV,G}(z) - \int_0^1 z\,\mathrm{d}z\, P^R_{HV,G}(z), \tag{3.70}$$

$$P^V_{H,2}(q) = -\frac{3}{4}\left[\int_0^{1-\frac{m_V}{q}} z\,\mathrm{d}z\, P^R_{HH,G}(z)+\int_0^1 z\,\mathrm{d}z\, P^R_{VH,G}(z)\right], \tag{3.71}$$

from which the Sudakov factor can be constructed using Eq. (3.28).

An important aspect of the SU(2) evolution equations is that, contrary to the other gauge groups, the dependence on the ratio m_V/q does not cancel between the real and virtual splitting functions. As an example, consider the evolution equation for an up-type fermion, given on the first line of Eq. (3.63), with the virtual contribution given by the first

line of Eq. (3.69). The sum of the contributions of real and virtual splitting functions is given by

$$\frac{\alpha_2}{\pi}\int_0^{1-\frac{m_V}{q}} \mathrm{d}z\,\frac{1}{4}P^R_{ff,G}(z)\left[2\,f_{d_L}(x/z)+f_{u_L}(x/z)-3\,f_{u_L}(x)\right]+\dots\,, \tag{3.72}$$

where $\dots$ represents less singular terms. Thus, the SU(2) breaking in the proton, which renders $f_u(z)\neq f_d(z)$, gives rise to a logarithmic dependence on m_V/q, which leads to a double-logarithmic dependence upon integration over q. As we will see later, the effect of this dependence is to double-logarithmically suppress the SU(2) breaking effects at high energies.

$I = Y$: Yukawa interactions

The interaction of Higgs particles with fermions is described by the Yukawa interactions. In this work we only keep the top Yukawa coupling, setting all others to zero. This gives the following couplings

$$C_{q_L^3 t_R,Y}=C_{H^0 t_R,Y}=C_{H^+ t_R,Y}=C_{t_R q_L^3,Y}=C_{\bar{H}^0 t_L,Y}=C_{H^- b_L,Y}=1\,, \tag{3.73}$$

where q_L^3 denotes either the left-handed top or bottom quark. We furthermore need

$$C_{t^R H^0,Y}=C_{t^R H^+,Y}=C_{t^L \bar{H}^0,Y}=C_{b_L H^-,Y}=N_C\,. \tag{3.74}$$

This gives contributions to the top quark PDFs, as well as the left-handed bottom PDF:

$$\left[\Delta_{q_L^3,Y}\,q\frac{\partial}{\partial q}\frac{f_{t_L}}{\Delta_{q_L^3,Y}}\right]_Y = \frac{\alpha_Y}{\pi}\left\{P^R_{ff,Y}\otimes f_{t_R}+N_C P_{fH,Y}\otimes f_{\bar{H}^0}\right\}, \tag{3.75}$$

$$\left[\Delta_{t_R,Y}\,q\frac{\partial}{\partial q}\frac{f_{t_R}}{\Delta_{t_R,Y}}\right]_Y = \frac{\alpha_Y}{\pi}\left\{P^R_{ff,Y}\otimes [f_{t_L}+f_{b_L}]+N_C P_{fH,Y}\otimes [f_{H^0}+f_{H^+}]\right\}, \tag{3.76}$$

$$\left[\Delta_{q_L^3,Y}\,q\frac{\partial}{\partial q}\frac{f_{b_L}}{\Delta_{q_L^3,Y}}\right]_Y = \frac{\alpha_Y}{\pi}\left\{P^R_{ff,Y}\otimes f_{t_R}+N_C P_{fH,Y}\otimes f_{H^-}\right\}. \tag{3.77}$$

It also contributes to the evolution of the Higgs bosons:

$$\left[\Delta_{H,Y}\,q\frac{\partial}{\partial q}\frac{f_{H^+}}{\Delta_{H,Y}}\right]_Y = \frac{\alpha_Y}{\pi}P^R_{Hf,Y}\otimes\left[f_{t_R}+f_{\bar{b}_L}\right], \tag{3.78}$$

$$\left[\Delta_{H,Y}\,q\frac{\partial}{\partial q}\frac{f_{H^0}}{\Delta_{H^0,Y}}\right]_Y = \frac{\alpha_Y}{\pi}P^R_{Hf,Y}\otimes\left[f_{t_R}+f_{\bar{t}_L}\right]. \tag{3.79}$$

The Sudakov factors can be obtained using Eq. (3.28) with

$$P^V_{q_L^3,Y}(q)=\frac{1}{2}P^V_{t_R,Y}(q)=-\int_0^1 z\,\mathrm{d}z\,P^R_{ff,Y}(z)-\int_0^1 z\,\mathrm{d}z\,P^R_{Hf,Y}(z)\,, \tag{3.80}$$

$$P^V_{H,Y}(q)=-2N_C\int_0^1 z\,\mathrm{d}z\,P^R_{fH,Y}(z)\,. \tag{3.81}$$

$I = M$: Mixed $B - W_3$ interactions

Finally, we need to consider the evolution involving the mixed BW boson PDF. The non-vanishing couplings are

$$C_{BWf_u,M} = -C_{BWf_d,M} = 2\frac{Y_f}{2}, \tag{3.82}$$

$$C_{f_uBW,M} = -C_{f_dBW,M} = N_f\frac{Y_f}{2}, \tag{3.83}$$

where f_u and f_d represent the up- and down-type left-handed fermions and anti-fermions of all generations. Since $Y_{\bar{f}} = -Y_f$ and $T_{3\bar{f}} = -T_{3f}$, the couplings for fermions and anti-fermions are identical. The factor of 2 in the first line comes from our definition of f_{BW} as the sum of BW and WB contributions. The diagonal coefficients $C_{f_uf_u,M}$ and $C_{f_df_d,M}$ are zero because there is no vector boson with both U(1) and SU(2) interactions. For the same reason, there are no Sudakov factors associated with the mixed interaction. The couplings involving the Higgs bosons are

$$C_{BWH^+,M} = -C_{BWH^0,M} = \frac{1}{2}, \tag{3.84}$$

$$C_{H^+BW,M} = -C_{H^0BW,M} = \frac{1}{4}, \tag{3.85}$$

where, as for the fermions, the same relations hold for the charge-conjugate states.

Plugging these into the general evolution equation gives

$$\left[q\frac{\partial}{\partial q}f_{f_u}\right]_M = \frac{\alpha_M}{\pi}\frac{Y_f}{2}N_f P^R_{fV,G}\otimes f_{BW}, \tag{3.86}$$

$$\left[q\frac{\partial}{\partial q}f_{f_d}\right]_M = -\frac{\alpha_M}{\pi}\frac{Y_f}{2}N_f P^R_{fV,G}\otimes f_{BW}, \tag{3.87}$$

$$\begin{aligned}\left[q\frac{\partial}{\partial q}f_{BW}\right]_M = \frac{\alpha_M}{\pi}\Big[&\sum_{f_u} Y_f P^R_{Vf,G}\otimes f_{f_u} - \sum_{f_d} Y_f P^R_{Vf,G}\otimes f_{f_d} \\ &+\frac{1}{2}\sum_{h_u} P^R_{VH,G}\otimes f_{h_u} - \frac{1}{2}\sum_{h_d} P^R_{VH,G}\otimes f_{h_d}\Big],\end{aligned} \tag{3.88}$$

$$\left[q\frac{\partial}{\partial q}f_{h_u}\right]_M = \frac{\alpha_M}{\pi}\frac{1}{4}P^R_{HV,G}\otimes f_{BW}, \tag{3.89}$$

$$\left[q\frac{\partial}{\partial q}f_{h_d}\right]_M = -\frac{\alpha_M}{\pi}\frac{1}{4}P^R_{HV,G}\otimes f_{BW}. \tag{3.90}$$

As already discussed, the mixed gauge field PDF f_{BW} has Sudakov factors associated with the U(1) and SU(2) interactions, given by Eq. (3.28). Since there is no corresponding real emission term in the evolution equation for f_{BW}, it evolves double-logarithmically and is suppressed at high scales relative to the unmixed PDFs.

3.2 Implementation details

Our treatment assumes that the SM PDFs at very high energies can be obtained by smoothly matching the broken and unbroken symmetry regimes at a matching scale $q_V \sim m_V$, which in practice we take to be 100 GeV. Our input PDFs at 100 GeV are obtained as follows. We take the CT14qed PDF set [66] at 10 GeV and replace the photon PDF by that of the LUXqed set [67]. We do not use the CT14qed photon because the LUXqed photon, while being consistent with CT14qed, has much smaller uncertanties and a smoother x dependence. The LUXqed PDF set combines the PDF4LHC15_nnlo_100 parton set [68] with a determination of the photon PDF from structure function and elastic form factor fits in electron-proton scattering. However, we do not use the LUXqed partons, because being NNLO they are not positive-definite, which we require for our LO treatment and is satisfied by CT14qed.

We evolve this hybrid CT14-LUX PDF set from 10 to 100 GeV using leading-order QCD plus QED evolution, which incidentally generates the charged leptons. The resulting parton, photon and lepton PDFs form our input to the unbroken SM evolution upwards from 100 GeV. The input left- and right-handed fermion PDFs are identical. The input W^3, B and mixed B/W^3 PDFs are determined by the photon (and the absence of the Z^0) at the matching scale according to Eq. (3.7). The remaining vector boson, neutrino and Higgs PDFs are all generated dynamically starting from zero at the matching scale.

The equations given in Sections 3.1 completely define the evolution of all parton distribution functions in the unbroken symmetry regime. However, as already explained, one can rewrite the equations slightly to make them more amenable to a numerical implementation. First, switching to a basis of states with well-defined isospin decouples the set of 52 equations to some degree. In this new basis another transformation eliminates the double logarithmic sensitivity to the ratio m_V/q. Second, by combining the virtual and real splitting functions into +-distributions, one can reduce numerical sensitivity to the cutoff of the z integrations. We will now discuss these simplifications in turn.

Switching to a basis of conserved quantum numbers

As we already explained in Section 3.1, the set of 52 evolution equations can be decoupled to some degree by switching to a basis of well-defined isospin **T** and CP. Writing a fermion PDF with **T** and CP as $f_i^{\mathbf{T}\mathrm{CP}}$, we write the left-handed fermions as

$$f_{f_L}^{0+} = \frac{1}{4}\left(f_{u_L} + f_{d_L} + f_{\bar{d}_L} + f_{\bar{u}_L}\right) , \qquad f_{f_L}^{1+} = \frac{1}{4}\left(f_{u_L} - f_{d_L} - f_{\bar{d}_L} + f_{\bar{u}_L}\right) , \tag{3.91}$$

$$f_{f_L}^{0-} = \frac{1}{4}\left(f_{u_L} + f_{d_L} - f_{\bar{d}_L} - f_{\bar{u}_L}\right) , \qquad f_{f_L}^{1-} = \frac{1}{4}\left(f_{u_L} - f_{d_L} + f_{\bar{d}_L} - f_{\bar{u}_L}\right) , \tag{3.92}$$

where u_L and d_L refer to left-handed up- and down-type fermions. Right-handed fermions are given by

$$f_{f_R}^{0+} = \frac{1}{2}\left(f_{f_R} + f_{\bar{f}_R}\right) , \qquad f_{f_R}^{0-} = \frac{1}{2}\left(f_{f_R} - f_{\bar{f}_R}\right) . \tag{3.93}$$

The SU(3) and U(1) boson PDFs have $\mathbf{T} = 0$, CP $= +$

$$f_g^{0+} = f_g\,, \qquad\qquad f_B^{0+} = f_B\,, \tag{3.94}$$

while the SU(2) boson PDFs can have $\mathbf{T} = 0, 1, 2$ with respectively CP $= +, -, +$

$$f_W^{0+} = \frac{1}{3}\left(f_{W^+} + f_{W^-} + f_{W^0}\right), \quad f_W^{1-} = \frac{1}{2}\left(f_{W^+} - f_{W^-}\right), \tag{3.95}$$

$$f_W^{2+} = \frac{1}{6}\left(f_{W^+} + f_{W^-} - 2f_{W^0}\right). \tag{3.96}$$

The mixed BW boson state is a combination of 0^- and 1^- and therefore its PDF has $\mathbf{T} = 1$, CP $= +$

$$f_{BW}^{1+} = f_{BW}\,. \tag{3.97}$$

For the Higgs boson, one writes similarly to the fermions

$$f_H^{0+} = \frac{1}{4}\left(f_{H^+} + f_{H^0} + f_{\bar{H}^0} + f_{H^-}\right), \quad f_H^{1+} = \frac{1}{4}\left(f_{H^+} - f_{H^0} - f_{\bar{H}^0} + f_{H^-}\right), \tag{3.98}$$

$$f_H^{0-} = \frac{1}{4}\left(f_{H^+} + f_{H^0} - f_{\bar{H}^0} - f_{H^-}\right), \quad f_H^{1+} = \frac{1}{4}\left(f_{H^+} - f_{H^0} + f_{\bar{H}^0} - f_{H^-}\right). \tag{3.99}$$

In terms of these states the longitudinal vector boson and Higgs PDFs are then, using Eq. (3.15),

$$f_{W_L^+} = f_H^{0+} + f_H^{1+} + f_H^{0-} + f_H^{1-}\,, \tag{3.100}$$

$$f_{W_L^-} = f_H^{0+} + f_H^{1+} - f_H^{0-} - f_H^{1-}\,, \tag{3.101}$$

$$f_{Z_L} = f_h = f_H^{0+} - f_H^{1+}\,. \tag{3.102}$$

Cancellation of double-logarithmic dependence in evolution equations

In the $\{\mathbf{T}, \mathrm{CP}\}$ basis the singular contributions to the evolution equations (those that are proportional to the splitting functions $P^R_{ff,G}(z)$, $P^R_{VV,G}(z)$ and $P^R_{HH,G}(z)$, which diverge in the limit $z \to 1$) are diagonal,

$$\left[\Delta_{i,I}\, q\frac{\partial}{\partial q}\frac{f_i^{\mathbf{T}\mathrm{CP}}}{\Delta_{i,I}}\right]_I = \frac{\alpha_I}{\pi} D_{i,I}^{\mathbf{T}\mathrm{CP}} P^R_{ii,I} \otimes f_i^{\mathbf{T}\mathrm{CP}} + \dots\,, \tag{3.103}$$

such that the PDF multiplying the divergent splitting function is the same as that appearing on the left-hand side. Here, as in $f_i^{\mathbf{T}CP}$, the label i now refers to a parton species f, V, H rather than a particular parton. Recalling that the Sudakov factor takes the form

$$\begin{aligned}\Delta_{i,I}(q) &= \exp\left[\int_{q_V}^{q}\frac{\mathrm{d}q'}{q'}\frac{\alpha_I(q')}{\pi}P^V_{i,I}(q')\right] \\ &= \exp\left[-C_{i,I}\int_{q_V}^{q}\frac{\mathrm{d}q'}{q'}\frac{\alpha_I(q')}{\pi}\int_0^{z^{ii,I}_{\max}(q)} z\,\mathrm{d}z\, P^R_{ii,I}(z) + \dots\right],\end{aligned} \tag{3.104}$$

where ... represents less divergent terms, and

$$C_{i,I} = \sum_{k\in i} C_{kl,I} \,\text{for}\, l \in i\,, \tag{3.105}$$

where k and l are particular partons, we have

$$\begin{aligned}\left[q\frac{\partial}{\partial q} f_i^{\mathbf{T}\mathrm{CP}}\right]_I &= \frac{\alpha_I}{\pi}\left[D_{i,I}^{\mathbf{T}\mathrm{CP}} P_{ii,I}^R \otimes f_i^{\mathbf{T}\mathrm{CP}} + P_{i,I}^V f_i^{\mathbf{T}\mathrm{CP}}\right] + \dots\,, \\ &= \frac{\alpha_I}{\pi}\left[D_{i,I}^{\mathbf{T}\mathrm{CP}} P_{ii,I}^+ \otimes f_i^{\mathbf{T}\mathrm{CP}} + \left(1 - \frac{D_{i,I}^{\mathbf{T}\mathrm{CP}}}{C_{i,I}}\right) P_{i,I}^V f_i^{\mathbf{T}\mathrm{CP}}\right] + \dots\,,\end{aligned} \tag{3.106}$$

where

$$\begin{aligned} P_{ii,I}^+ \otimes f_i &\equiv P_{ii,I}^R \otimes f_i + \frac{P_{i,I}^V}{C_{i,I}} f_i \\ &= \int_0^{z_{\max}^{ii,I}(q)} \mathrm{d}z\, \left[P_{ii,I}^R(z)\theta(z>x) f(x/z,q) - z P_{ii,I}^R(z) f(x,q)\right] + \dots\,. \end{aligned} \tag{3.107}$$

The +-prescription defined by Eq. (3.107) regulates the divergence in the integrand as $z \to 1$ and therefore if we define the modifying factor

$$\begin{aligned} F_{i,I}^{\mathbf{T}\mathrm{CP}}(q) &= \exp\left[\left(1 - \frac{D_{i,I}^{\mathbf{T}\mathrm{CP}}}{C_{i,I}}\right)\int_{q_V}^{q} \frac{\mathrm{d}q'}{q'}\frac{\alpha_I(q')}{\pi} P_{i,I}^V(q')\right] \\ &= \left[\Delta_{i,I}(q)\right]^{1 - D_{i,I}^{\mathbf{T}\mathrm{CP}}/C_{i,I}}\,, \end{aligned} \tag{3.108}$$

then the evolution equation (3.103) becomes

$$\left[F_{i,I}^{\mathbf{T}\mathrm{CP}}\, q\frac{\partial}{\partial q}\frac{f_i^{\mathbf{T}\mathrm{CP}}}{F_{i,I}^{\mathbf{T}\mathrm{CP}}}\right]_I = \frac{\alpha_I}{\pi} D_{i,I}^{\mathbf{T}\mathrm{CP}} P_{ii,I}^+ \otimes f_i^{\mathbf{T}\mathrm{CP}} + \dots\,, \tag{3.109}$$

with no logarithmic dependence on m_V/q on the right-hand side.

For all interactions except SU(2), one can show that $D_{i,I}^{\mathbf{T}\mathrm{CP}} = C_{i,I}$, so that the modifying factor (3.108) is unity[7]. For SU(2) we have explicitly:[8]

$$C_{f,2} = C_{H,2} = \frac{3}{4}\,, \quad C_{V,2} = 2\,, \tag{3.110}$$

[7]For the U(1) interaction one has $D_{i,1}^{\mathbf{T}\mathrm{CP}} = C_{i,1} = 0$, and we choose to set the modifying factor to 1 in this case.

[8]Here we have used the numerical values for the Casimir operator eigenvalues for the corresponding SU(2) representations, $C_F^{\mathrm{SU}(2)} = 3/4$, $C_A^{\mathrm{SU}(2)} = 2$.

while

$$D_{f,2}^{0\pm} = D_{H,2}^{0\pm} = \frac{3}{4}\,, \quad D_{f,2}^{1\pm} = D_{H,2}^{1\pm} = -\frac{1}{4}\,, \tag{3.111}$$

$$D_{V,2}^{0+} = 2\,, \quad D_{V,2}^{1-} = 1\,, \quad D_{V,2}^{2+} = -1\,, \tag{3.112}$$

so that

$$F_{f,2}^{0\pm} = F_{H,2}^{0\pm} = 1\,, \quad F_{f/H,2}^{1\pm} = \Delta_{f/H,2}^{4/3}\,, \tag{3.113}$$

$$F_{V,2}^{0+} = 1\,, \quad F_{V,2}^{1-} = \Delta_{V,2}^{1/2}\,, \quad F_{V,2}^{2+} = \Delta_{V,2}^{3/2}\,. \tag{3.114}$$

For the mixed PDF f_{BW} we have $D_{BW,2}^{1+} = 0$ and therefore

$$F_{BW,2}^{1+} = \Delta_{BW,2} = \Delta_{V,2}^{1/2} = F_{V,2}^{1-} \tag{3.115}$$

The equations finally used to evolve the PDFs in the conserved-quantum-number basis are given in Appendix A.

3.3 Results

We begin by showing how the PDFs of strongly interacting particles are changed by including the evolution of the full Standard Model. Figure 3.1 shows results on the evolution of left- and right-handed quark PDFs, shown solid and dashed respectively, normalized to their values assuming pure QCD evolution. In each plot we show the results at three different scales, namely $q = 10^4$ GeV, $q = 10^6$ GeV and $q = 10^8$ GeV. The values of 10^6 and 10^8 GeV are of course far away from energy scales one can reach at any collider in the near or distant future. However, showing the results at such unattainable values helps to illustrate their approach to asymptotic behavior.

All the light quarks (and antiquarks, not shown) evolve to lower values compared to pure QCD at small x, due to an overall loss of energy to the electroweak gauge bosons through the additional splittings $q \to qW$ and $q \to qB$. At higher x values, the up and down quarks (top row) exhibit different behaviors, with the left-handed up PDF evolving more rapidly to lower values compared to pure QCD, while the down quark eventually evolves to higher values. This is because the left-handed up and down distributions evolve towards each other, their difference being double-logarithmically suppressed at high scales. The right-handed quark PDFs have no double-logarithmic component and evolve to slightly lower values than pure QCD, due to energy loss through the additional splitting $q_R \to q_R B$.

The asymmetry between left-handed charm and strange quarks also evolves double-logarithmically towards zero, primarily through a more rapid decrease of the strange PDF. At high x the behavior is more complicated because the input CT14qed charm PDF is larger than the strange above $x \sim 0.7$. The right-handed quarks behave qualitatively the same as those of the first generation.

The left-handed top and bottom quarks also must evolve towards equal values, which in this case means that the top has higher values than in pure QCD, while the bottom evolution looks similar to strange, relative to pure QCD. The right-handed b-quark behaves qualitatively like the right-handed quarks of the first and second generation, while the right-handed top quark, being generated purely dynamically, behaves differently at large x. Since the right-handed top has vanishing initial condition, the splitting $t_R \to t_R B$, which would decrease the PDF, is sub-dominant compared to the process $B \to t_R \bar{t}_R$. This means that at large x the right-handed top PDF is increased, rather than decreased.

The effect on the gluon PDF is shown in last row of Fig. 3.1. While the effects are quite small up to $q \sim 10^4$ GeV, at larger scales the back-reaction from the changing quark PDFs is affecting the gluon PDF at an appreciable level.

It is interesting to study how rapidly electroweak symmetry is restored. To illustrate this, we show the asymmetry

$$A^{q_L} = \frac{f_{u_L} - f_{d_L}}{f_{u_L} + f_{d_L}}, \tag{3.116}$$

compared to the result if only QCD evolution were turned on. This asymmetry ratio is shown in Figure 3.2 for the three generation of quarks as a function of q, for various values of x. For all generations the asymmetry decreases as q gets larger, driving the PDFs of the different isospin states towards each other. The onset of the deviation from pure QCD is in the range $1 - 10$ TeV. The ratio between the full asymmetry and the result using only QCD evolution is given by

$$A^{q_L}(x,q) \sim [\Delta_{f,2}(q)]^{4/3}\, A^{q_L}_{\rm QCD}(x,q) \tag{3.117}$$

where $\Delta_{f,2}(q)$ is the fermion Sudakov factor, as given in Eq. (3.108), independent of the generation.

Next, we study the size of the PDFs of particles not charged under the strong interaction. Since these PDFs are only generated by emissions due to the U(1), SU(2) or Yukawa interactions, they are vanishing at all scales if one is including only SU(3) evolution. The only exception is the photon, which has a non-vanishing initial condition at $q = 100$ GeV. Figure 3.3 shows results on the electroweak boson PDFs normalized to the gluon PDF, both evolved using the full Standard Model. One can see that the electroweak gauge boson PDFs become a significant fraction of the gluon PDF, especially at large values of x. The photon PDF is the largest mainly because it has a non-zero input. The PDF for the W^+ boson is initially larger than the W^- boson PDF at large x because the W^+ is mainly generated through emissions from the up-quark, whose PDF is larger than the down-quark which mainly generates the W^-. Since the difference between W^+ and W^- has isospin 1, the W^+ evolves more slowly and the W^- more rapidly, so that they approach each other at high q. At low x they are more similar as are the up-quark and down-quark PDFs. The Z^0 PDF is similar to the W^+ but it is smaller at low x and larger at large x. The mixed γZ PDF is small and positive at small x and negative at large x. There is no constraint to be positive definite for a mixed PDF as it is the product of two amplitudes rather than the square modulus of one. Its absolute value becomes very large at large x and q.

We also show the PDFs for the longitudinally polarized gauge bosons, the Higgs boson, the mixed PDF between the Higgs and the Z_L and the leptons. The Z_L PDF is the same as the Higgs in our approximation, see Eq. (3.15), so we do not make a separate plot for it. The boson PDFs are shown in Fig. 3.4, and the leptons in Fig. 3.5, both normalized to the gluon. Both are expected to be much smaller than the transverse vector boson PDFs, because they are generated via a second order effect of emission from the vector bosons and via Yukawa emission from the top and bottom quarks, which are much smaller than the up and down quarks. The mixed PDF is even smaller because it is generated by the asymmetry between transverse W^+ and W^- PDFs and the top and anti-top PDFs. The W_L^+ and W_L^- PDFs are very similar, for the same reason.

As a final result, we study several parton luminosities, choosing a future 100 TeV pp collider as a reference. While the energy scales that can be reached at such a collider are not quite large enough to get $\mathcal{O}(1)$ effects, the effects of the full Standard Model evolution are still numerically relevant. In Figure 3.6 we show the $q_L\bar{q}_L$ luminosities for the six different quark flavors, normalized to their values if only QCD evolution is taken into account. One can see that all except the $t\bar{t}$ luminosity are reduced appreciably from their values if only QCD evolution were taken into account. This will affect searches for Z'-like particles at a future 100 TeV collider. The $d\bar{d}$ luminosity is decreasing more slowly as the double-logarithmic evolution drives it larger than QCD at high x (see Fig. 3.1).

We also show selected luminosities of vector bosons combined with quarks, normalized to the average of the $u\bar{u}$ and $d\bar{d}$ luminosities. One can see that luminosities involving one transverse vector boson become of comparable magnitude to the $q\bar{q}$ luminosities. Luminosities involving the longitudinal gauge and Higgs bosons are much smaller.

Finally, to illustrate the uncertainties associated with subleading terms, we show in Tables 3.2 and 3.3 the dependence of some integrated PDFs (momentum fractions) on the infrared cutoff m_V and matching scale q_V. We see that there are variations in the electroweak PDFs of the order of $\pm 10\%$ at 10 TeV and 5% at 100 TeV for the ranges of parameters indicated. The relative variations in the light quark PDFs are smaller as they are dominated by QCD evolution. There are of course in addition the usual uncertainties associated with the input PDFs and higher-order QCD corrections.

m_V/GeV	q_V/GeV	u_L	t_L	W_T^+	W_T^-	e_L^-	ν_e	h
100	100	8.51	0.43	0.46	0.33	0.0019	0.0012	0.0026
50	100	8.42	0.43	0.46	0.34	0.0019	0.0012	0.0027
50	200	8.48	0.44	0.39	0.29	0.0017	0.0009	0.0025
100	200	8.56	0.43	0.39	0.29	0.0017	0.0009	0.0024
200	200	8.64	0.42	0.39	0.28	0.0017	0.0009	0.0024

Table 3.2: Momentum fractions (%) carried by various parton species at scale $q = 10$ TeV.

m_V/GeV	q_V/GeV	u_L	t_L	W_T^+	W_T^-	e_L^-	ν_e	h
100	100	7.53	0.56	0.64	0.50	0.0031	0.0025	0.0061
50	100	7.43	0.61	0.63	0.51	0.0031	0.0026	0.0062
50	200	7.48	0.61	0.58	0.47	0.0028	0.0021	0.0059
100	200	7.58	0.60	0.58	0.46	0.0028	0.0021	0.0055
200	200	7.68	0.59	0.58	0.45	0.0028	0.0020	0.0054

Table 3.3: Momentum fractions (%) carried by various parton species at scale $q = 100$ TeV.

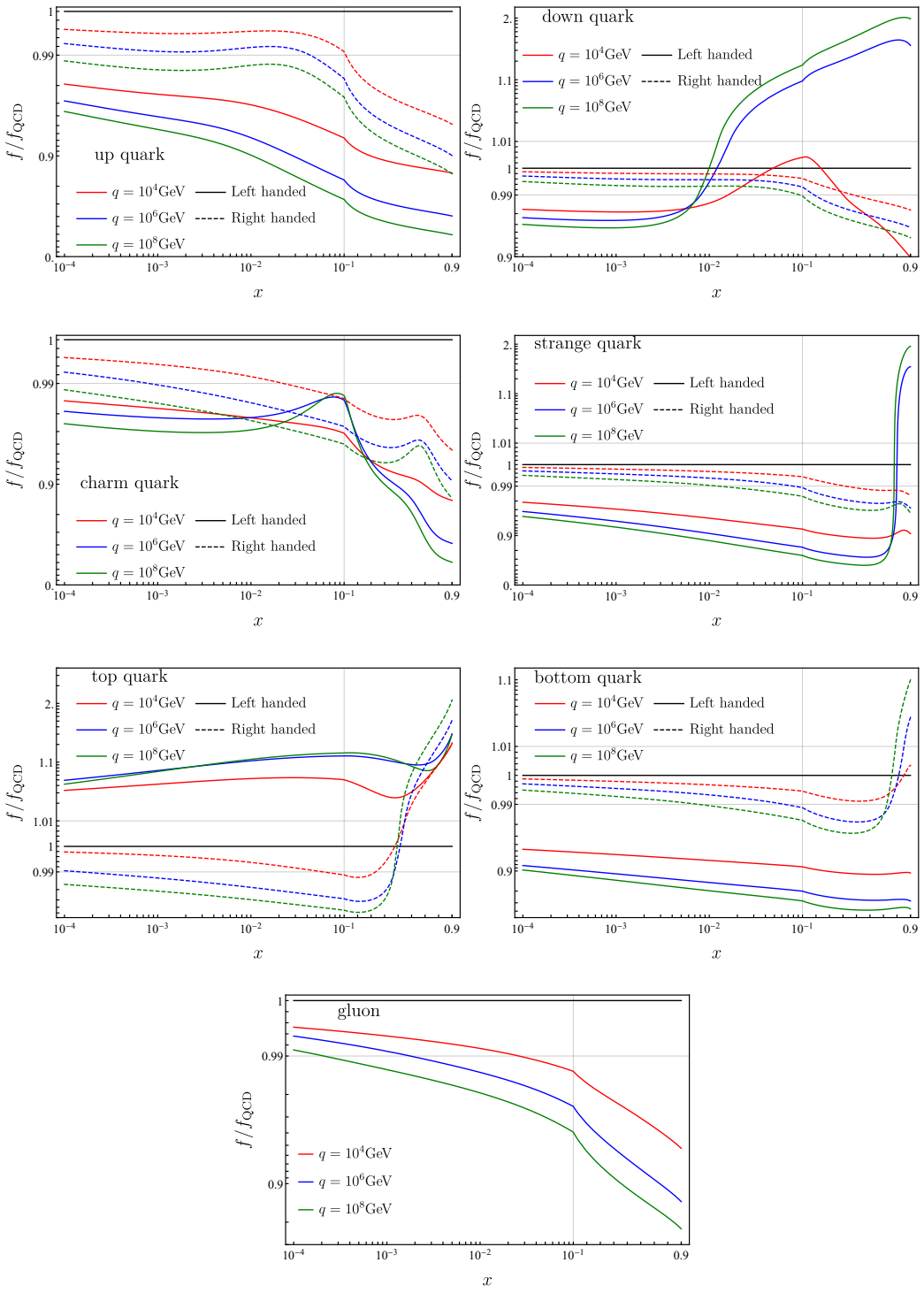

Figure 3.1: Quark and gluon PDFs in the full unbroken SM, divided by their values assuming pure QCD evolution only. Left- and right-handed quark chiralities are solid and dashed, respectively. The thin gray lines show where the scales on the x- and/or y-axes switch between linear and logarithmic.

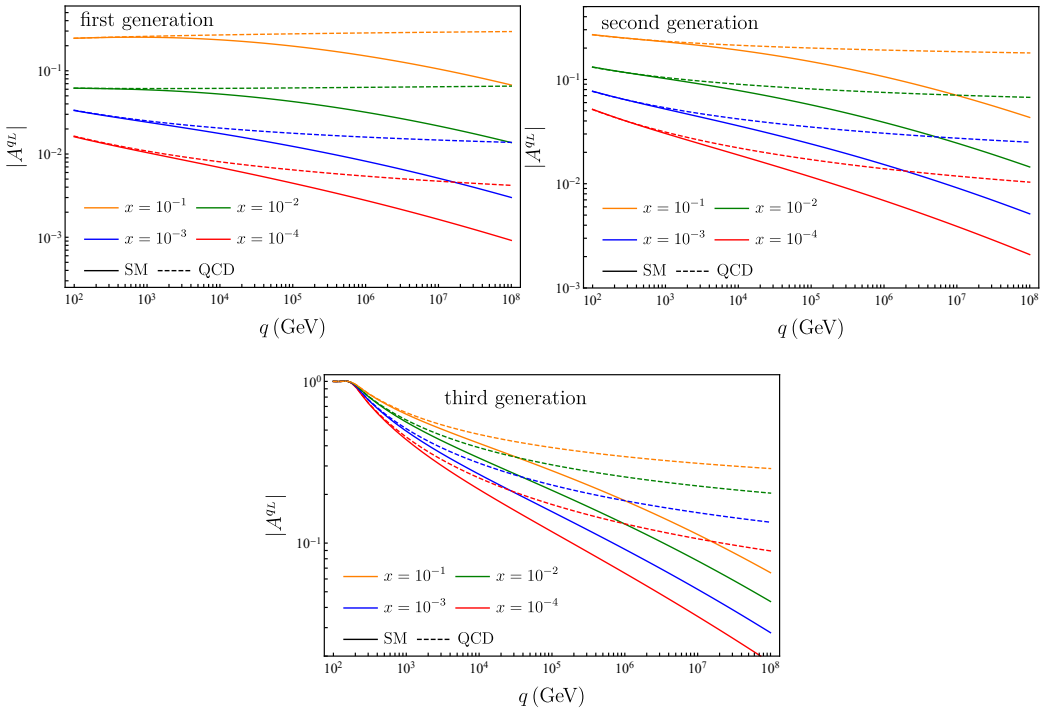

Figure 3.2: Asymmetry between up-isospin and down-isospin left-handed quark PDFs, defined in Eq. (3.116), in the full unbroken SM, compared to the result when only QCD evolution is included.

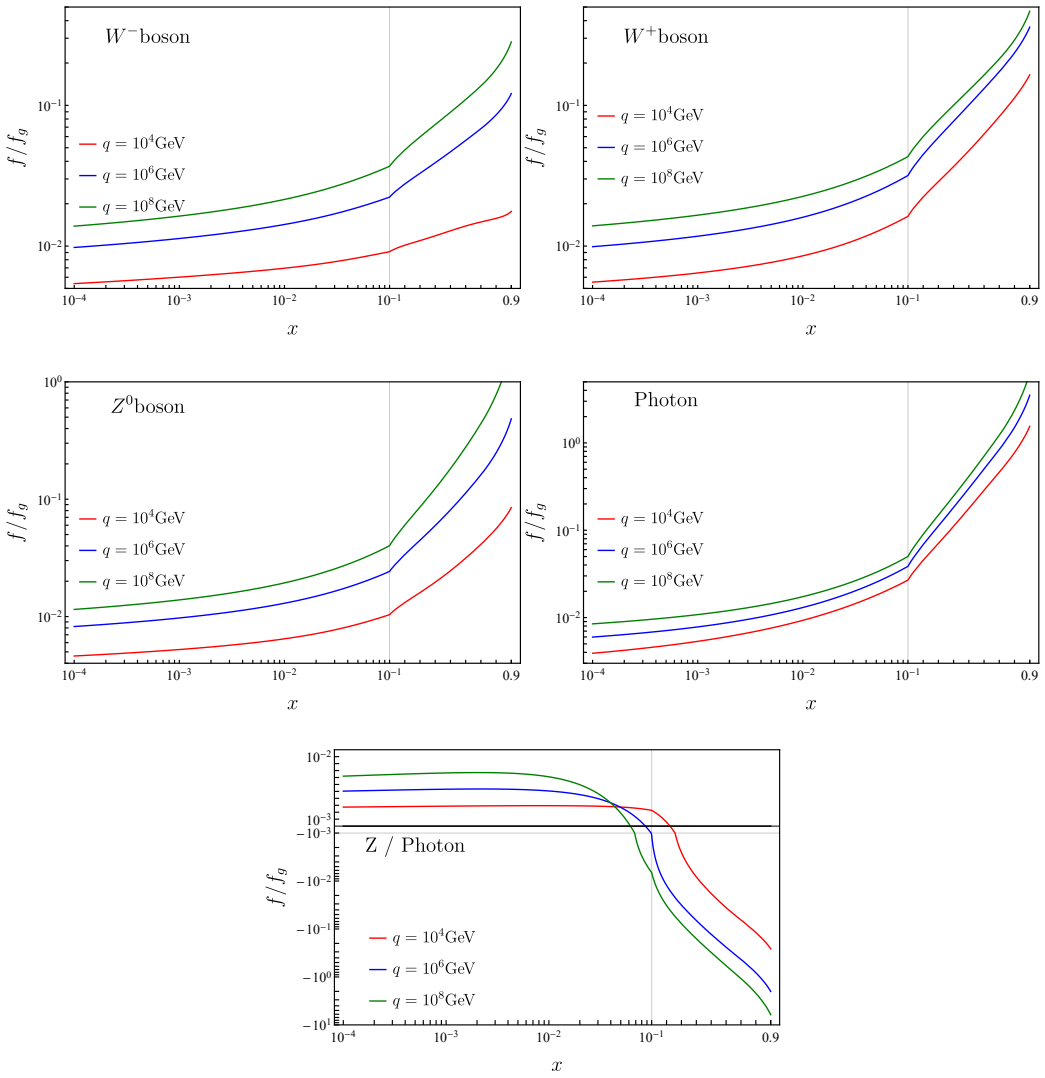

Figure 3.3: Electroweak bosons PDF normalized by the gluon PDF. The thin gray lines show where the scales on the x- and/or y-axes switch between linear and logarithmic.

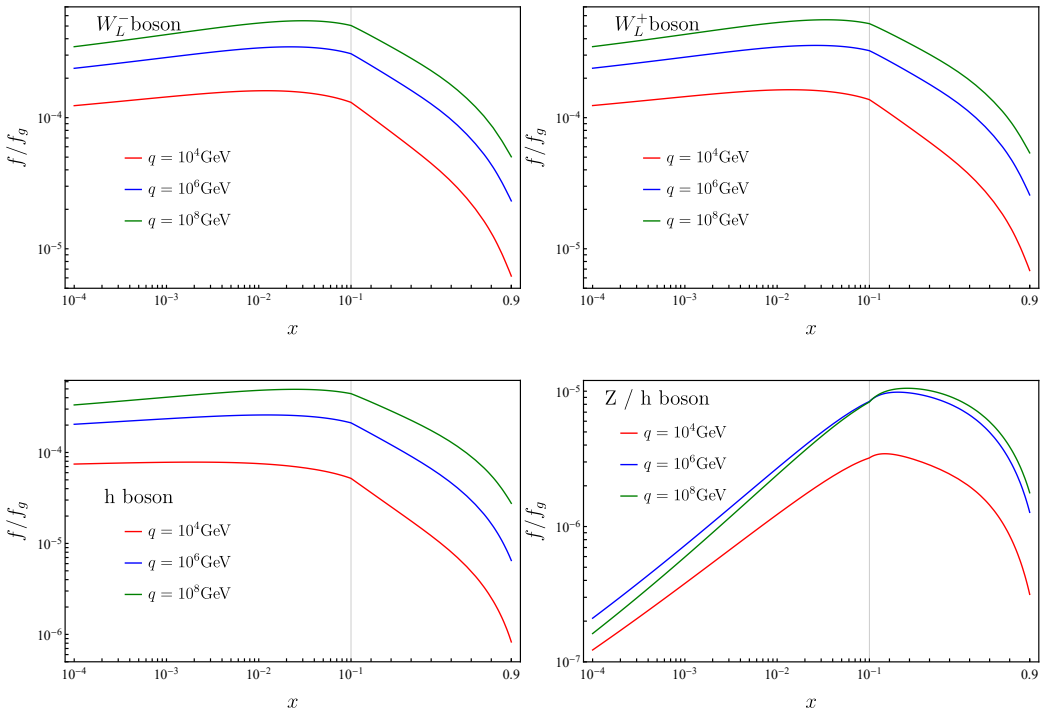

Figure 3.4: Longitudinal gauge and Higgs bosons PDFs normalized by the gluon PDF. The Z_L PDF is the same as the h PDF. The hZ_L PDF is purely imaginary and we show the result divided by i. The thin gray line shows where the scales on the x- and/or y-axes switch between linear and logarithmic.

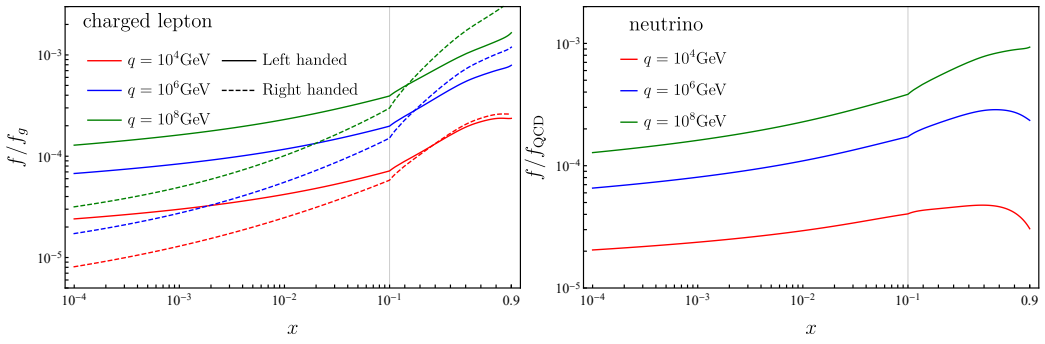

Figure 3.5: First generation lepton PDFs normalized by the gluon PDF. Since we treat leptons as massless, and all leptons have the same initial condition, the results for the other 2 generations are identical. The thin gray line shows where the scales on the x- and/or y-axes switch between linear and logarithmic.

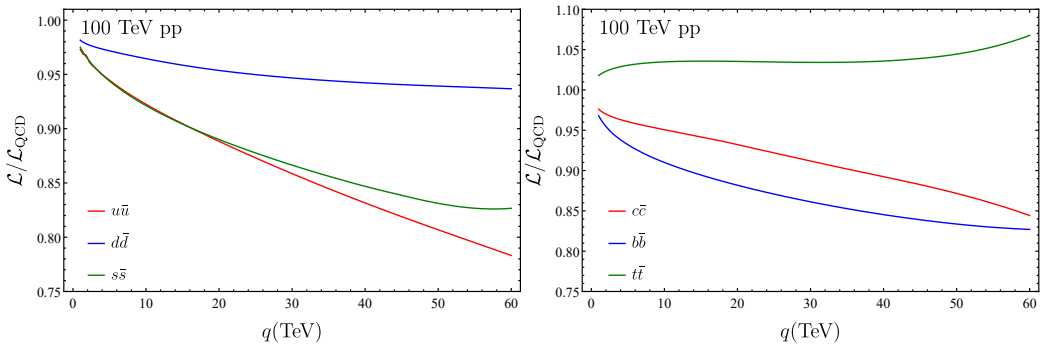

Figure 3.6: Quark anti-quark luminosity in the full unbroken SM, divided by their values assuming pure QCD evolution only.

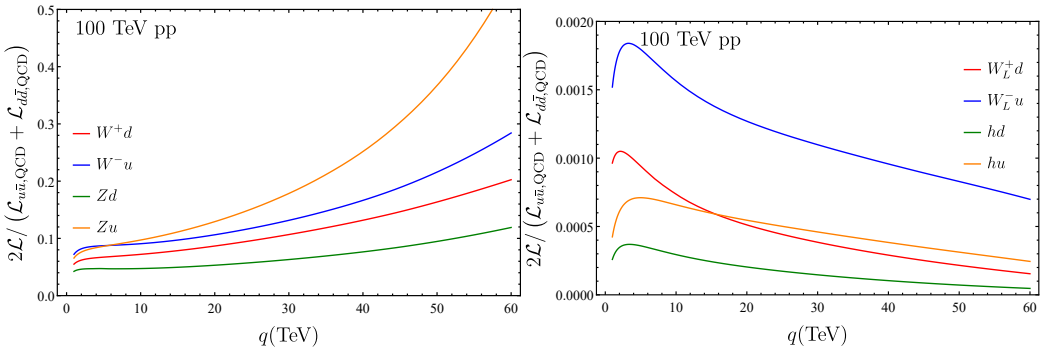

Figure 3.7: Vq and Hq luminosity in the full unbroken SM, divided by the average of $u\bar{u}$ and $d\bar{d}$ luminosity assuming pure QCD evolution only.

Chapter 4

Combining initial-state resummation with fixed-order calculations of electroweak corrections

In the previous chapter, we developed a set of parton distribution function valid at very high energy when we can neglect the electroweak symmetry breaking. It corresponds to resum the initial-state electroweak corrections. It is interesting to combine those corrections with fixed-order calculations in a way that is valid at all energies.

We present a way to resum double logarithms associated with the asymmetry of the initial state, and to match the results with those of fixed-order EW calculations.[1] For this purpose, we will study completely inclusive observables, which are defined to sum over a completely SU(2) symmetric final state. The example we use later in the chapter is inclusive di-lepton production at a pp collider, which is defined to include a lepton-antilepton pair of a given generation and any number of extra gauge bosons in the final state. So to next-to-leading order (NLO) EW accuracy, this process sums over the final states $\ell^+\ell^-(+V)$, $\ell^+\nu_\ell(+V)$, $\bar{\nu}_\ell\ell^-(+V)$, $\bar{\nu}_\ell\nu_\ell(+V)$, where ℓ denotes, for example, the electron and ν_ℓ the electron neutrino and the $(+V)$ denotes the possible addition of a γ, Z or $W^\pm$ boson. Since the final state is SU(2) symmetric, the only SU(2) breaking effect is coming from the fact that the initial state protons are not SU(2) symmetric. The large logarithmic terms from the initial state radiation can be resummed through a DGLAP evolution [57–59] using the interactions of the full Standard Model [12], which was performed recently in [18]. By performing the DGLAP evolution to first order in electroweak effects, one sums all double logarithms and a large class of the single logarithms, namely those coming from the hard collinear parts of the splitting functions. Not included are subleading logarithms such as those coming from precise limits of integration and higher-order corrections to splitting functions and running couplings. This resummation is called leading logarithmic (LL). [2]

[1] For recent examples of NLO EW calculations see [69–73] and references therein.

[2] A similar resummation of final-state logarithms in non-symmetric final states could be performed though

This DGLAP evolution uses $\mathrm{SU}(3) \otimes \mathrm{U}(1)_{\mathrm{em}}$ for scales q less than some matching scale q_V of order m_V, and the full unbroken $\mathrm{SU}(3) \otimes \mathrm{SU}(2) \otimes \mathrm{U}(1)$ for $q > q_V$. Performing this evolution up to the scale $\sqrt{s}$ of the process results in the PDFs

$$f_A^{\mathrm{SM}}(x, \sqrt{s}) \tag{4.1}$$

for all SM parton species A. Given these PDFs, the logarithms are resummed at leading logarithmic accuracy by writing

$$\langle O \rangle_{\mathrm{LL}} = \sum_{AB} \int \mathrm{d}\Phi_n \, O_n(\Phi_n) \, \mathcal{L}_{AB}^{\mathrm{SM}}(x_A, x_B; \sqrt{s}) B_{AB}(\widehat{\Phi}_n) \,, \tag{4.2}$$

where $\widehat{\Phi}_n$ denotes the phase space of the partonic process, $B_{AB}(\widehat{\Phi}_n)$ is the cross section for the process initiated by partons A and B and $\mathrm{d}\Phi_n$ is the phase-space element including their momentum fractions:

$$\mathrm{d}\Phi_n = \mathrm{d}x_A \, \mathrm{d}x_B \, \mathrm{d}\widehat{\Phi}_n \,. \tag{4.3}$$

$O(\Phi_n)$ denotes the value of the given observable calculated from the phase space point Φ_n, and

$$\mathcal{L}_{AB}^{\mathrm{SM}}(x_A, x_B; \sqrt{s}) = f_A^{\mathrm{SM}}(x_A, \sqrt{s}) \, f_B^{\mathrm{SM}}(x_B, \sqrt{s}) \tag{4.4}$$

is the parton luminosity evaluated with the full SM PDFs. Note that since the parton luminosity in the full SM has contributions from initial states not usually present, such as electroweak gauge bosons, one requires knowledge of partonic cross sections that are not usually considered.

Which initial-state partons A and B are required depends on the partonic process (inclusive di-lepton production in our case) and how one counts powers of the coupling constants. We summarize the scaling of the various PDFs with the electroweak coupling in Table 4.1. Gluons obviously do not contribute at the order we are working. One can see that in the strict LL limit, where one only requires to reproduce $\alpha^n \mathrm{L}_s^{2n}$ terms, one only needs to keep quarks in the initial state. However, transverse vector bosons (the photon as well as massive vector bosons) are only suppressed by one power of the logarithm, and their relative contribution grows with increasing partonic center-of-mass energy. This makes them phenomenologically quite relevant and we will keep them in our analysis. Leptons, longitudinal gauge bosons[3] and Higgs bosons are further suppressed, and their contributions will be neglected in the following discussion, although their effects, together with the Yukawa couplings to the top quark, have been kept in the solution to the evolution equations.

DGLAP evolution of electroweak fragmentation functions but will not be implemented here.

[3]Note that longitudinal gauge bosons can become very important in situations where the partonic process is sensitive to non-gauge interactions, for example in Higgs and heavy quark production. In such cases one should include their effects in fixed order. An alternative approach is proposed in [56].

PDF	leading α power	log scaling
q	0	$\alpha^n \mathrm{L}_s^{2n}$
g	0	$\alpha^n \mathrm{L}_s^{n}$
γ	1	$\alpha^n \mathrm{L}_s^{2n-1}$
V_T	1	$\alpha^n \mathrm{L}_s^{2n-1}$
V_L	2	$\alpha^n \mathrm{L}_s^{2n-2}$
ℓ	2	$\alpha^n \mathrm{L}_s^{2n-2}$
h	2	$\alpha^n \mathrm{L}_s^{2n-2}$

Table 4.1: The scaling of the PDFs with the EW coupling constant.

Since the DGLAP evolution assumes the unbroken Standard Model (SM) above the matching scale $q_V \sim m_V$, it drops all terms of order $m_V/\sqrt{s}$, which clearly misses important threshold effects around the electroweak scale.[4] Furthermore, single logarithmic terms of order $\alpha\,\mathrm{L}_s$ are not fully accounted for in the DGLAP evolution. While these effects do not need to be resummed for any scale $\sqrt{s}$ of interest, at first order they can still give a relatively large effect and introduce an uncertainty in the SM PDFs even for $\sqrt{s} \gg q_V$. One way to estimate their importance is to vary the values of q_V and m_V chosen in the DGLAP evolution, and it was shown in [18] that this can give an effect for certain PDFs at the 10% level, even for $\sqrt{s} \sim 10$ TeV.

The threshold effects, as well as the single logarithmic terms, are properly included in any fixed-order EW calculation. This means that one way to obtain a result that includes the resummation of the LL logarithms, threshold effects, as well as single logarithmic terms is to combine a fixed-order EW calculation with the LL resummation. This is accomplished by the simple equation

$$\langle O\rangle_{\mathrm{NLO/LL}} = \langle O\rangle_{\mathrm{NLO}} + \langle O\rangle_{\mathrm{LL}} - \left[\langle O\rangle_{\mathrm{LL}}\right]_\alpha \,. \tag{4.5}$$

Here $\langle O\rangle_{\mathrm{NLO}}$ denotes the fixed-order EW calculation at next-to-leading order, and $\left[\langle O\rangle_{\mathrm{LL}}\right]_\alpha$ denotes the expansion of $\langle O\rangle_{\mathrm{LL}}$ in α up to the same order as included in the fixed-order expansion; in our case that requires an expansion to first order. This term is required to subtract the $O(1)$ and $O(\alpha)$ terms that are double counted between the NLO and the LL result. It can be written as

$$\left[\langle O\rangle_{\mathrm{LL}}\right]_\alpha = \sum_{AB} \int \mathrm{d}\Phi_n\, O_n(\Phi_n)\, \left[\mathcal{L}_{AB}^{\mathrm{SM}}(x_A, x_B; \sqrt{s})\right]_\alpha B_{AB}(\widehat{\Phi}_n)\,, \tag{4.6}$$

where $\left[\mathcal{L}_{AB}^{\mathrm{SM}}(x_A, x_B; \sqrt{s})\right]_\alpha$ is the expansion of the SM parton luminosity.

In summary, to combine a fixed-order EW calculation with the LL resummation of the logarithms one requires only knowledge of the partonic cross sections $B_{AB}(\Phi_n)$ with A, B

[4] Some terms of this nature may be included by using modified splitting functions [56].

including any SM particle (which are already required for the LL resummed result), as well as the expansion of the SM parton luminosity. We perform the calculation of the latter in Section 4.1, where we also study the convergence of the PDFs and parton luminosities in detail. In Section 4.2 we show the numerical impact of adding the LL resummation to a fixed order computation for the example of di-lepton production. We give the results of the required partonic cross sections in Appendix B.

4.1 Standard Model parton luminosities and their expansion

The parton luminosities in the SM, as defined in Eq. (4.4), require PDFs using the full SM evolution. The corresponding DGLAP equations are, in the notation of Chap. 3,[5] to leading order in all coupling constants

$$q\frac{\partial}{\partial q}f_i^{\mathrm{SM}}(x,q) \;=\; \sum_I \frac{\alpha_I(q)}{\pi}\left[P_{i,I}^V(q)\, f_i^{\mathrm{SM}}(x,q) + \sum_j C_{ij,I}\int_x^{z_{\max}^{ij,I}(q)}\frac{\mathrm{d}z}{z}\,P_{ij,I}^R(z) f_j^{\mathrm{SM}}(x/z,q)\right], \tag{4.7}$$

where the sum over I goes over all possible different interactions[6] in the Standard Model: $I = 1$ for U(1), $I = 2$ for SU(2), $I = 3$ for SU(3) and $I = M$ for mixed interactions proportional to $\alpha_M(q) = \sqrt{\alpha_1(q)\,\alpha_2(q)}$. The latter represent interference between processes initiated by U(1) and SU(2) bosons. As in [18] we choose $q_V = m_V = 100$ GeV. Note that one might want to go to higher orders in the QCD evolution, and for that one can use the known higher-order splitting kernels.

Since the evolution in the unbroken Standard Model only applies for scales $q > q_V$, one requires a boundary condition at the scale q_V, which we write as

$$f_i^{\mathrm{SM}}(x,q_V) = f_i^{\mathrm{noEW}}(x,q_V)\,. \tag{4.8}$$

The precise definition of f^{noEW} required depends on what level of accuracy is desired. One clearly needs to include the QCD evolution from the hadronic scale $q_0 \sim 1$ GeV to the scale q_V, since $\alpha_s \ln q_V/q_0 \sim 1$. QED evolution gives rise to single logarithmic effects, and by including this evolution one includes terms of order $\alpha^n \ln^n q_V/q_0$, which should be subdominant to the double logarithmic terms generated by the EW evolution above q_V. However, by including this evolution also below q_V one is using $\mathcal{O}(\alpha)$ evolution both above and below q_V. For this reason, we choose as boundary condition

$$f_i^{\mathrm{noEW}}(x,q_V) = f_i^{\mathrm{QCED}}(x,q_V)\,, \tag{4.9}$$

[5] However, contrary to Chap. 3, the PDFs here represent the actual momentum fraction distributions rather than the x-weighted distributions.

[6] In this chapter we neglect Yukawa interactions and the Higgs self-interaction, which make only very small contributions.

where the PDF set QCED is obtained by $SU(3) \otimes U(1)_{\rm em}$ evolution from scales below q_V. Specifically, as in [18], we use the CT14qed PDF set [66] at 10 GeV and replace the photon PDF by that of the LUXqed set [67, 74]. The strongly interacting partons are rescaled to obtain exact momentum conservation. The resulting PDF set is then evolved up to the matching scale $q_V = 100$ GeV using leading-order (LO) DGLAP equations that include QCD and QED effects. In this way we obtain a LO PDF set at the matching scale which is consistent with our LO evolution above that scale.

The first contribution in Eq. (4.7), proportional to $P^V_{i,I}$, denotes the virtual contribution to the PDF evolution (the disappearance of a flavor i), while the second contribution is the real contribution (the appearance of flavor i due to the splitting of a flavor j). The maximum value of z in the integration of the real contribution is given by Eq. (3.18) depends on the type of splitting and interaction

This implies that an infrared cutoff m_V is applied when a U(1) boson B or SU(2) boson W is emitted. The physical origin of this cutoff is that the energy of a massive vector boson is bounded by its mass[7]. It is also required, since contrary to the standard SU(3) and U(1) evolution equations, which are regular as $z \to 1$ due to a cancellation between real and virtual contributions, the SU(2) evolution equations are not regular as $z \to 1$ due to the non-singlet nature of the initial state.

Before we expand the resulting PDFs, it is worth recalling where the double-logarithmic sensitivity is coming from, since this is not present in the usual DGLAP evolution. One can understand this by looking for example at the evolution of an up-type left-handed fermion due to the SU(2) interaction:

$$q\frac{\partial}{\partial q} f^{\rm SM}_{u_L} = \frac{\alpha_2}{\pi}\int_0^{1-\frac{m_V}{q}} \frac{{\rm d}z}{z} P^R_{ff,G}(z)\left[\frac{f^{\rm SM}_{d_L}(x/z,q)}{2} + \frac{f^{\rm SM}_{u_L}(x/z,q)}{4} - \frac{3z f^{\rm SM}_{u_L}(x,q)}{4}\right] + \dots \quad (4.10)$$

where the terms ... do not contribute to double logarithms. The splitting function $P^R_{ff,G}(z)$ is singular as $z \to 1$. If the initial state were SU(2) symmetric, one would have $f_{u_L}(x,q) = f_{d_L}(x,q) \equiv f_{Q_L}(x,q)$ and the combination in the square bracket would be of the form $3/4\,[f_{Q_L}(x/z,q) - z\, f_{Q_L}(x,q)]$, such that the divergence in $z \to 1$ would cancel in the difference. Since $f_{u_L}(x,q) \neq f_{d_L}(x,q)$, this cancellation does not happen, generating logarithmic sensitivity to the ratio m_V/q from the integral over z. This soft dependence gives rise to the double logarithmic sensitivity in the solution of the DGLAP equation. As was shown in [12, 18], in a basis of definite weak isospin, this double logarithmic sensitivity drives any terms with non-zero isospin to zero as $q \to \infty$, thereby restoring EW symmetry asymptotically. For the PDFs included, we will retain all DGLAP effects, even those that do not give rise to double-logarithmic terms.

As explained earlier, our aim is to obtain not only the luminosities resulting from the resummed SM PDFs but also their expansion to first order in α_I. This will permit matching

[7]Note that the precise value of the mass m_V does not matter at LL accuracy. In [18] the effect of varying m_V by a factor of 2 was used to obtain an estimate of the uncertainties from higher logarithmic effects.

to exact fixed-order calculations and assessment of the contribution of terms beyond fixed order. To expand the PDFs to first order in $\alpha_{I\neq 3}$ we define

$$\left[f_i^{\mathrm{SM}}(x,q)\right]_\alpha = f_i^{\mathrm{noEW}}(x,q) + g_i(x,q) \tag{4.11}$$

such that $\left[f_i^{\mathrm{SM}}(x,q)\right]_\alpha$ only includes the linear terms in $\alpha_{I\neq 3}$. This implies

$$f_i^{\mathrm{SM}}(x,q) = \left[f_i^{\mathrm{SM}}(x,q)\right]_\alpha + \mathcal{O}(\alpha_{I\neq 3}^2)\,. \tag{4.12}$$

The boundary condition for g_i is

$$g_i(x, q < q_V) = 0\,. \tag{4.13}$$

The definition of the function $g_i(x,q)$ obviously depends on the definition of $f_i^{\mathrm{noEW}}(x,q)$. The function g_i vanishes for $q < q_V$, so f_i^{noEW} coincides with f_i^{SM} for those values. Since the SM evolution for $q > q_V$ is adding the full $\mathrm{SU}(2) \otimes \mathrm{U}(1)$ evolution, it makes sense to choose $f_i^{\mathrm{noEW}}(x,q)$ to only include the SU(3) evolution above that scale. In other words, we choose

$$f_i^{\mathrm{noEW}}(x,q) = \begin{cases} \text{QCED evolution} & q < q_V\,, \\ \text{QCD evolution} & q > q_V\,. \end{cases} \tag{4.14}$$

One could also choose a definition that includes the QED evolution for $q > q_V$. This would introduce spurious single logarithmic $[\alpha \mathrm{L}_s]^n$ terms in the difference between f_i^{SM} and $[f_i^{\mathrm{SM}}(x,q)]_\alpha$, which are in principle beyond the claimed accuracy. However, the definition Eq. (4.14) trivially avoids these spurious terms, which is why it is our choice for the remainder of this chapter.

The DGLAP equation for $[f_i^{\mathrm{SM}}(x,q)]_\alpha$ can easily be obtained by expanding Eq. (4.7) to obtain

$$\begin{aligned} &q\frac{\partial}{\partial q}\left[f_i^{\mathrm{SM}}(x,q)\right]_\alpha \\ &\quad= \frac{\alpha_3(q)}{\pi}\left[P_{i,3}^V(q)\,\left[f_i^{\mathrm{SM}}(x,q)\right]_\alpha + \sum_j C_{ij,I}\int_x^1 \frac{\mathrm{d}z}{z} P_{ij,3}^R(z)\,\left[f_i^{\mathrm{SM}}(x/z,q)\right]_\alpha\right] \\ &\quad+ \sum_{I\in 1,2,M}\frac{\alpha_I(q)}{\pi}\left[P_{i,I}^V(q)\, f_i^{\mathrm{noEW}}(x,q) + \sum_j C_{ij,I}\int_x^{z_{\max}^{ij,I}(q)} \frac{\mathrm{d}z}{z} P_{ij,I}^R(z) f_j^{\mathrm{noEW}}(x/z,q)\right]. \end{aligned} \tag{4.15}$$

In other words, we have simply set $[f_i^{\mathrm{SM}}(x,q)]_\alpha = f_i^{\mathrm{noEW}}$ in the second line, since the dropped terms give rise to second order effects. This gives

$$\begin{aligned} &q\frac{\partial}{\partial q} g_i(x,q) \\ &\quad= \frac{\alpha_3(q)}{\pi}\left[P_{i,3}^V(q)\, g_i(x,q) + \sum_j C_{ij,I}\int_x^1 \frac{\mathrm{d}z}{z}\, P_{ij,3}^R(z) g_j(x/z,q)\right] \\ &\quad+ \sum_{I\in 1,2,M}\frac{\alpha_I(q)}{\pi}\left[P_{i,I}^V(q)\, f_i^{\mathrm{noEW}}(x,q) + \sum_j C_{ij,I}\int_x^{z_{\max}^{ij,I}(q)} \frac{\mathrm{d}z}{z}\, P_{ij,I}^R(z) f_j^{\mathrm{noEW}}(x/z,q)\right]. \end{aligned} \tag{4.16}$$

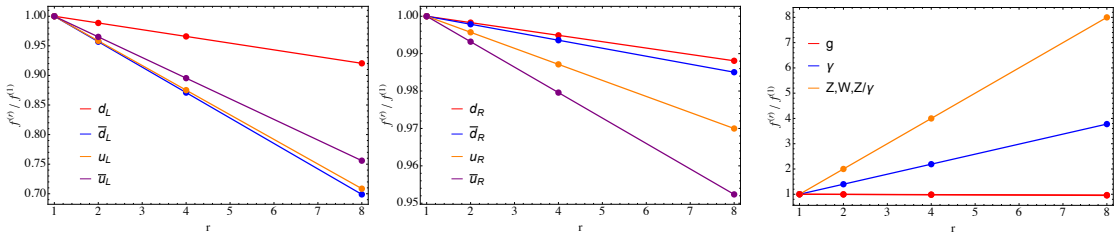

Figure 4.1: Scaling of the expanded PDFs with the parameter r, which multiplies $\alpha_{I=1,2,M}$. On the left, we show the left-handed quarks of the first generation, in the middle the right-handed quarks of the first generation, and on the right the vector bosons. One can clearly see that the expanded PDFs are linear in α_I.

We have implemented the DGLAP equation Eq. (4.16) with boundary condition Eq. (4.13) and solved for $g_i(x,q)$. As a cross check on the resulting expanded PDFs one can validate that the result is indeed linear in the coupling constants $\alpha_{I=1,2,M}$. For this, we perform the rescaling $\alpha_I \to r\alpha_I$, and then plot $[f_i^{\mathrm{SM}}(x,q)]_\alpha$ for various values of r (normalized to the result with $r=1$). Figure 4.1 clearly verifies the expected linear behavior.

Given the resummed result for the SM PDFs, together with this first-order expansion, one can obtain a first estimate of the higher-order effects, and the convergence of electroweak perturbation theory. For this, we define the two ratios

$$r_i^{\mathrm{noEW}}(x,q) \equiv \frac{f_i^{\mathrm{noEW}}(x,q)}{f_i^{\mathrm{SM}}(x,q)}\,, \qquad r_i^{\mathrm{SM},\alpha}(x,q) \equiv \frac{\left[f_i^{\mathrm{SM}}(x,q)\right]_\alpha}{f_i^{\mathrm{SM}}(x,q)}\,. \tag{4.17}$$

Defining the function $h_i(x,q)$ to be the difference between $[f_i^{\mathrm{SM}}]_\alpha$ and f_i^{SM} we can write

$$f_i^{\mathrm{SM}}(x,q) = f_i^{\mathrm{noEW}}(x,q) + g_i(x,q) + h_i(x,q)\,, \tag{4.18}$$

where $g_i(x,q)$ is the same function used in Eq. (4.11). As already discussed, the function $g_i(x,q)$ is of order α_I, while the function $h_i(x,q)$ contains the resummed terms of α_I^2 and higher. With these definitions, one can write

$$\begin{aligned} r_i^{\mathrm{noEW}}(x,q) &= 1 - \frac{g_i(x,q)+h_i(x,q)}{f_i^{\mathrm{SM}}(x,q)} \sim 1 + \mathcal{O}(\alpha_I)\,, \\ r_i^{\mathrm{SM},\alpha}(x,q) &= 1 - \frac{h_i(x,q)}{f_i^{\mathrm{SM}}(x,q)} \sim 1 + \mathcal{O}(\alpha_I^2)\,. \end{aligned} \tag{4.19}$$

Thus, the deviation from unity of the first ratio shows the size of the first-order correction, while the deviation of the second ratio shows the size of the higher-order corrections. Note that for PDFs for which $f_i^{\mathrm{noEW}}(x,q)$ vanishes (in our case the massive vector bosons) the first ratio vanishes, and the second ratio gives

$$r_i^{\mathrm{SM},\alpha}(x,q) = 1 - \frac{h_i(x,q)}{g_i(x,q)} \sim 1 + \mathcal{O}(\alpha_I) \tag{4.20}$$

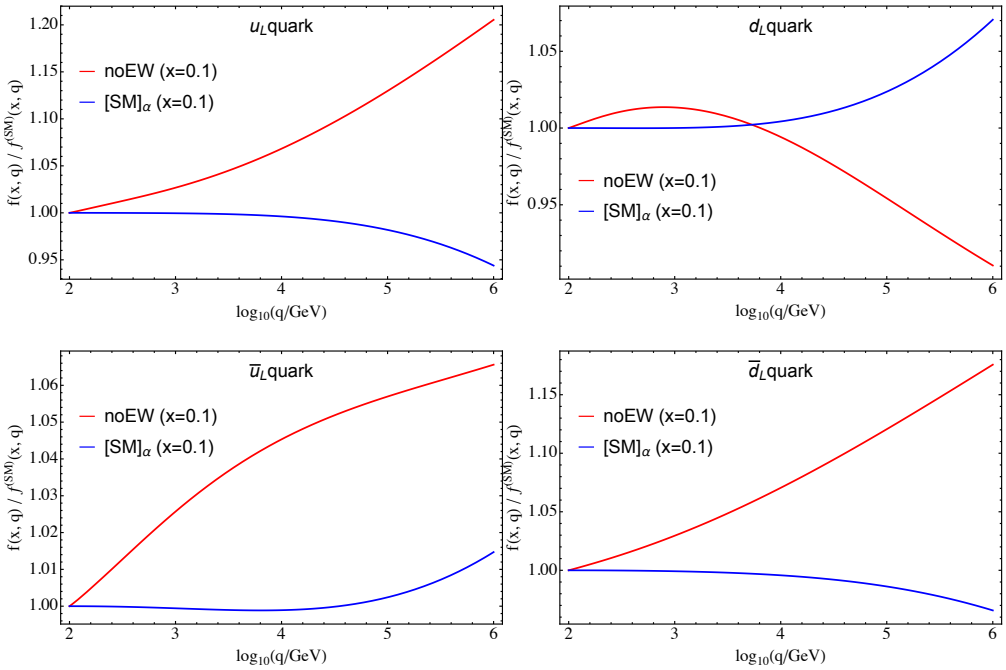

Figure 4.2: The ratio of the "noEW" and expanded SM PDFs relative to the PDF evaluated in the full SM for left-handed quarks.

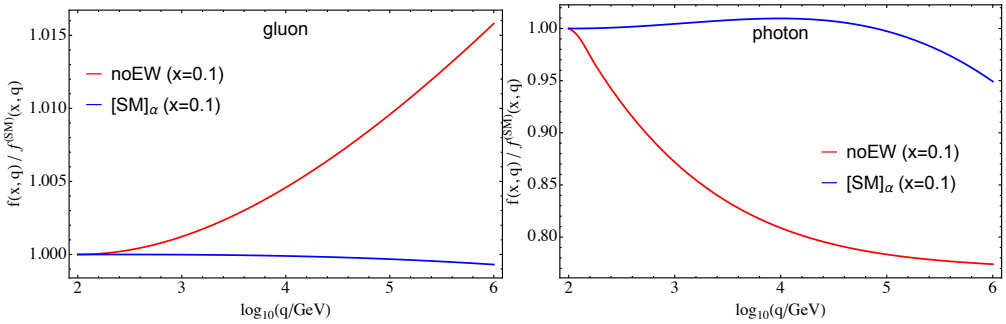

Figure 4.3: The ratio of the "noEW" and expanded SM PDFs relative to the PDF evaluated in the full SM for the massless vector bosons.

and is therefore an estimate of the size of the second-order term relative to the first-order term.

The results are shown in Fig. 4.2 for left-handed up and down (anti)quarks. One can clearly see that at low values of q the second-order correction is much smaller than the first-order correction, which is indicative of an absence of large logarithmic corrections. For $q \gtrsim 10^4$ GeV, however, the logarithmic contributions become noticeable, and the second-order correction grows relative to the first order, becoming comparable to the latter, at least

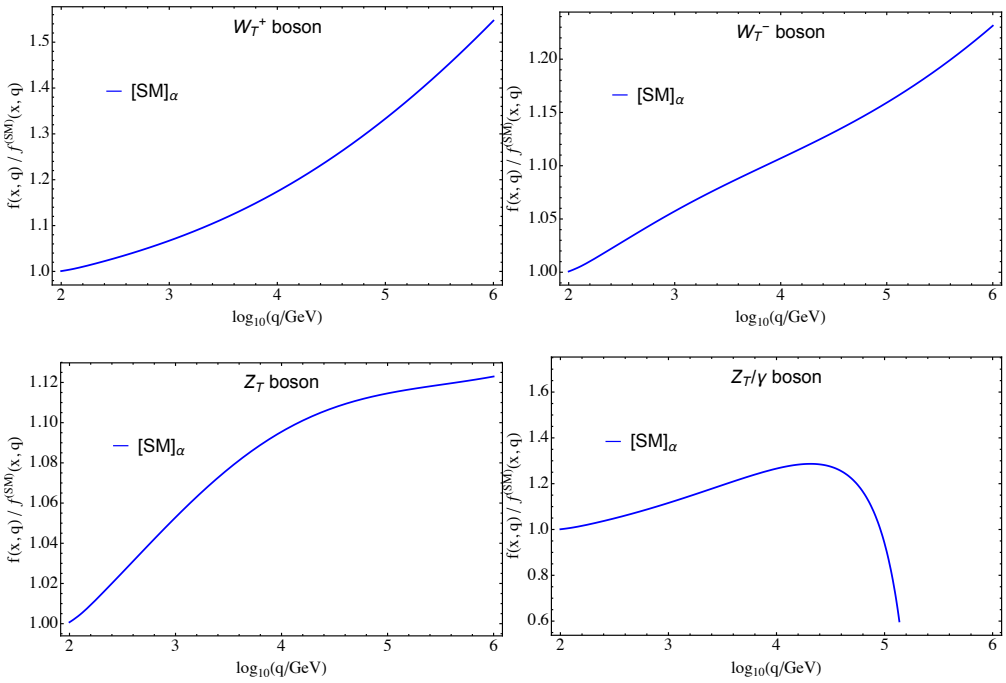

Figure 4.4: The ratio of the "noEW" and expanded SM PDFs relative to the PDF evaluated in the full SM for the transversely-polarized massive vector bosons.

for some of the PDFs, by $q \sim 10^6$ GeV. Notice that at high q the left-handed up and down quarks move in opposite directions, to restore isospin symmetry asymptotically.

For the gluon and photon, the results are shown in Fig. 4.3. The gluon does not couple to the massive vector bosons directly, so the electroweak effect is strongly suppressed. Since the "noEW" PDFs include only QCD evolution, the photon does not evolve at all in that case, and receives a large first-order EW correction. In higher orders it can couple directly to the massive bosons, so its PDF is double-logarithmically sensitive to the ratio m_V/q. Therefore, although the higher-order corrections are much smaller than the first order for $q \sim q_V$, they grow much more rapidly at high values of q.

For massive vector bosons $r^{\rm noEW}(x,q)$ is zero, since their PDFs vanish when only QCD effects are included for $q > q_V$. Therefore, given our results, the validity of the perturbative expansion can only be studied through the ratio $r^{{\rm SM},\alpha}(x,q)$, whose deviation from unity starts at first order in α_I as given in Eq. (4.20). In Fig. 4.4 one sees clearly the poor convergence of the perturbative expansion of massive boson PDFs: the deviation from unity is much larger than one power of α_I, which of course is due to the double-logarithmic dependence on m_V/q. The ratio between the expanded PDF and the full PDF can deviate from unity by an amount in excess of 10%.

Given these PDFs and their expansions, one can find the first-order expansion of the SM

luminosity

$$\left[\mathcal{L}_{AB}^{\mathrm{SM}}(x_A, x_B; \sqrt{s})\right]_\alpha = f_A^{\mathrm{noEW}}(x_A, \sqrt{s})\, f_B^{\mathrm{noEW}}(x_B, \sqrt{s}) + f_A^{\mathrm{noEW}}(x_A, \sqrt{s})\, g_B(x_B, \sqrt{s}) + g_A(x_A, \sqrt{s})\, f_B^{\mathrm{noEW}}(x_B, \sqrt{s})\,. \tag{4.21}$$

From the definition Eq. (4.11) this obviously satisfies

$$\mathcal{L}_{AB}^{\mathrm{SM}}(x_A, x_B; \sqrt{s}) - \left[\mathcal{L}_{AB}^{\mathrm{SM}}(x_A, x_B; \sqrt{s})\right]_\alpha = \mathcal{O}(\alpha_I^2)\,. \tag{4.22}$$

Thus the difference in Eq. (4.22) can be used to add resummation terms to a NLO calculation, since it excludes all terms in the luminosity $\mathcal{L}_{AB}^{\mathrm{SM}}$ at $\mathcal{O}(1)$ and $\mathcal{O}(\alpha_I)$ while including all LL terms of higher order.

Parton luminosities involving two massive gauge bosons (such as $\mathcal{L}_{ZZ}$, $\mathcal{L}_{W^+W^-}$) only start to contribute at order α_I^2, since the PDF of each such boson is suppressed by one power of α_I. This means that their effect is not included in the first-order expansion of the luminosity discussed above. However, vector-boson fusion (VBF) processes (those involving two massive gauge bosons in the initial state) can be significant numerically. For this reason, one might want to include their effects exactly at lowest order, and only rely on the LL approximation to predict their higher-order terms. This requires subtraction of the $\mathcal{O}(\alpha_I^2)$ terms from $\mathcal{L}_{VV}$ when computing the expanded luminosity. The resulting modified expanded luminosity

$$\left[\mathcal{L}_{AB}^{\mathrm{SM}}(x_A, x_B; \sqrt{s})\right]_\alpha^{\mathrm{mod}} = f_A^{\mathrm{noEW}}(x_A, \sqrt{s})\, f_B^{\mathrm{noEW}}(x_B, \sqrt{s}) + f_A^{\mathrm{noEW}}(x_A, \sqrt{s})\, g_B(x_B, \sqrt{s}) + g_A(x_A, \sqrt{s})\, f_B^{\mathrm{noEW}}(x_B, \sqrt{s}) + g_A(x_A, \sqrt{s})\, g_B(x_B, \sqrt{s})\delta_{AB,VV}\,, \tag{4.23}$$

coinciding with Eq. (4.21) for all channels except V_TV_T, allows the inclusion of the exact lowest-order V_TV_T contribution together with all resummed higher-order terms in that and the other channels. Thus to combine a fixed-order calculation including all EW effects at NLO, as well as the VBF process V_TV_T at LO, which we denote by

$$\langle O\rangle_{\mathrm{NLO+VV}} \equiv \langle O\rangle_{\mathrm{NLO}} + \langle O\rangle_{\mathrm{LO}}^{\mathrm{VV}}\,, \tag{4.24}$$

one would compute

$$\langle O\rangle_{\mathrm{NLO+VV+LL}} = \langle O\rangle_{\mathrm{NLO+VV}} + \langle O\rangle_{\mathrm{LL}} - \left[\langle O\rangle_{\mathrm{LL}}\right]_\alpha^{\mathrm{mod}}\,. \tag{4.25}$$

where

$$\left[\langle O\rangle_{\mathrm{LL}}\right]_\alpha^{\mathrm{mod}} = \sum_{AB}\int \mathrm{d}\Phi_n\, O_n(\Phi_n)\, \left[\mathcal{L}_{AB}^{\mathrm{SM}}(x_A, x_B; \sqrt{s})\right]_\alpha^{\mathrm{mod}} B_{AB}(\Phi_n)\,. \tag{4.26}$$

In Fig. 4.5 we show the results for a few selected parton luminosities

$$\mathcal{L}_{\mathcal{AB}}(m_{\ell\ell}) = \int \mathrm{d}x_A\, \mathrm{d}x_B\, \mathcal{L}_{AB}^{\mathrm{SM}}\left(x_A, x_B; m_{\ell\ell}\right)\, \delta\left(m_{\ell\ell} - \sqrt{x_1 x_2 S}\right)\,, \tag{4.27}$$

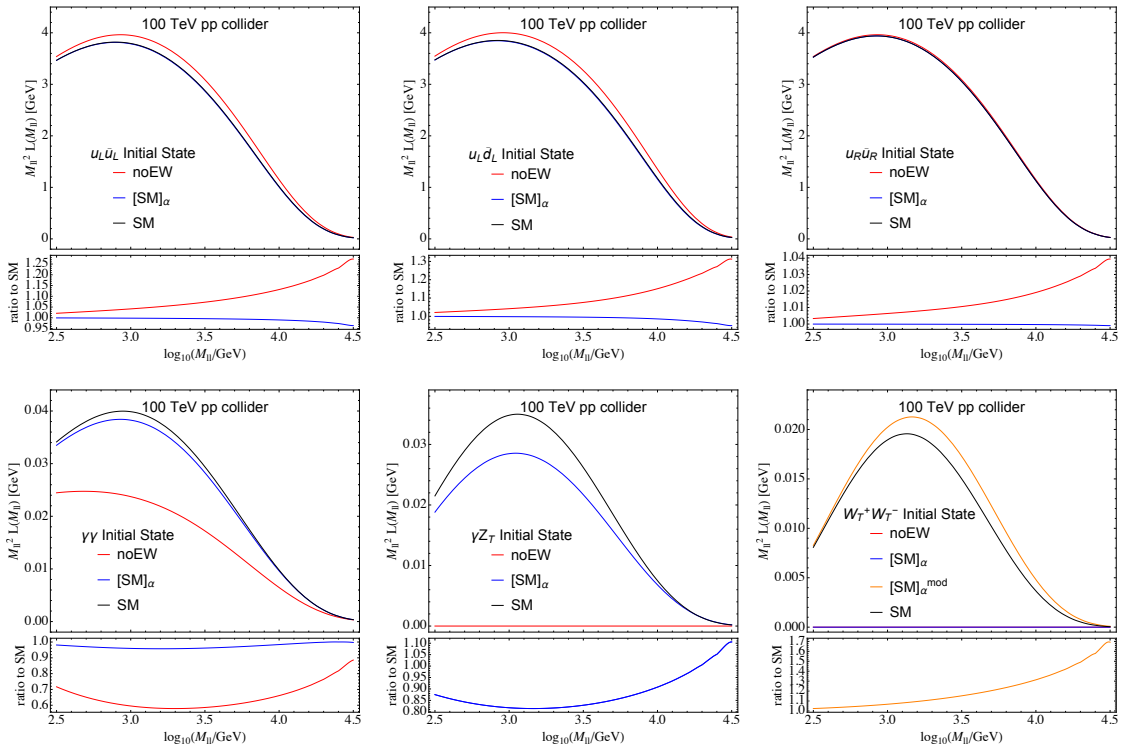

Figure 4.5: Plots showing luminosities for various choices of initial states. We show in black $\mathcal{L}^{\text{SM}}$, in red $\mathcal{L}^{\text{noEW}}$, in blue $\left[\mathcal{L}^{\text{SM}}\right]_\alpha$ and for V_TV_T initial states in orange $\left[\mathcal{L}^{\text{SM}}\right]_\alpha^{\text{mod}}$.

for pp collisions at $\sqrt{S} = 100$ TeV, rescaled by the square of the invariant mass $m_{\ell\ell}$ to overcome the steeply falling nature of the functions. We show in black $\mathcal{L}^{\text{SM}}$, in red $\mathcal{L}^{\text{noEW}}$, in blue $\left[\mathcal{L}^{\text{SM}}\right]_\alpha$ and for VV initial states in orange $\left[\mathcal{L}^{\text{SM}}\right]_\alpha^{\text{mod}}$. One can see that for left-handed quarks the difference between $\mathcal{L}^{\text{noEW}}$ and $\mathcal{L}^{\text{SM}}$ is larger than the difference between $\left[\mathcal{L}^{\text{SM}}\right]_\alpha$ and $\mathcal{L}^{\text{SM}}$ for all values of $m_{\ell\ell}$ considered, indicating that the double logarithms are not yet large enough to have $\alpha \ln^2(m_{\ell\ell}^2/m_V^2) \gtrsim 1$. However, for $m_{\ell\ell} \gtrsim$ a few TeV the higher-order terms become significant. For right-handed quarks, there are no double logarithms and the coupling is smaller, so the convergence of the perturbation series is much faster. For the $\gamma\gamma$ initial state, recall that the "noEW" photon PDF is frozen at the matching scale $q_V = 100$ GeV so the order α correction is large and dominates the expansion. For the γZ luminosity the higher-order terms are more significant. Finally, the W^+W^- luminosity vanishes for $\left[\mathcal{L}^{\text{SM}}\right]_\alpha$. Using the modified expansion reproduces the dominant features of the full luminosity, but higher order terms are still very important for $m_{\ell\ell} \gtrsim$ few TeV.

4.2 Resummation of logarithms in inclusive di-lepton production

In this section, we study the effects of higher-order leading logarithms in the process of fully inclusive di-lepton production. This will allow us to assess the correction from logarithmic resummation that needs to be applied to fixed-order calculations in order to achieve NLO+LL accuracy. Note, however, that we do not include the fixed-order calculation here.

The definition of fully inclusive di-lepton production was given in the introduction, but we will repeat it here for completeness. The inclusive process is defined to include a lepton-antilepton pair of any charge of a given generation and any number of extra gauge bosons in the final state. So to NLO EW accuracy, this process sums over the final states $\ell^+\ell^-(+V)$, $\ell^+\nu_\ell(+V)$, $\bar{\nu}_\ell\ell^-(+V)$, $\bar{\nu}_\ell\nu_\ell(+V)$. Here ℓ denotes, for example, the electron and ν_ℓ the electron neutrino and the $(+V)$ denotes the possible addition of a γ, Z or $W^\pm$ boson. Since we are summing over both electrons and neutrinos, and we are including the radiation of extra electroweak gauge bosons, the final state of this process is SU(2) symmetric, as required. In order to regulate the strong enhancement of forward lepton production in vector boson fusion, we impose a cut on the transverse momentum of each lepton $p_T > 100$ GeV. This implies that the accessible di-lepton invariant masses are $m_{\ell\ell} > 200$ GeV.

To compute the partonic Born cross section $B_{AB}(\widehat{\Phi}_n)$ in Eq. (4.2), one relates it to the square of the relevant matrix element via

$$B_{AB}(\Phi_n) \equiv \frac{1}{4p_A\cdot p_B}\left|M(AB\to\ell\ell)\right|^2 , \tag{4.28}$$

where ℓ denotes either a charged lepton or a neutrino. As discussed in Section 4, for the initial states A and B one needs $q\bar{q}$ of all possible quark flavors and helicities, as well as VV, where V can be any one of the electroweak gauge bosons, $\gamma, Z^0, W^\pm$, or the mixed γ/Z^0 representing interference contributions. The contributions of initial-state leptons, longitudinal gauge bosons and Higgs bosons are much smaller and will be neglected. Details of the cross-section calculations are given in the Appendix.

The leading-logarithmic differential cross section $\mathrm{d}\sigma/\mathrm{d}m_{\ell\ell}$ is shown for a 100 TeV pp collider in Fig 4.6. In order to make the plot easier to read, we have multiplied the differential cross section by $m_{\ell\ell}^4$ to overcome its steeply falling nature. We have stacked the contributions of the various initial states $q\bar{q}$, $\gamma\gamma$, γV_T and V_TV_T (where V_T now denotes a sum over massive transversely polarized electroweak gauge bosons) on top of each other. In the lower part of the plot, we show the ratio to the total contribution, giving a better estimate of the relative size of each contribution. One can see that the dominant contribution is from the $q\bar{q}$ initial states, but the relative size of the initial states with two vector bosons grows with increasing $m_{\ell\ell}$. For a 100 TeV collider, the contributions with vector bosons in the initial state are around 25% for $m_{\ell\ell} = 10^{4.5}$ GeV ~ 30 TeV.

Next, we take each of the four contributions and investigate their convergence under EW perturbation theory. For this, we compare the result of the LL-resummed cross section

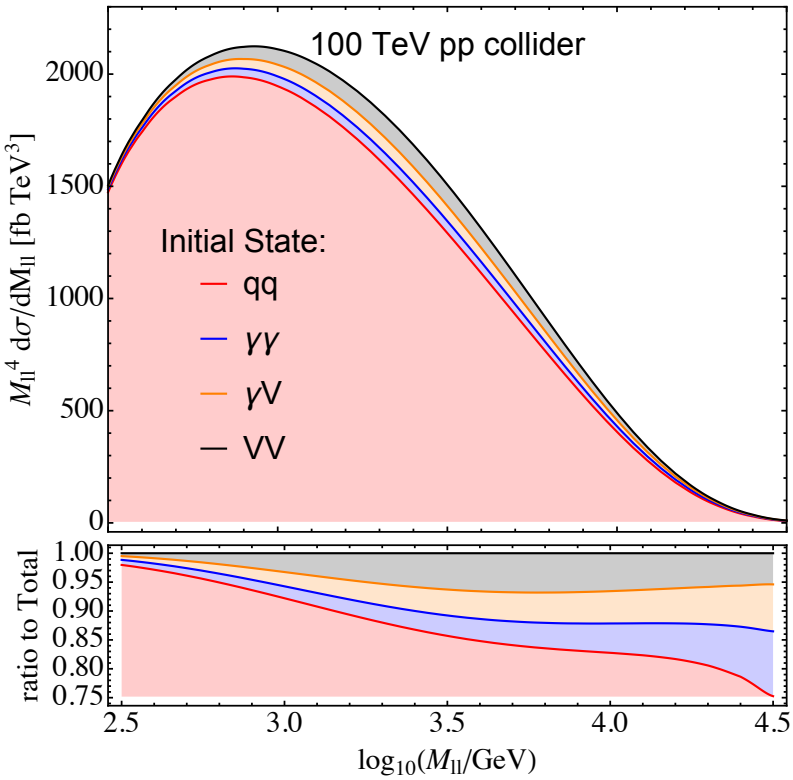

Figure 4.6: The differential cross section $m_{\ell\ell}^4 \mathrm{d}\sigma/\mathrm{d}m_{\ell\ell}(p_{T\ell} > 100\ \mathrm{GeV})$ for a 100 TeV collider, showing the makeup of the total cross section in terms of the individual initial states.

$m_{\ell\ell}^4 \mathrm{d}\sigma_{\mathrm{LL}}/\mathrm{d}m_{\ell\ell}$ with its first-order expansion $[m_{\ell\ell}^4 \mathrm{d}\sigma_{\mathrm{LL}}/\mathrm{d}m_{\ell\ell}]_\alpha$ for the various initial states. The results are shown for a 100 TeV pp collider in Fig. 4.7, where in black we show the resummed result, and in blue its first-order expansion. The difference between these two is the correction that should be added to a fixed-order calculation to achieve NLO+LL accuracy. For comparison, we also show in red the "noEW" result. The difference between the blue and red curves shows the logarithmically enhanced order-α contribution. As one can see, for the $q\bar{q}$ channel, the expansion of the LL result is quite close to the full LL result, indicating that the higher-order corrections are quite small. This is due to two facts: First, the right-handed quarks do not receive any double-logarithmic contributions (and their single logarithmic terms come with coupling constant α_1 rather than α_2). Second, since sea quarks are mostly iso-singlet, the double logarithms only arise from iso-vector contributions of the valence quarks. Each of these facts reduces the double logarithmic effect by roughly a factor of 2, such that overall the effect is smaller by a factor of 4 compared to an individual $q_L\bar{q}_L$ parton luminosity. Note that one of these factors of two would be absent for a $p\bar{p}$ collider, so one would expect the effect to be larger there by a factor of 2.

For $\gamma\gamma$ initial states, one needs to keep in mind that our definition of f^{noEW} does not

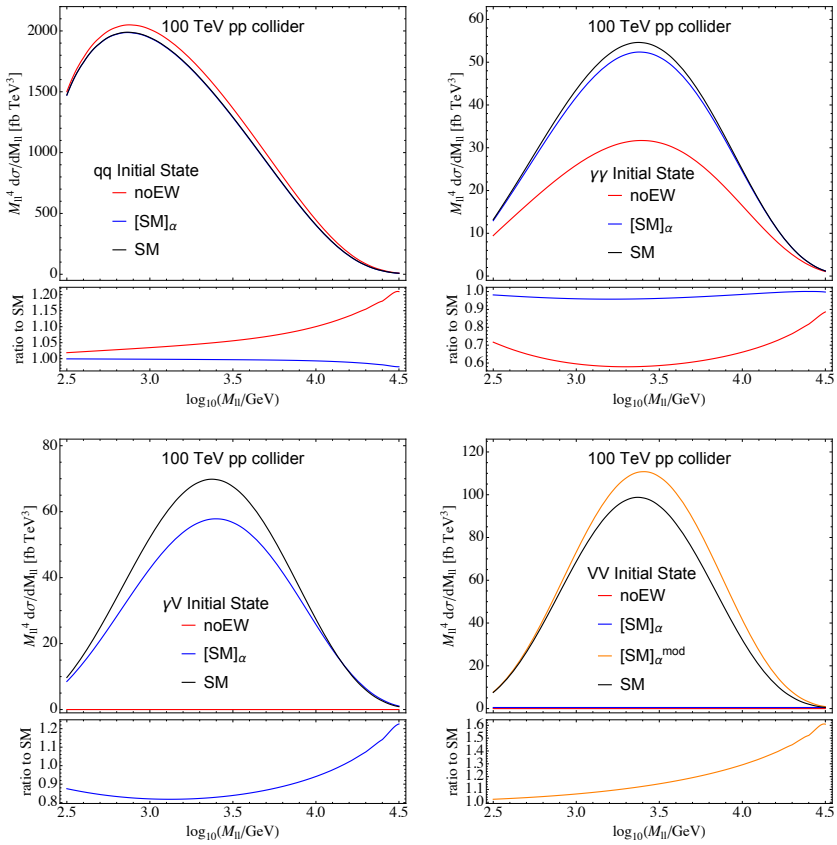

Figure 4.7: The expansion of the various contributions to $m_{\ell\ell}^4 \mathrm{d}\sigma/\mathrm{d}m_{\ell\ell}(p_{T\ell} > 100\ \mathrm{GeV})$ for a 100 TeV collider. We show in black the result obtained using $\mathcal{L}^{\mathrm{SM}}$, in red that using $\mathcal{L}^{\mathrm{noEW}}$, in blue that using $\left[\mathcal{L}^{\mathrm{SM}}\right]_\alpha$ and for $V_T V_T$ initial states in orange that using $\left[\mathcal{L}^{\mathrm{SM}}\right]_\alpha^{\mathrm{mod}}$.

include any QED evolution for $q > q_V$. This means that the photon PDF freezes out at the scale q_V for this PDF. Since the effect of the evolution is of the same size as the value of the PDF at $q = q_V$, the first order (difference of red and black) gives an $\mathcal{O}(1)$ effect. The second order (difference of blue and black) is considerably smaller than the first order for all values of $m_{\ell\ell}$, but from the absolute value of the correction it is also clear that the expansion parameter is much larger than α_{em}/π as one might naively expect. For example, for $m_{\ell\ell} \sim 1$ TeV, the second-order correction is almost 5%.

Any process with massive bosons in the initial states is suppressed by one power of α for each. Therefore the "noEW" luminosity vanishes for γV_T and $V_T V_T$, and for $V_T V_T$ the $[\mathrm{SM}]_\alpha$ luminosity also vanishes, as indicated by the red and blue lines in the last two plots. However, for γV_T the second-order correction (the difference between the blue and the black line) reaches tens of percent at high $m_{\ell\ell}$, indicating that the higher order perturbative corrections are significant. For $V_T V_T$ initial states, we also show in orange the result of the modified expansion Eq. (4.23), which includes the leading $\mathcal{O}(\alpha^2)$ term. The difference

between the orange and black curve denotes $\mathcal{O}(\alpha^3)$ terms, which are tens of percent of the leading $\mathcal{O}(\alpha^2)$ terms, indicating again a poorly convergent perturbation series.

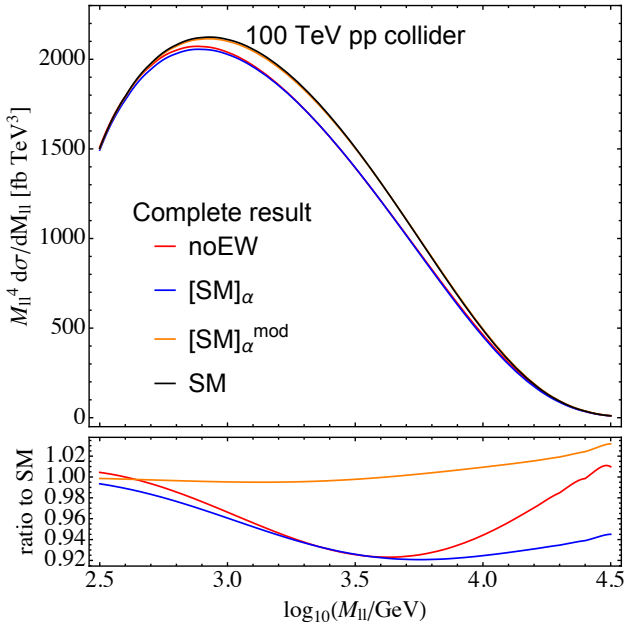

Figure 4.8: The expansion of the complete result $m_{\ell\ell}^4 \mathrm{d}\sigma/\mathrm{d}m_{\ell\ell}(p_{T\ell} > 100\ \mathrm{GeV})$ for a 100 TeV collider. The colors are the same as in Fig. 4.7.

Putting these results together, we show in Fig. 4.8 the combination of the various channels. One can see that perturbation theory is not very well behaved and for $m_{\ell\ell} \gtrsim 5$ TeV, the second order correction is essentially of the same size as the first order correction (there is an accidental cancellation for very large $m_{\ell\ell}$ which makes the first order correction become small). The overall effect of the corrections of order α_I^2 and higher for $m_{\ell\ell} \gtrsim$ a few TeV is of the order of 5%. Most of this comes from the VBF processes, so the correction to the modified expansion Eq. (4.23) is much smaller.

To understand how these results depend on the center-of-mass energy of the collider, we also show results at 27 TeV, which is the energy that might be achieved by a high-energy upgrade of the LHC using novel magnet technology [75], and a fictitious 1 PeV collider. In Fig. 4.9 the relative importance of the various channels is shown. One obvious effect is that at high energies one has access to larger values of the di-lepton invariant mass, for which the logarithmic enhancement is stronger. However, even at fixed invariant mass the relative importance of the initial states with vector bosons is diminished (enhanced) for a 27 TeV (1 PeV) collider. This is because at higher energies one is probing smaller values of x, and the vector boson PDFs, like that of the gluon, rise rapidly with decreasing x. For a 1 PeV collider at the highest accessible di-lepton invariant mass, the contribution of vector boson initial states is almost 50% of the total cross section.

Finally, we study the convergence of perturbation theory for individual channels for a 27 TeV and 1 PeV collider in Figs. 4.10 and 4.11, respectively, and the complete result in Fig. 4.12. Qualitatively the effects are the same as for a 100 TeV collider, but the overall size of the effects are decreased (increased) for the 27 TeV (1 PeV) collider.

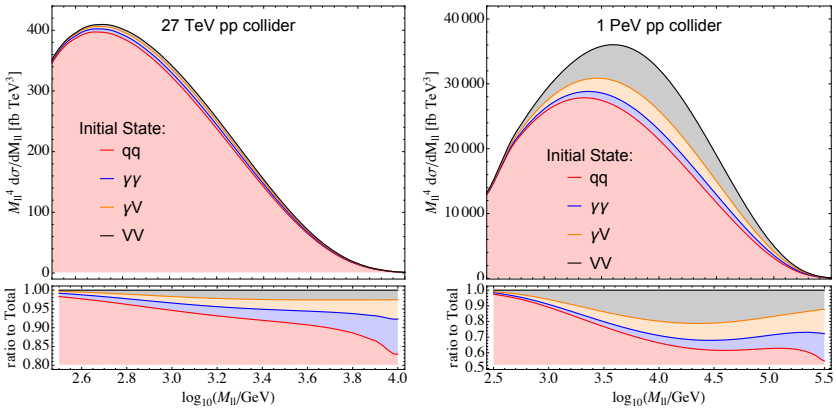

Figure 4.9: The differential cross section $m_{\ell\ell}^4 \mathrm{d}\sigma/\mathrm{d}m_{\ell\ell}(p_{T\ell} > 100\ \mathrm{GeV})$ for a 27 TeV and 1 PeV collider, showing the makeup of the total cross section in terms of the individual initial states.

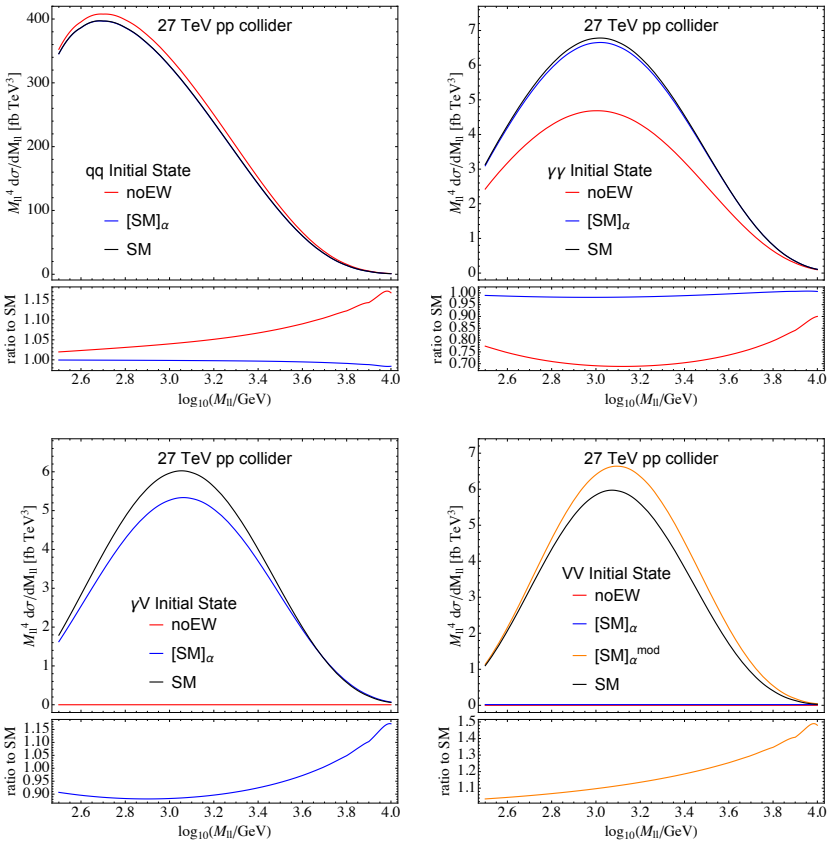

Figure 4.10: The expansion of the various contributions to $m_{\ell\ell}^4 \mathrm{d}\sigma/\mathrm{d}m_{\ell\ell}(p_{T\ell} > 100$ GeV) for a 27 TeV collider. The colors are the same as in Fig. 4.7.

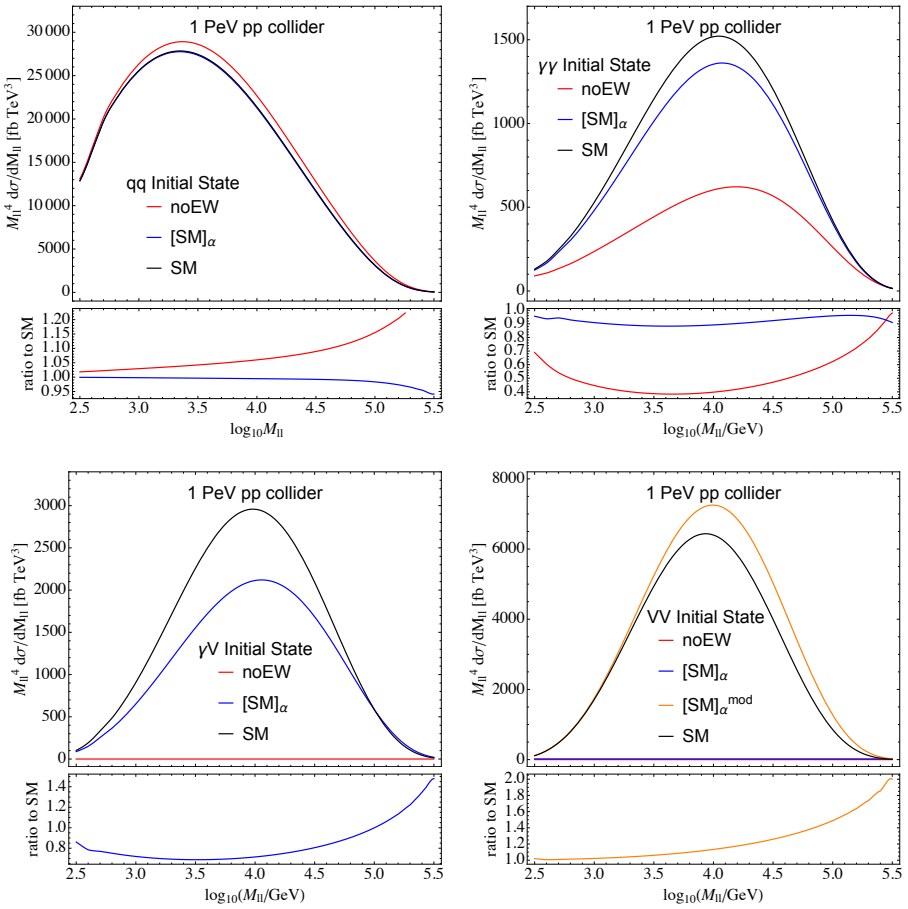

Figure 4.11: The expansion of the various contributions to $m_{\ell\ell}^4 \mathrm{d}\sigma/\mathrm{d}m_{\ell\ell}(p_{T\ell} > 100$ GeV) for a 1 PeV collider. The colors are the same as in Fig. 4.7.

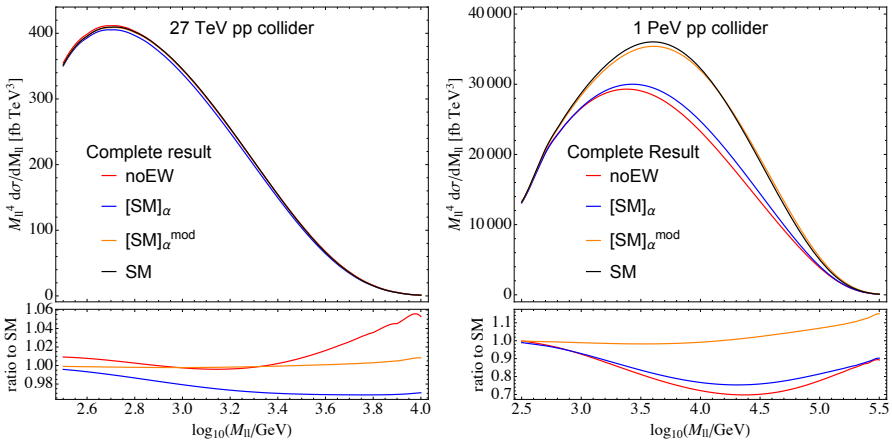

Figure 4.12: The expansion of the complete result $m_{\ell\ell}^4 \mathrm{d}\sigma/\mathrm{d}m_{\ell\ell}(p_{T\ell} > 100\ \mathrm{GeV})$ for a 27 TeV and 1 PeV collider. The colors are the same as in Fig. 4.7

Chapter 5

Conclusions

The LHC experiments explore the energy scale around and beyond the electroweak scale. As of now, there has been no discovery of physics beyond the Standard Model. For this reason, it is interesting to examine the assumption that the Standard Model is valid up to very high energies. At energy significantly higher than the electroweak scale, one can assume that the electroweak symmetry is unbroken.

We have shown that at high energy, the resummation of the electroweak Sudakov logarithms has a large impact of the result of cross-sections with radiation of electroweak bosons. We considered Drell-Yan production of leptons at a hadron collider, and presented result for the logarithmic resummation at LL accuracy for electroweak corrections to the total cross-section in simple analytic form.

Using these analytical results, we have analyzed the size of the corrections numerically for the 13 TeV LHC and a possible future 100 TeV pp collider. Our results show than the real resummation is as important as the virtual resummation and its importance increases fast with the partonic center of mass energy: at the LHC, the resummation effect over the fixed order goes from around 10% at 1 TeV to around 20% at 3 TeV for the virtual with any leptonic final state and goes from around 20% at 1 TeV to around 50% at 3 TeV for all kinds of real emissions with any leptonic final state. The resummed virtual over the Born cross-section goes from around 10% at 1 TeV to 30% at 3 TeV, while each resummed reals are around the third of the resummed virtual. At a future 100 TeV pp collider, the resummation effects over the fixed order can be much larger, and are around 50% for the virtual and 200% for the real at 25 TeV in most cases. The resummed virtual over the Born cross-section is around 80% at 25 TeV.

For final states with fixed lepton flavors, summing the virtual and real corrections does not reduce the magnitude of the double logarithmic terms, as expected for a result that is not inclusive. After summing over all lepton flavors, a large cancellation is observed at fixed order, but a small logarithmic sensitivity remains, due to the fact that protons are not SU(2) singlets. On the other hand, for the resummed results, a large effect remains because we are including only the first emission for the real. The cancellation will happen only for an inclusive result, that is summing the virtual and the real for any number of emitted bosons.

We have implemented numerically the full set of generalized DGLAP evolution equations for all the parton species and interactions of the unbroken SM in leading order. The input PDFs of 5 quark flavors, the gluon, photon and charged leptons at a starting scale $q_V = 100$ GeV for the full SM evolution are obtained from parton and photon PDFs at 10 GeV by QCD plus QED evolution. The input left- and right-handed fermion PDFs are thus identical at scale q_V but they evolve differently above that scale. The top quark PDFs (not present in the input) start to evolve from the top mass scale. The input photon is resolved into its U(1), SU(2) and mixed components, which are evolved independently from scale q_V and reassembled into the photon and transversely polarized Z^0 at higher scales. The charged and longitudinal vector boson, Higgs and neutrino PDFs are generated dynamically starting from zero at scale q_V. This simplified treatment misses some symmetry-breaking effects around the electroweak scale, but these are power-suppressed at higher scales and our results should provide a guide to the ways in which the PDFs deviate from pure QCD evolution.

Amongst the most interesting features of the SM is the distinction between left- and right-handed fermions. The evolution of the right-handed PDFs deviates little from pure QCD, owing to the weakness of the U(1) interaction. The left-handed PDFs generally deviate from pure QCD at the 5-10% level by 10 TeV.

Another important SM characteristic is the restoration of isospin symmetry at high scales. This is manifest in the decreasing asymmetry between the up- and down-type quark PDFs, which sets in at $1 - 10$ TeV, the up-type being pulled down in the first generation and conversely in the third. The suppression of the asymmetry is a double-logarithmic effect that can be treated in fixed order at present energies but is resummed to all orders in the evolution.

The electroweak bosons are generated quite copiously, the W^+ in particular at high x due to splitting $u \to dW^+$. The photon and Z^0 PDFs also grow rapidly, eventually exceeding the gluon at high x. The PDFs of the longitudinal vector bosons, the Higgs boson and the leptons are generally much smaller as they arise from second-order splittings.

Finally, we have used the generated PDFs to present some parton-parton luminosities at a 100 TeV pp collider. These results are just an illustration of the size of the effects that can be expected at such a future collider, and a more detailed phenomenological analysis will be presented in a forthcoming publication.

We found a rich structure in the proton when probed beyond the electroweak scale. The associated PDFs are interesting and useful in their own right. They also represent a key component of event generators that aim to embody the full Standard Model in initial-state parton showering, a topic we plan to explore further.

We have proposed a method for combining resummation with fixed-order electroweak calculations, without double counting of terms already included. This is done by expanding the evolution equations to fixed order in the electroweak couplings and computing the terms that need to be subtracted to avoid double counting. The remaining terms then provide a resummed estimate of the higher-order effects beyond those that have been computed exactly in fixed order. The relative size of the first- and higher-order terms provides an indication of the convergence of electroweak perturbation theory.

In order to combine resummed and fixed-order calculations without double counting, one needs to specify carefully the terms included in each case. In particular, the PDF sets used for the latter should not include terms present in the electroweak evolution equations used for the former. We therefore propose a "noEW" scheme for fixed-order calculations, in which there is no $\mathrm{U}(1)_{\mathrm{em}}$ evolution above the electroweak scale. In particular, the photon PDF used in the fixed-order calculation is frozen at a matching scale $q_V \sim m_V \sim 100$ GeV, and the resummation takes care of all the photon evolution above that scale.

Using this scheme, we have presented comparisons between "noEW" results, the full leading-logarithmic resummation (SM) and the resummed results expanded to fixed order ($[\mathrm{SM}]_\alpha$), at the level of PDFs, parton-parton luminosities and fully-inclusive di-lepton cross sections. The difference between $[\mathrm{SM}]_\alpha$ and "noEW" represents the part that should be replaced by an exact order-α calculation for improved precision. The difference between SM and $[\mathrm{SM}]_\alpha$ then indicates the extra contribution from the resummation of enhanced terms of yet higher orders. Our results are shown mainly in the context of a future pp collider of center-of-mass energy 100 TeV, but we also show some effects at a possible 27 TeV high-energy upgrade of the LHC and at much higher energy.

A notable feature of our findings is that there are relatively large contributions to the PDFs of the electroweak vector bosons beyond order α, reaching tens of percent beyond scales of ~ 10 TeV. This is reflected in their contributions to luminosities and the di-lepton cross section. Even at fixed invariant mass, the relative importance of the initial states with vector bosons increases with collider energy. This is because at higher energies one is probing smaller values of x. Since the contributions of vector boson fusion processes begin at order α^2, one may wish to make an extra subtraction of this piece from the resummation, resulting in a scheme we call $[\mathrm{SM}]_\alpha^{\mathrm{mod}}$. In this scheme one can include the exact lowest-order VBF contribution, the difference between SM and $[\mathrm{SM}]_\alpha^{\mathrm{mod}}$ then indicating the effect of remaining resummed terms. We find that the latter are still quite significant, again reaching tens of percent beyond scales of ~ 10 TeV.

Our approach naturally to compute resummed PDFs that can be combined with fixed-order calculations invites a number of future developments. Foremost of these would be the inclusion of exact order-α calculations in the way we have proposed, together with order-α^2 VBF contributions. The fully-inclusive di-lepton process that we have considered is not experimentally relevant, owing to the presence of unobservable neutrinos. This could be rectified either by including Sudakov factors for a fully exclusive e^+e^- or $\mu^+\mu^-$ final state, or by computing fragmentation functions for the inclusive production of charged leptons. Ultimately, fully exclusive final states containing all combinations of jets, leptons, photons and massive bosons could be simulated by an event generator based on complete Standard Model evolution equations for initial- and final-state parton showers.

In conclusion, we calculated that the logarithmic resummation of real electroweak corrections will have an significant impact on the cross-section predictions for the next generation of colliders. We implemented the PDFs using the full SM evolution and implemented PDFs that can be combined with fixed order calculations to get both NLO and LL accuracy.

Bibliography

[1] R. Contino et al., *Physics at a 100 TeV pp collider: Higgs and EW symmetry breaking studies*, *CERN Yellow Report* (2017) 255–440, [1606.09408].

[2] N. Arkani-Hamed, T. Han, M. Mangano and L.-T. Wang, *Physics opportunities of a 100 TeV proton-proton collider*, *Phys. Rept.* **652** (2016) 1–49, [1511.06495].

[3] M. L. Mangano et al., *Physics at a 100 TeV pp collider: Standard Model processes*, 1607.01831.

[4] P. Ciafaloni and D. Comelli, *Sudakov enhancement of electroweak corrections*, *Phys. Lett.* **B446** (1999) 278–284, [hep-ph/9809321].

[5] P. Ciafaloni and D. Comelli, *Electroweak Sudakov form-factors and nonfactorizable soft QED effects at NLC energies*, *Phys. Lett.* **B476** (2000) 49–57, [hep-ph/9910278].

[6] M. Ciafaloni, P. Ciafaloni and D. Comelli, *Bloch-Nordsieck violating electroweak corrections to inclusive TeV scale hard processes*, *Phys. Rev. Lett.* **84** (2000) 4810–4813, [hep-ph/0001142].

[7] M. Ciafaloni, P. Ciafaloni and D. Comelli, *Electroweak double logarithms in inclusive observables for a generic initial state*, *Phys. Lett.* **B501** (2001) 216–222, [hep-ph/0007096].

[8] M. Ciafaloni, P. Ciafaloni and D. Comelli, *Electroweak Bloch-Nordsieck violation at the TeV scale: 'Strong' weak interactions?*, *Nucl. Phys.* **B589** (2000) 359–380, [hep-ph/0004071].

[9] M. Ciafaloni, P. Ciafaloni and D. Comelli, *Enhanced electroweak corrections to inclusive boson fusion processes at the TeV scale*, *Nucl. Phys.* **B613** (2001) 382–406, [hep-ph/0103316].

[10] M. Ciafaloni, P. Ciafaloni and D. Comelli, *Towards collinear evolution equations in electroweak theory*, *Phys. Rev. Lett.* **88** (2002) 102001, [hep-ph/0111109].

[11] P. Ciafaloni, D. Comelli and A. Vergine, *Sudakov electroweak effects in transversely polarized beams*, *JHEP* **07** (2004) 039, [hep-ph/0311260].

[12] P. Ciafaloni and D. Comelli, *Electroweak evolution equations*, *JHEP* **11** (2005) 022, [hep-ph/0505047].

[13] P. Ciafaloni and D. Comelli, *The Importance of weak bosons emission at LHC*, *JHEP* **09** (2006) 055, [hep-ph/0604070].

[14] M. Ciafaloni, P. Ciafaloni and D. Comelli, *Electroweak double-logs at small x*, *JHEP* **05** (2008) 039, [0802.0168].

[15] P. Ciafaloni and A. Urbano, *Infrared weak corrections to strongly interacting gauge bosons scattering*, *Phys. Rev.* **D81** (2010) 085033, [0902.1855].

[16] P. Ciafaloni, D. Comelli, A. Riotto, F. Sala, A. Strumia and A. Urbano, *Weak Corrections are Relevant for Dark Matter Indirect Detection*, *JCAP* **1103** (2011) 019, [1009.0224].

[17] S. Forte et al., *The Standard Model from LHC to future colliders*, *Eur. Phys. J.* **C75** (2015) 554, [1505.01279].

[18] C. W. Bauer, N. Ferland and B. R. Webber, *Standard Model Parton Distributions at Very High Energies*, *JHEP* **08** (2017) 036, [1703.08562].

[19] V. S. Fadin, L. N. Lipatov, A. D. Martin and M. Melles, *Resummation of double logarithms in electroweak high-energy processes*, *Phys. Rev.* **D61** (2000) 094002, [hep-ph/9910338].

[20] J. H. Kühn, A. A. Penin and V. A. Smirnov, *Summing up subleading Sudakov logarithms*, *Eur. Phys. J.* **C17** (2000) 97–105, [hep-ph/9912503].

[21] A. Denner and S. Pozzorini, *One loop leading logarithms in electroweak radiative corrections. 1. Results*, *Eur. Phys. J.* **C18** (2001) 461–480, [hep-ph/0010201].

[22] A. Denner and S. Pozzorini, *One loop leading logarithms in electroweak radiative corrections. 2. Factorization of collinear singularities*, *Eur. Phys. J.* **C21** (2001) 63–79, [hep-ph/0104127].

[23] B. Feucht, J. H. Kühn, A. A. Penin and V. A. Smirnov, *Two loop Sudakov form-factor in a theory with mass gap*, *Phys. Rev. Lett.* **93** (2004) 101802, [hep-ph/0404082].

[24] B. Jantzen, J. H. Kühn, A. A. Penin and V. A. Smirnov, *Two-loop electroweak logarithms*, *Phys. Rev.* **D72** (2005) 051301, [hep-ph/0504111].

[25] B. Jantzen, J. H. Kühn, A. A. Penin and V. A. Smirnov, *Two-loop electroweak logarithms in four-fermion processes at high energy*, *Nucl. Phys.* **B731** (2005) 188–212, [hep-ph/0509157].

[26] M. Beccaria, F. M. Renard and C. Verzegnassi, *Top quark production at future lepton colliders in the asymptotic regime*, *Phys. Rev.* **D63** (2001) 053013, [hep-ph/0010205].

[27] M. Hori, H. Kawamura and J. Kodaira, *Electroweak Sudakov at two loop level*, *Phys. Lett.* **B491** (2000) 275–279, [hep-ph/0007329].

[28] W. Beenakker and A. Werthenbach, *Electroweak two loop Sudakov logarithms for on-shell fermions and bosons*, *Nucl. Phys.* **B630** (2002) 3–54, [hep-ph/0112030].

[29] A. Denner, M. Melles and S. Pozzorini, *Two loop electroweak angular dependent logarithms at high-energies*, *Nucl. Phys.* **B662** (2003) 299–333, [hep-ph/0301241].

[30] S. Pozzorini, *Next to leading mass singularities in two loop electroweak singlet form-factors*, *Nucl. Phys.* **B692** (2004) 135–174, [hep-ph/0401087].

[31] B. Jantzen and V. A. Smirnov, *The Two-loop vector form-factor in the Sudakov limit*, *Eur. Phys. J.* **C47** (2006) 671–695, [hep-ph/0603133].

[32] J.-y. Chiu, F. Golf, R. Kelley and A. V. Manohar, *Electroweak Sudakov corrections using effective field theory*, *Phys. Rev. Lett.* **100** (2008) 021802, [0709.2377].

[33] J.-y. Chiu, F. Golf, R. Kelley and A. V. Manohar, *Electroweak Corrections in High Energy Processes using Effective Field Theory*, *Phys. Rev.* **D77** (2008) 053004, [0712.0396].

[34] J.-y. Chiu, R. Kelley and A. V. Manohar, *Electroweak Corrections using Effective Field Theory: Applications to the LHC*, *Phys. Rev.* **D78** (2008) 073006, [0806.1240].

[35] J.-y. Chiu, A. Fuhrer, A. H. Hoang, R. Kelley and A. V. Manohar, *Soft-Collinear Factorization and Zero-Bin Subtractions*, *Phys. Rev.* **D79** (2009) 053007, [0901.1332].

[36] J.-y. Chiu, A. Fuhrer, A. H. Hoang, R. Kelley and A. V. Manohar, *Using SCET to calculate electroweak corrections in gauge boson production*, *PoS* **EFT09** (2009) 009, [0905.1141].

[37] J.-y. Chiu, A. Fuhrer, R. Kelley and A. V. Manohar, *Factorization Structure of Gauge Theory Amplitudes and Application to Hard Scattering Processes at the LHC*, *Phys. Rev.* **D80** (2009) 094013, [0909.0012].

[38] J.-y. Chiu, A. Fuhrer, R. Kelley and A. V. Manohar, *Soft and Collinear Functions for the Standard Model*, *Phys. Rev.* **D81** (2010) 014023, [0909.0947].

[39] A. Fuhrer, A. V. Manohar, J.-y. Chiu and R. Kelley, *Radiative Corrections to Longitudinal and Transverse Gauge Boson and Higgs Production*, *Phys. Rev.* **D81** (2010) 093005, [1003.0025].

[40] M. Melles, *Electroweak radiative corrections in high-energy processes*, *Phys. Rept.* **375** (2003) 219–326, [hep-ph/0104232].

[41] A. V. Manohar and M. Trott, *Electroweak Sudakov Corrections and the Top Quark Forward-Backward Asymmetry*, *Phys. Lett.* **B711** (2012) 313–316, [1201.3926].

[42] C. W. Bauer and I. W. Stewart, *Invariant operators in collinear effective theory*, *Phys. Lett.* **B516** (2001) 134–142, [hep-ph/0107001].

[43] C. W. Bauer, S. Fleming and M. E. Luke, *Summing Sudakov logarithms in B —¿ X(s gamma) in effective field theory*, *Phys. Rev.* **D63** (2000) 014006, [hep-ph/0005275].

[44] C. W. Bauer, S. Fleming, D. Pirjol and I. W. Stewart, *An Effective field theory for collinear and soft gluons: Heavy to light decays*, *Phys. Rev.* **D63** (2001) 114020, [hep-ph/0011336].

[45] C. W. Bauer, D. Pirjol and I. W. Stewart, *Soft collinear factorization in effective field theory*, *Phys. Rev.* **D65** (2002) 054022, [hep-ph/0109045].

[46] U. Baur, *Weak Boson Emission in Hadron Collider Processes*, *Phys. Rev.* **D75** (2007) 013005, [hep-ph/0611241].

[47] A. Manohar, B. Shotwell, C. Bauer and S. Turczyk, *Non-cancellation of electroweak logarithms in high-energy scattering*, *Phys. Lett.* **B740** (2015) 179–187, [1409.1918].

[48] G. Bell, J. H. Kühn and J. Rittinger, *Electroweak Sudakov Logarithms and Real Gauge-Boson Radiation in the TeV Region*, *Eur. Phys. J.* **C70** (2010) 659–671, [1004.4117].

[49] C. W. Bauer and N. Ferland, *Resummation of electroweak Sudakov logarithms for real radiation*, *JHEP* **09** (2016) 025, [1601.07190].

[50] C. W. Bauer, N. Ferland and B. R. Webber, *Combining initial-state resummation with fixed-order calculations of electroweak corrections*, 1712.07147.

[51] T. Kinoshita, *Mass singularities of Feynman amplitudes*, *J. Math. Phys.* **3** (1962) 650–677.

[52] T. Sjostrand, S. Mrenna and P. Z. Skands, *PYTHIA 6.4 Physics and Manual*, *JHEP* **05** (2006) 026, [hep-ph/0603175].

[53] A. Buckley et al., *General-purpose event generators for LHC physics*, *Phys. Rept.* **504** (2011) 145–233, [1101.2599].

[54] T. Sjostrand, *A Model for Initial State Parton Showers*, *Phys. Lett.* **B157** (1985) 321–325.

[55] R. K. Ellis, W. J. Stirling and B. R. Webber, *QCD and collider physics*, *Camb. Monogr. Part. Phys. Nucl. Phys. Cosmol.* **8** (1996) 1–435.

[56] J. Chen, T. Han and B. Tweedie, *Electroweak Splitting Functions and High Energy Showering*, *JHEP* **11** (2017) 093, [1611.00788].

[57] V. N. Gribov and L. N. Lipatov, *Deep inelastic e p scattering in perturbation theory*, *Sov. J. Nucl. Phys.* **15** (1972) 438–450.

[58] Y. L. Dokshitzer, *Calculation of the Structure Functions for Deep Inelastic Scattering and e+ e- Annihilation by Perturbation Theory in Quantum Chromodynamics.*, *Sov. Phys. JETP* **46** (1977) 641–653.

[59] G. Altarelli and G. Parisi, *Asymptotic Freedom in Parton Language*, *Nucl. Phys.* **B126** (1977) 298–318.

[60] H. Spiesberger, *QED radiative corrections for parton distributions*, *Phys. Rev.* **D52** (1995) 4936–4940, [hep-ph/9412286].

[61] A. D. Martin, R. G. Roberts, W. J. Stirling and R. S. Thorne, *Parton distributions incorporating QED contributions*, *Eur. Phys. J.* **C39** (2005) 155–161, [hep-ph/0411040].

[62] M. Roth and S. Weinzierl, *QED corrections to the evolution of parton distributions*, *Phys. Lett.* **B590** (2004) 190–198, [hep-ph/0403200].

[63] NNPDF collaboration, R. D. Ball, V. Bertone, S. Carrazza, L. Del Debbio, S. Forte, A. Guffanti et al., *Parton distributions with QED corrections*, *Nucl. Phys.* **B877** (2013) 290–320, [1308.0598].

[64] R. Sadykov, *Impact of QED radiative corrections on Parton Distribution Functions*, 1401.1133.

[65] S. Carrazza, *Parton distribution functions with QED corrections*. PhD thesis, Milan U., 2015. 1509.00209.

[66] C. Schmidt, J. Pumplin, D. Stump and C. P. Yuan, *CT14QED parton distribution functions from isolated photon production in deep inelastic scattering*, *Phys. Rev.* **D93** (2016) 114015, [1509.02905].

[67] A. Manohar, P. Nason, G. P. Salam and G. Zanderighi, *How bright is the proton? A precise determination of the photon parton distribution function*, *Phys. Rev. Lett.* **117** (2016) 242002, [1607.04266].

[68] J. Butterworth et al., *PDF4LHC recommendations for LHC Run II*, *J. Phys.* **G43** (2016) 023001, [1510.03865].

[69] S. Kallweit, J. M. Lindert, P. Maierhöfer, S. Pozzorini and M. Schönherr, *NLO electroweak automation and precise predictions for W+multijet production at the LHC*, *JHEP* **04** (2015) 012, [1412.5157].

[70] S. Kallweit, J. M. Lindert, P. Maierhöfer, S. Pozzorini and M. Schönherr, *NLO QCD+EW predictions for V + jets including off-shell vector-boson decays and multijet merging*, *JHEP* **04** (2016) 021, [1511.08692].

[71] S. Kallweit, J. M. Lindert, S. Pozzorini and M. Schönherr, *NLO QCD+EW predictions for $2\ell 2\nu$ diboson signatures at the LHC*, *JHEP* **11** (2017) 120, [1705.00598].

[72] F. Granata, J. M. Lindert, C. Oleari and S. Pozzorini, *NLO QCD+EW predictions for HV and HV +jet production including parton-shower effects*, *JHEP* **09** (2017) 012, [1706.03522].

[73] M. Chiesa, N. Greiner, M. Schönherr and F. Tramontano, *Electroweak corrections to diphoton plus jets*, *JHEP* **10** (2017) 181, [1706.09022].

[74] A. V. Manohar, P. Nason, G. P. Salam and G. Zanderighi, *The Photon Content of the Proton*, 1708.01256.

[75] D. Tommasini et al., *The 16 T Dipole Development Program for FCC*, *IEEE Trans. Appl. Supercond.* **27** (2016) 4000405.

Appendix A

Equations used in the forward evolution

A.1 SU(3) interaction

- $\mathbf{T} = 0$ and CP $= +$:

$$\left[q\frac{\partial}{\partial q}f_q^{0+}\right]_3 = \frac{\alpha_3}{\pi}\left[C_F P^+_{ff,G}\otimes f_q^{0+} + T_R P^R_{fV,G}\otimes f_g\right], \tag{A.1}$$

$$\left[q\frac{\partial}{\partial q}f_g\right]_3 = \frac{\alpha_3}{\pi}\left[C_A P^+_{VV,G}\otimes f_g + C_F P^R_{Vf,G}\otimes f^{0+}_{\sum_g}\right]. \tag{A.2}$$

Here

$$f^{0+}_{\sum_g} = 4\sum_{q_L} f^{0+}_{q_L} + 2\sum_{q_R} f^{0+}_{q_R}, \tag{A.3}$$

where the sums run over all left-handed quark doublets and all right-handed quarks. The factors of 4 and 2 are due to the different normalizations in Eqs. (3.91) and (3.93).

- All other states:

$$\left[q\frac{\partial}{\partial q}f_q\right]_3 = \frac{\alpha_3}{\pi}C_F P^+_{ff,G}\otimes f_q\,. \tag{A.4}$$

A.2 U(1) interaction

- $\mathbf{T} = 0$ and CP $= +$:

$$\left[q\frac{\partial}{\partial q}f_f^{0+}\right]_1 = \frac{\alpha_1}{\pi}Y_i^2\left[P_{ff,G}^{+}\otimes f_f^{0+} + N_f P_{fV,G}^{R}\otimes f_B\right], \tag{A.5}$$

$$\left[q\frac{\partial}{\partial q}f_B\right]_1 = \frac{\alpha_1}{\pi}\left[P_{B,1}^{V}f_B + P_{Vf,G}^{R}\otimes f_{\sum_B f}^{0+} + P_{VH,G}^{R}\otimes f_H^{0+}\right], \tag{A.6}$$

$$\left[q\frac{\partial}{\partial q}f_H^{0+}\right]_1 = \frac{\alpha_1}{\pi}\frac{1}{4}\left[P_{HH,G}^{+}\otimes f_H^{0+} + P_{HV,G}^{R}\otimes f_B\right], \tag{A.7}$$

where

$$f_{\sum_B f}^{0+} = 4\sum_{f_L} Y_{f_L}^2 f_{f_L}^{0+} + 2\sum_{f_R} Y_{f_R}^2 f_{f_R}^{0+}. \tag{A.8}$$

- $\mathbf{T} = 1$ and CP $= +$:

$$\left[q\frac{\partial}{\partial q}f_{BW}^{1+}\right]_1 = \frac{\alpha_1}{\pi}\frac{1}{2}P_{B,1}^{V}f_{BW}^{1+}. \tag{A.9}$$

- All other states:

$$\left[q\frac{\partial}{\partial q}f_f\right]_1 = \frac{\alpha_1}{\pi}Y_f^2 P_{ff,G}^{+}\otimes f_f, \tag{A.10}$$

$$\left[q\frac{\partial}{\partial q}f_H\right]_1 = \frac{\alpha_1}{\pi}\frac{1}{4}P_{HH,G}^{+}\otimes f_H. \tag{A.11}$$

A.3 SU(2) interaction

- $\mathbf{T} = 0$ and CP $= +$:

$$\left[q\frac{\partial}{\partial q}f_{f_L}^{0+}\right]_2 = \frac{\alpha_2}{\pi}\frac{3}{4}\left[P_{ff,G}^{+}\otimes f_{f_L}^{0+} + N_f P_{fV,G}^{R}\otimes f_W^{0+}\right], \tag{A.12}$$

$$\left[q\frac{\partial}{\partial q}f_W^{0+}\right]_2 = \frac{\alpha_2}{\pi}\left[2P_{VV,G}^{+}\otimes f_W^{0+} + \sum_{f_L} P_{Vf,G}^{R}\otimes f_{f_L}^{0+} + P_{VH,G}^{R}\otimes f_H^{0+}\right], \tag{A.13}$$

$$\left[q\frac{\partial}{\partial q}f_H^{0+}\right]_2 = \frac{\alpha_2}{\pi}\frac{3}{4}\left[P_{HH,G}^{+}\otimes f_H^{0+} + P_{HV,G}^{R}\otimes f_W^{0+}\right]. \tag{A.14}$$

- $\mathbf{T} = 0$ and CP $= -$:

$$\left[q\frac{\partial}{\partial q}f_{f_L}^{0-}\right]_2 = \frac{\alpha_2}{\pi}\frac{3}{4}P_{ff,G}^{+}\otimes f_{f_L}^{0-}, \tag{A.15}$$

$$\left[q\frac{\partial}{\partial q}f_H^{0-}\right]_2 = \frac{\alpha_2}{\pi}\frac{3}{4}P_{HH,G}^{+}\otimes f_H^{0-}. \tag{A.16}$$

- $\mathbf{T} = 1$ and CP $= +$:

$$\left[\Delta_{f,2}^{4/3} q \frac{\partial}{\partial q} \frac{f_{f_L}^{1+}}{\Delta_{f,2}^{4/3}}\right]_2 = -\frac{\alpha_2}{\pi}\frac{1}{4} P_{ff,G}^{+} \otimes f_{f_L}^{1+} \tag{A.17}$$

$$\left[\Delta_{H,2}^{4/3} q \frac{\partial}{\partial q} \frac{f_{H}^{1+}}{\Delta_{H,2}^{4/3}}\right]_2 = -\frac{\alpha_2}{\pi}\frac{1}{4} P_{HH,G}^{+} \otimes f_{H}^{1+} \tag{A.18}$$

$$\left[\Delta_{V,2}^{1/2} q \frac{\partial}{\partial q} \frac{f_{BW}^{1+}}{\Delta_{V,2}^{1/2}}\right]_2 = 0\,. \tag{A.19}$$

- $\mathbf{T} = 1$ and CP $= -$:

$$\left[\Delta_{f,2}^{4/3} q \frac{\partial}{\partial q} \frac{f_{f_L}^{1-}}{\Delta_{f,2}^{4/3}}\right]_2 = \frac{\alpha_2}{\pi}\left[-\frac{1}{4} P_{ff,G}^{+} \otimes f_{f_L}^{1-} + \frac{1}{2} N_f P_{fV,G}^{R} \otimes f_{W}^{1-}\right] \tag{A.20}$$

$$\left[\Delta_{V,2}^{1/2} q \frac{\partial}{\partial q} \frac{f_{W}^{1-}}{\Delta_{V,2}^{1/2}}\right]_2 = \frac{\alpha_2}{\pi}\left[P_{VV,G}^{+} \otimes f_{W}^{1-} + \sum_{f_L} P_{Vf} \otimes f_{f_L}^{1-} + P_{VH} \otimes f_{H}^{1-}\right] \tag{A.21}$$

$$\left[\Delta_{H,2}^{4/3} q \frac{\partial}{\partial q} \frac{f_{H}^{1-}}{\Delta_{H,2}^{4/3}}\right]_2 = \frac{\alpha_2}{\pi}\left[-\frac{1}{4} P_{HH,G}^{+} \otimes f_{H}^{1-} + \frac{1}{2}\, P_{HV,G} \otimes f_{W}^{1-}\right]. \tag{A.22}$$

- $\mathbf{T} = 2$ and CP $= +$:

$$\left[\Delta_{V,2}^{3/2} q \frac{\partial}{\partial q} \frac{f_{W}^{2+}}{\Delta_{V,2}^{3/2}}\right]_2 = -\frac{\alpha_2}{\pi} P_{VV}^{+} \otimes f_{W}^{2+}\,. \tag{A.23}$$

A.4 Yukawa interaction

- $\mathbf{T} = 0$ and CP $= +$:

$$\left[q \frac{\partial}{\partial q} f_{q_L^3}^{0+}\right]_Y = \frac{\alpha_Y}{\pi}\left[P_{q_L^3,Y}^{V} f_{q_L^3}^{0+} + P_{ff,Y}^{R} \otimes f_{t_R}^{0+} + N_c P_{fH,Y} \otimes f_{H}^{0+}\right] \tag{A.24}$$

$$\left[q \frac{\partial}{\partial q} f_{t_R}^{0+}\right]_Y = \frac{\alpha_Y}{\pi}\, 2\left[P_{t_R,Y}^{V} f_{t_R}^{0+} + P_{ff,Y}^{R} \otimes f_{q_L^3}^{0+} + N_C P_{fH,Y} \otimes f_{H}^{0+}\right] \tag{A.25}$$

$$\left[q \frac{\partial}{\partial q} f_{H}^{0+}\right]_Y = \frac{\alpha_Y}{\pi}\left[P_{H,Y}^{V} f_{H}^{0+} + P_{Hf,Y}^{R} \otimes f_{\sum_H f}^{0+}\right], \tag{A.26}$$

where

$$f_{\sum_H f}^{0+} = f_{t_R}^{0+} + f_{q_L^3}^{0+}\,. \tag{A.27}$$

- $\mathbf{T} = 0$ and CP $= -$:

$$\left[q\frac{\partial}{\partial q}f^{0-}_{q^3}\right]_Y = \frac{\alpha_Y}{\pi}\left[P^V_{q^3_L,Y}f^{0-}_{q^3_L} + P^R_{ff,Y}\otimes f^{0-}_{t_R} - N_c P_{fH,Y}\otimes f^{0-}_H\right] \quad (A.28)$$

$$\left[q\frac{\partial}{\partial q}f^{0-}_{t_R}\right]_Y = \frac{\alpha_Y}{\pi}2\left[P^V_{t_R,Y}f^{0-}_{t_R} + P^R_{ff,Y}\otimes f^{0-}_{q^3} + N_C P_{fH,Y}\otimes f^{0-}_H\right] \quad (A.29)$$

$$\left[q\frac{\partial}{\partial q}f^{0-}_H\right]_Y = \frac{\alpha_Y}{\pi}\left[P^V_{H,Y}f^{0-}_H + P^R_{Hf,Y}\otimes f^{0-}_{\sum_H f}\right], \quad (A.30)$$

where

$$f^{0-}_{\sum_H f} = f^{0-}_{t_R} - f^{0-}_{q^3_L}\,. \quad (A.31)$$

- $\mathbf{T} = 1$ and CP $= +$:

$$\left[q\frac{\partial}{\partial q}f^{1+}_{q^3_L}\right]_Y = \frac{\alpha_Y}{\pi}\left[P^V_{q^3_L,Y}f^{1+}_{q^3_L} - N_c P_{fH,Y}\otimes f^{1+}_H\right] \quad (A.32)$$

$$\left[q\frac{\partial}{\partial q}f^{1+}_H\right]_Y = \frac{\alpha_Y}{\pi}\left[P^V_{H,Y}f^{1+}_H - P^R_{Hf}\otimes f^{1+}_{q^3_L}\right] \quad (A.33)$$

- $\mathbf{T} = 1$ and CP $= -$:

$$\left[q\frac{\partial}{\partial q}f^{1-}_{t_L}\right]_Y = \frac{\alpha_Y}{\pi}\left[P^V_{t_L,Y}f^{1-}_{t_L} + N_c P_{fH,Y}\otimes f^{1-}_H\right] \quad (A.34)$$

$$\left[q\frac{\partial}{\partial q}f^{1-}_H\right]_Y = \frac{\alpha_Y}{\pi}\left[P^V_{H,Y}f^{1-}_H + P^R_{Hf,Y}\otimes f^{1-}_{q^3_L}\right] \quad (A.35)$$

A.5 Mixed interaction

- $\mathbf{T} = 1$ and CP $= +$:

$$\left[q\frac{\partial}{\partial q}f^{1+}_f\right]_M = \frac{\alpha_M}{\pi}\frac{Y_f}{2}N_f P^R_{fV,G}\otimes f^{1+}_{BW}\,, \quad (A.36)$$

$$\left[q\frac{\partial}{\partial q}f^{1+}_{BW}\right]_M = \frac{\alpha_M}{\pi}\left[4\sum_{f_L}Y_f P^R_{Vf,G}\otimes f^{1+}_f + 2P^R_{VH,G}\otimes f^{1+}_H\right], \quad (A.37)$$

$$\left[q\frac{\partial}{\partial q}f^{1+}_H\right]_M = \frac{\alpha_M}{\pi}\frac{1}{4}P^R_{HV,G}\otimes f^{1+}_{BW}\,, \quad (A.38)$$

Equation (A.37) differs slightly from Ref. [12] where, taking into account the definition there of $f_{B3} = f_{BW}/2$, an 8 would appear in place of 4 in the first term on the right-hand side.

Appendix B

The partonic Born cross sections for di-lepton production

The expressions for the Born cross sections with $AB = q\bar{q}$ and $AB = W^+W^-$ are given in Table B.1, with the various functional dependences on the Mandelstam variables s, t, u,

$$s = (p_A + p_B)^2\,, \qquad t = (p_A - p_\ell)^2\,, \qquad u = (p_B - p_\ell)^2\,, \tag{B.1}$$

$AB \to \ell\bar{\ell}'$	B_{AB}
$q_{L/R}\,\bar{q}_{L/R} \to \ell_{L/R}\,\bar{\ell}_{L/R}$	$\frac{8\pi^2}{s}\, f_{L/R,L/R}(s,t,u)\, \left(\alpha_1 Y_q Y_\ell + \alpha_2 I_q I_\ell\right)^2$
$q_{L/R}\,\bar{q}_{L/R} \to \ell_{R/L}\,\bar{\ell}_{R/L}$	$\frac{8\pi^2}{s}\, f_{L/R,R/L}(s,t,u)\, \alpha_1^2 Y_q^2 Y_\ell^2$
$q_L\,\bar{q}'_L \to \ell_L\,\bar{\ell}'_L$	$\frac{8\pi^2}{s}\, f_{C,L}(s,t,u)\, \alpha_2^2$
$W^+\,W^- \to e_L\bar{e}_L$	$\frac{8\pi^2}{s}\, f^{(1)}_{(+,-)}(s,t,u)\, \alpha_2^2$
$W^+\,W^- \to \nu_L\bar{\nu}_L$	$\frac{8\pi^2}{s}\, f^{(2)}_{(+,-)}(s,t,u)\, \alpha_2^2$

Table B.1: Born cross sections for $q\bar{q}$ and W^+W^- going to lepton pairs. Here e stands for the charged lepton. The cross sections for $BA \to \ell\bar{\ell}'$ are the same as $AB \to \ell\bar{\ell}'$ with $t \leftrightarrow u$.

given by[1]

$$
\begin{aligned}
f_{L/R,L/R}(s,t,u) &= \frac{4}{3}\frac{u^2}{s^2} \\
f_{L/R,R/L}(s,t,u) &= \frac{4}{3}\frac{t^2}{s^2} \\
f_{C,L}(s,t,u) &= \frac{1}{3}\frac{u^2}{s^2} \\
f^{(1)}_{(+,-)}(s,t,u) &= \frac{t}{4u}\frac{t^2+u^2}{s^2} \\
f^{(2)}_{(+,-)}(s,t,u) &= \frac{u}{4t}\frac{t^2+u^2}{s^2}\,.
\end{aligned}
\tag{B.2}
$$

For the scattering involving neutral gauge bosons in the initial state one can either work in the unbroken basis (where the neutral bosons required are B, W_3 or mixed $M = B/W_3$) or in the broken basis (where the neutral bosons required are γ, Z or mixed $\tilde{M} = \gamma/Z$). For the unbroken basis the results are given in Table B.2 with

$$
\begin{aligned}
f_N(s,t,u) &= \frac{t^2+u^2}{ut} \\
f_{(\pm,3)}(s,t,u) &= \frac{1}{8}\frac{u^2+t^2}{ut}\frac{(t-u)^2}{s^2} \\
f_{(\pm,B)}(s,t,u) &= \frac{1}{8}\frac{u^2+t^2}{ut} \\
f_{(\pm,M)}(s,t,u) &= \pm\frac{1}{8}\frac{u^2+t^2}{ut}\frac{t-u}{s}\,,
\end{aligned}
\tag{B.3}
$$

while for the broken basis the results are in Table B.3 with

$$
\begin{aligned}
f_{+,\gamma}(s,t,u) &= \frac{1}{2}\frac{u^2+t^2}{s^2}\frac{u}{t} \\
f_{-,\gamma}(s,t,u) &= \frac{1}{2}\frac{u^2+t^2}{s^2}\frac{t}{u}, \\
f_{+,Z}(s,t,u) &= \frac{1}{8}\frac{u^2+t^2}{ut}\left(\frac{s+2c_W^2 u}{c_W s_W s}\right)^2 \\
f_{-,Z}(s,t,u) &= \frac{1}{8}\frac{u^2+t^2}{ut}\left(\frac{s+2c_W^2 t}{c_W s_W s}\right)^2 \\
f_{+,\tilde{M}}(s,t,u) &= \frac{1}{4}\frac{u^2+t^2}{st}\frac{s+2c_W^2 u}{c_W s_W s} \\
f_{-,\tilde{M}}(s,t,u) &= \frac{1}{4}\frac{u^2+t^2}{su}\frac{s+2c_W^2 t}{c_W s_W s}\,,
\end{aligned}
\tag{B.4}
$$

where s_W and c_W represent the sine and cosine of the weak mixing angle, respectively.

[1]In keeping with our neglect of power-suppressed terms above the electroweak scale, all fermion and boson masses are set to zero.

$AB \to \ell\bar{\ell}'$	B_{AB}
$W^3\,W^3 \to \ell\bar{\ell}$	$\frac{8\pi^2}{s}\, f_N(s,t,u)\, \alpha_2^2\, I_\ell^4$
$W^3\,B \to \ell\bar{\ell}$	$\frac{8\pi^2}{s}\, f_N(s,t,u)\, \alpha_1\, \alpha_2\, Y_\ell^2\, I_\ell^2$
$W^3\,M \to \ell\bar{\ell}$	$\frac{8\pi^2}{s}\, f_N(s,t,u)\, \sqrt{\alpha_1\alpha_2}\, \alpha_2\, Y_\ell\, I_\ell^3$
$B\,B \to \ell\bar{\ell}$	$\frac{8\pi^2}{s}\, f_N(s,t,u)\, \alpha_1^2\, Y_\ell^4$
$B\,M \to \ell\bar{\ell}$	$\frac{8\pi^2}{s}\, f_N(s,t,u)\, \sqrt{\alpha_1\alpha_2}\, \alpha_1\, Y_\ell^3\, I_\ell$
$M\,M \to \ell\bar{\ell}$	$\frac{8\pi^2}{s}\, f_N(s,t,u)\, \alpha_1\, \alpha_2\, Y_\ell^2\, I_\ell^2$
$W^\pm\,W^3 \to \ell_L\bar{\ell}'_L$	$\frac{8\pi^2}{s}\, f_{(\pm,3)}(s,t,u)\, \alpha_2^2$
$W^\pm\,B \to \ell_L\bar{\ell}'_L$	$\frac{8\pi^2}{s}\, f_{(\pm,B)}(s,t,u)\, \alpha_1\, \alpha_2$
$W^\pm\,M \to \ell_L\bar{\ell}'_L$	$\frac{8\pi^2}{s}\, f_{(\pm,M)}(s,t,u)\, \sqrt{\alpha_1\alpha_2}\, \alpha_2$

Table B.2: Born cross sections for VV in the unbroken basis going to lepton pairs. Here M stands for the mixed B/W_3 PDF. The cross sections for $BA \to \ell\bar{\ell}'$ are the same as $AB \to \ell\bar{\ell}'$ with $t \leftrightarrow u$.

$AB \to \ell\bar{\ell}'$	B_{AB}
$\gamma\,\gamma \to \ell\bar{\ell}$	$\frac{8\pi^2}{s}\, f_N(s,t,u)\, \alpha^2\, Q_\ell^4$
$\gamma\,Z \to \ell\bar{\ell}$	$\frac{8\pi^2}{s}\, f_N(s,t,u)\, \alpha^2\, Q_\ell^2\, R_\ell^2$
$\gamma\,\tilde{M} \to \ell\bar{\ell}$	$\frac{8\pi^2}{s}\, f_N(s,t,u)\, \alpha^2\, Q_\ell^3\, R_\ell$
$Z\,Z \to \ell\bar{\ell}$	$\frac{8\pi^2}{s}\, f_N(s,t,u)\, \alpha^2\, R_\ell^4$
$Z\,\tilde{M} \to \ell\bar{\ell}$	$\frac{8\pi^2}{s}\, f_N(s,t,u)\, \alpha^2\ Q_\ell\, R_\ell^3$
$\tilde{M}\,\tilde{M} \to \ell\bar{\ell}$	$\frac{8\pi^2}{s}\, f_N(s,t,u)\, \alpha^2\, Q_\ell^2\, R_\ell^2$
$W^\pm\,\gamma \to \ell_L\bar{\ell}'_L$	$\frac{8\pi^2}{s}\, f_{(\pm,\gamma)}(s,t,u)\, \alpha\, \alpha_2$
$W^\pm\,Z \to \ell_L\bar{\ell}'_L$	$\frac{8\pi^2}{s}\, f_{(\pm,Z)}(s,t,u)\, \alpha\, \alpha_2$
$W^\pm\,\tilde{M} \to \ell_L\bar{\ell}'_L$	$\frac{8\pi^2}{s}\, f_{(\pm,\tilde{M})}(s,t,u)\, \alpha\, \alpha_2$

Table B.3: Born cross sections for VV in the broken basis going to lepton pairs. Here $\tilde{M}$ stands for the mixed γ/Z PDF. The cross sections for $BA \to \ell\bar{\ell}'$ are the same as $AB \to \ell\bar{\ell}'$ with $t \leftrightarrow u$.